H⁄A

HORMIGÓN y ACERO

El **Consejo Editorial** de la revista tiene como misión la definición de la política editorial (estilo de la revista, redacción, normas de presentación de originales, diseño, creación y orientación de las distintas secciones). **El Comité de Redacción** se constituye como un comité permanente del Consejo Editorial y se encarga de dirigir y supervisar la gestión diaria de la revista, controlar la selección de contribuciones y tomar las decisiones sobre los contenidos que han de conformar cada número de la revista. La función del **Consejo Asesor Científico** es la de velar por el prestigio científico y técnico de la revista, promoviendo e impulsando su difusión internacional.

Una descripción más amplia puede consultarse en *www.hormigonyacero.com*

SUMARIO | CONTENTS

MIEMBROS PATROCINADORES DE LA ASOCIACIÓN ESPAÑOLA DE INGENIERÍA ESTRUCTURAL (ACHE)

Según los Estatutos de la Asociación existen dos tipos de miembros, uno para personas jurídicas y otro para personas físicas. De entre los primeros, y por la importancia que tienen para la Asociación por su contribución económica, destacan los miembros Patrocinadores y los Protectores. Hasta la fecha de cierre del presente número de la Revista, figuran inscritos como **Miembros Patrocinadores** los que a continuación se indican, citados por orden alfabético:

ACCIONA INFRAESTRUCTURAS
Avda. de Europa, 18
28108 ALCOBENDAS (MADRID)

ALE HEAVYLIFT IBERICA, S.A
Pl. Los Frailes, Ctra Alcalá de Henares a Daganzo,
km 9, P 101-108, 28814 DAGANZO (MADRID)

**ARENAS & ASOCIADOS,
INGENIERÍA DE DISEÑO, S.L.P.**
C/ Marqués de la Ensenada, 11 - 3º
39009 SANTANDER

ACE
C/ Jordi Girona 31 - 2ª, Edifici 19-bis
08034 - BARCELONA

CALIDAD SIDERÚRGICA
C/ Orense, 58 - 10º
28006 MADRID

CARLOS FERNÁNDEZ CASADO, S.L.
OFICINA DE PROYECTOS
CARLOS FERNÁNDEZ CASADO, S.L.
C/ Orense, 10
28020 MADRID

CEDEX (Laboratorio Central)
C/ Alfonso XII, 3
28014 MADRID

CONSEJO GENERAL COLEGIOS ARQUITECTOS TÉCNICOS
Paseo de la Castellana, 155 - 1º
28046 MADRID

CYPE INGENIEROS, S.A.
Avda. Eusebio Sempere, 5 - Bajo
03003 ALICANTE

DRAGADOS, S.A.
Avda. Camino de Santiago, 50
28050 MADRID

EDARTEC CONSULTORES
C/ Manufactura, 4 - Planta 2 - Mod. 3
41927 MAIRENA DE ALJARAFE (SEVILLA)

E.T.S. INGENIEROS DE CAMINOS - DPTO. MECÁNICA
Ciudad Universitaria, s/n
28040 MADRID

EUROCONSULT
Avda. Camino de lo Cortao, 17 - Zona Industrial Sur
28703 SAN SEBASTIAN DE LOS REYES (MADRID)

FCC CONSTRUCCIÓN, S.A.
Avda. Camino de Santiago 40
28050 MADRID

FLORENTINO REGALADO INGENIERÍA & ARQUITECTURA S.L.P.
C/ Granja de Rocamora, 19
03015 ALICANTE

GRUPO MECÁNICA ESTRUCTURAL S.L.
C/ Amilcar González Díaz, 18
38550 ARAFO (SANTA CRUZ DE TENERIFE)

HILTI ESPAÑOLA, S.A.
Avda. Fuente de la Mora, 2 - Edificio I
28050 MADRID

INSTITUTO EDUARDO TORROJA
C/ Serrano Galvache, 4
28033 MADRID

IECA
C/ José Abascal, 53 - 2º
28003 MADRID

OVE ARUP & PARTNERS, S.A.
C/ Alfonso XI, 12
28014 Madrid

PUENTES Y CALZADAS, GRUPO DE EMPRESAS, S.A.
Ctra. de la Estación, s/n
15888 SIGÜEIRO-OROSO (A CORUÑA)
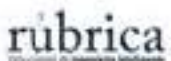
RÚBRICA INGENIERÍA Y ARQUITECTURA, S.L.
Avda. Hermanos Bou, 246
12003 CASTELLÓN

TECNALIA
Parque Tecnológico de Bizkaia - C/ Geldo - Edificio 700
48160 DERIO (VIZCAYA)

MIEMBROS PROTECTORES DE LA ASOCIACIÓN ESPAÑOLA DE INGENIERÍA ESTRUCTURAL (ACHE)

Según los Estatutos de la Asociación existen dos tipos de miembros; uno para personas jurídicas y otro para personas físicas. De entre los primeros, y por la importancia que tienen para la Asociación por su contribución económica, destacan los miembros Patrocinadores y los Protectores. Hasta la fecha de cierre del presente número de la Revista, figuran inscritos como **Miembros Protectores** los que a continuación se indican, citados por orden alfabético:

Este número especial de *Hormigón y Acero* está dedicado a Javier Manterola, una de las grandes figuras de la ingeniería estructural española, maestro de varias generaciones de ingenieros de la Escuela de Caminos de Madrid e inspirador de diseñadores de puentes en todo el mundo. No se realiza con ocasión de ningún hecho particular, sino más bien como sincera apreciación a su dilatada y fructífera trayectoria profesional. También agradecemos su intensa dedicación a la revista, en la que ha publicado 42 artículos por ahora, todos ellos disponibles en la *web*, y en la que ha trabajado como miembro del Consejo Editorial.

La edición del especial ha sido coordinada por José Romo, a quien agradezco muy especialmente su dedicación a esta tarea. Ha invitado a la mayoría de autores y ha organizado el proceso de edición y revisión, con la ayuda de Héctor Bernardo, Julio Sánchez Delgado, Miguel Ángel Astiz y Juan José Jorquera. No se trataba de tener un número con artículos *sobre* nuestro homenajeado, sino de trabajos *dedicados* a él. El resultado es una colección de contribuciones del máximo nivel firmadas por algunos de los mejores proyectistas y académicos en ingeniería de puentes.

Comienza con un artículo de Salvador Monleón, Carlos Lázaro y Josep Casanova, de la Univ. Politécnica de Valencia, sobre solicitaciones excéntricas en vigas curvas. Jiri Strasky (Univ. Técnica de Brno & Strasky, Husty and Partners) escribe sobre la búsqueda de la verdadera solución estructural. Contamos también con un artículo sobre puentes extradosados, cuyo autor es Akio Kasuga (Sumitomo Mitsui Construction & actual Vicepresidente de la *fib*), y otro sobre puentes atirantados, firmado por Naeem Hussain (ARUP). De Vincent de Ville de Goyet (Bureau Greisch & Univ. de Lieja) tenemos un artículo sobre arcos de acero. Mike Schlaich (SBP & Univ. Técnica de Berlín) analiza el enfoque en el diseño de Javier Manterola y estudia las similitudes con dicho enfoque que encuentra en puentes alemanes. José Romo (FHECOR & UPM) escribe sobre puentes híbridos como tendencia innovadora y, finalmente, de Klaus Ostenfeld (ahora consultor independiente, previamente director ejecutivo de COWI) tenemos un artículo sobre la evolución de los puentes colgantes. Gracias a todos ellos por su artículo para este especial.

Este número se presentará en la Sala Verde de la Escuela de Caminos de la UPM el jueves 20 de febrero de 2020 a las 16:30 h. Desde aquí invito a todos los lectores de *Hormigón y Acero* a que hagan un hueco en sus agendas y asistan al acto.

Gonzalo Ruiz
DIRECTOR DE HORMIGÓN Y ACERO

Es para mí un gran placer presentar aquí este número especial de la revista *Hormigón y Acero* dedicado a mi admirado Javier Manterola. Ha sido para mí un gran honor haber podido coordinar este número en el que colaboran ingenieros especialistas en puentes de todo el mundo.

Es evidente que Javier Manterola es uno de los ingenieros estructurales más destacado de las últimas décadas a nivel internacional; la gran cantidad de premios y galardones nacionales e internacionales que ha recibido a lo largo de su carrera dan fe de su prestigio como proyectista de puentes, y por ello Javier es más que merecedor del pequeño reconocimiento que hacemos con este número especial.

Me gustaría aprovechar para destacar la figura de Javier Manterola como ingeniero integral capaz de aproximarse al proyecto, con una visión general desde la propia especialización del ingeniero de puentes. Javier Manterola es indudablemente un gran dominador de lo técnico, pero al mismo tiempo tiene siempre una visión humanista, creativa y artística de la ingeniería que evidentemente se ve reflejada en su obra. Esta forma integral de abordar el proyecto se materializa en una obra muy personal, que constituye la formalización de una manera modélica de entender la labor del ingeniero; una forma de trabajar que es siempre fuente de admiración y de inspiración a otros proyectistas.

Este número, que dedicamos a Javier Manterola, presenta al lector una serie de artículos que resumen la evolución y el estado de la técnica de los distintos tipos estructurales de puentes. Para la realización de este monográfico, se ha contado con proyectistas de todo el mundo especialistas en los tipos estructurales contemporáneos de estas obras. Quiero destacar que ha sido muy sencillo contar con el apoyo entusiasta del grupo de proyectistas que colaboran en este número, gracias al aprecio y al reconocimiento profesional que todos ellos tienen por Javier Manterola. Agradezco enormemente a todos los autores su valiosa contribución a la revista.

A lo largo del número, el lector podrá descubrir que la mayor parte de las aportaciones de los autores se apartan de alguna forma de la ortodoxia de los escritos tradicionales académicos. Muchos de ellos trabajan únicamente en el mundo profesional del proyecto, en consecuencia, las contribuciones que aquí se incluyen son en muchos casos, no solo un resumen de la evolución y el estado de la técnica del proyecto de puentes, sino también un reflejo de la propia experiencia personal como proyectistas, lo que entiendo es un valor añadido para la revista.

Para concluir, espero que los lectores de *Hormigón y Acero* disfruten de este número especial en el que se ha intentado condensar la evolución y el estado de la técnica de puentes, que gustosamente y con admiración dedicamos a Javier Manterola.

José Romo
EDITOR ASOCIADO

La sección abierta y cerrada bajo solicitación excéntrica… en una viga curva. Un tributo a Javier Manterola

The open and closed cross-section under eccentric loading... on a curved beam. A tribute to Javier Manterola

Salvador Monleón, Carlos Lázaro* y Josep Casanova

*Universitat Politècnica de València. Mecánica de Medios Continuos y Teoría de Estructuras,
Escuela Técnica Superior de Ingenieros de Caminos, Canales y Puertos, Valencia, Spain*

RESUMEN

En este artículo se desarrolla una formulación elástico-lineal exacta para el análisis de vigas curvas de directriz plana. El propósito es idéntico al de un artículo que Javier Manterola publicó en 1976: profundizar en el comportamiento de las piezas esbeltas cuando estas se ven solicitadas excéntricamente por cargas transversales. Al incorporar la curvatura en la formulación, aparecen nuevos parámetros seccionales que condicionan el comportamiento de la pieza, cuya respuesta queda gobernada por la *esbeltez torsional*. A continuación se ha estudiado la relación de estos parámetros con la curvatura, y finalmente se ha evaluado la respuesta estructural de vigas de sección abierta y cerrada en función de la curvatura y de la *esbeltez torsional*. Este trabajo proporciona un método riguroso para evaluar la respuesta de las vigas curvas frente a la torsión, y constituye una extensión de los criterios tradicionalmente establecidos para vigas rectas.

© 2019 Asociación Española de Ingeniería Estructural (ACHE). Publicado por Cinter Divulgación Técnica S.L.L. Todos los derechos reservados.

PALABRAS CLAVE: Viga curva, acoplamiento flexión-torsión, esbeltez de torsión, torsión alabeada, torsión mixta

ABSTRACT

In this paper, an exact linear-elastic formulation for the analysis of curved beams with planar centerline has been developed. The purpose is identical to that of an article which Javier Manterola authored in 1976: to deepen in the behavior of beams when they are eccentrically loaded by transverse forces. When incorporating curvature in the formulation, new sectional parameters appear; they condition the structural behavior of the beam, which is governed by the *torsional slenderness*. The relation between these parameters and the curvature has been studied. Finally, the structural response of beams of open and closed cross-section has been evaluated in terms of curvature and torsional slenderness. This work provides a rigorous method to assess the response of curved beams under torsion and is therefore an extension of the traditionally established criteria for straight beams.

© 2019 Asociación Española de Ingeniería Estructural (ACHE). Published by Cinter Divulgación Técnica S.L.L. All rights reserved.

KEYWORDS: Curved beam, bending-torsion coupling, torsional slenderness, warped torsion, mixed torsion

1.
INTRODUCCIÓN

En el año 1976 la A.F.C.E. (Agrupación de Fabricantes de Cemento de España) publicó el Nº15 de su Serie Monográfica, dividido en tres volúmenes denominados Puentes I, II y III. En el segundo de ellos (Figura 1), Javier Manterola presentó un formidable artículo [1] que tituló *La sección abierta y cerrada bajo solicitación excéntrica*, en el que mostró con maestría cómo

la resistencia de materiales y en particular la teoría de vigas rectas podía extenderse más allá del modelo elemental de viga de Navier-Bernoulli-Timoshenko –que en lo sucesivo denominaremos Modelo de Viga Simple, o más brevemente MVS– adoptando para ello una intensidad de alabeo independiente de la intensidad de la rotación torsional al analizar la torsión no uniforme de vigas cajón y computando los efectos globales de flexión, torsión y distorsión producidos, en servicio, por las car-

---

* Autor para correspondencia.
Correo electrónico: carlafer@mes.upv.es (C. Lázaro).
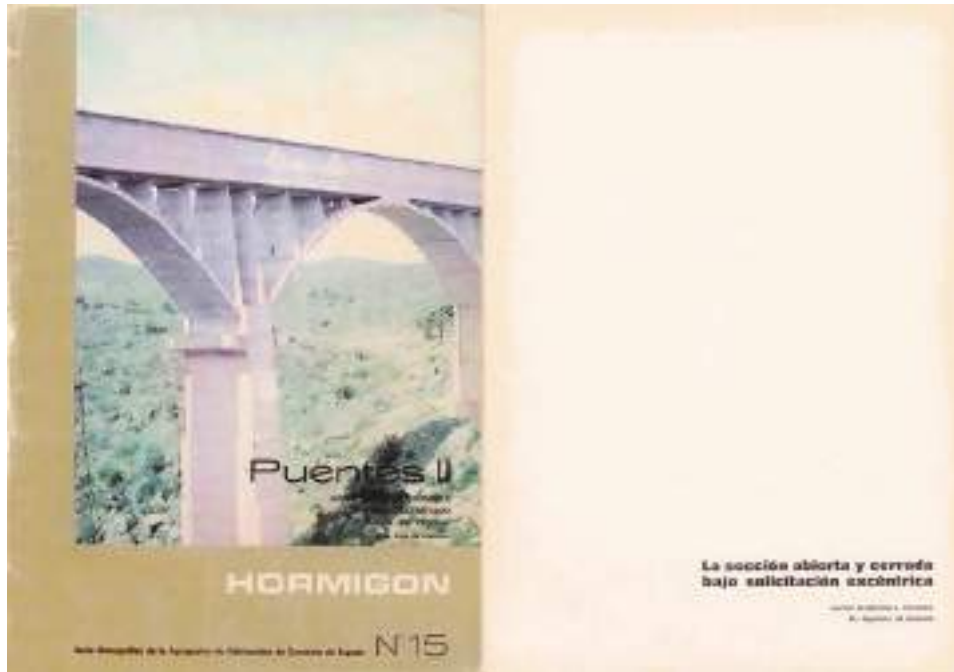
Figura 1. Portadas del Nº15 —Puentes II— de la Serie Monográfica de la A.F.C.E. y del artículo de Javier Manterola.

gas excéntricas sobre este mismo tipo de tableros, así como su evolución hasta rotura, evaluada mediante ensayos. Este trabajo formaba parte de una iniciativa mucho más amplia de Javier Manterola, orientada a la divulgación de nuevos métodos de cálculo especialmente apropiados para el análisis de tableros de puentes [2, 3], con el fin de actualizar y mejorar la praxis estructural en la España de la década de 1970. En particular, en lo que al modelo viga se refiere, destacaban las publicaciones de Vlassov [4] y Kollbrunner y Basler [5], referencias clave en el artículo del que hemos partido.

Nuestra modesta contribución al reconocimiento colectivo del inmenso trabajo desarrollado por Javier Manterola Armisén, ingeniero y profesor a lo largo de más de 50 años, consistirá en extender el problema anterior a las vigas curvas, como un primer paso hacia su generalización a los tableros de planta curva.

El problema de las piezas de directriz curva ha preocupado a los ingenieros desde hace mucho tiempo. El primero del que se tiene noticias de que lo abordara fue Kirchhoff [6], a mediados del siglo XIX. Desarrolló un modelo de viga muy esbelta, sin limitación en los desplazamientos de la directriz, considerando la deformabilidad de la sección debida al efecto Poisson y al alabeo torsional. Es válido para secciones macizas o cerradas en las que el centro de gravedad y el centro de esfuerzos cortantes pueden suponerse coincidentes. Aproximadamente en la misma época, Winkler [7] planteó un modelo lineal de viga curva, que se convirtió en la base de la formulación de este problema incluida en los manuales clásicos, como Timoshenko [8] o Courbon [9], que se centran en el problema del arco.

En 1959 Anderson [10] investigó las tensiones en vigas curvas con sección en doble T y en cajón, y proporcionó tablas y fórmulas para determinarlas. Posteriormente, Samartín y González de Cangas [11] dedujeron las ecuaciones generales del comportamiento de vigas curvas en el espacio y las aplicaron al caso de la viga balcón. El estudio no considera el

alabeo torsional ni la posible excentricidad del centro de esfuerzos cortantes. El trabajo de Gimena et al. [12] sistematiza el planteamiento exacto del problema basándose en hipótesis similares (sin consideración del alabeo). Cabe mencionar también otros estudios analíticos más recientes relacionados con la torsión de vigas como Barretta et al. [13] y Romano et al. [14], que tratan de la distribución de tensiones debidas a la torsión en vigas rectas de sección arbitraria, y de la posición relativa de centros de torsión y de cortante, respectivamente.

En las últimas décadas, la investigación en vigas curvas se ha centrado en la resolución numérica del problema empleando modelos de elementos finitos, y específicamente en el tratamiento de la principal dificultad asociada: el bloqueo de cortante y de membrana [15-18]. En el ámbito de las vigas con grandes desplazamientos, Reissner [19] desarrolló una teoría no lineal sin considerar alabeo de la sección, que fue la base para la formulación de modelos de elementos finitos como los desarrollados por Simó, primero sin incorporar alabeo [20] y más adelante considerándolo [21].

Nuestra aportación consistirá en el desarrollo de las ecuaciones exactas de la formulación lineal del problema de la viga curva de directriz contenida en un plano, con sección abierta o cerrada, considerando tanto el alabeo torsional como la posible excentricidad del centro de esfuerzos cortantes. Esto amplia el ámbito de aplicación de las referencias clásicas [8,9] y también de la referencia [11], más reciente.

Para ello, comenzaremos por unas consideraciones generales sobre las piezas curvas, de carácter geométrico, acompañadas de algún resultado mecánico apropiado para nuestros desarrollos futuros. A continuación, en la sección 3, abordaremos la parte central del trabajo, que consiste en la formulación de la estática lineal de la viga curva sometida a cargas transversales, desarrollada en el marco de la teoría unificada de vigas (*UBT* por sus siglas en inglés) [22]. Esta formulación permite, sin abandonar el modelo viga, identificar las características mecá-

nicas de la sección que influyen en la respuesta, y definir la esbeltez torsional como parámetro que gobierna (junto con la curvatura) el reparto de la torsión entre la parte de Saint-Venant y la parte debida al alabeo. El problema estudiado no ha sido tratado en la citada referencia y constituye por tanto una aportación original. En la sección 4 estudiaremos en primer lugar la influencia de la curvatura en los parámetros asociados a la sección transversal en tres tipos de sección: rectangular hueca, doble T y U; a continuación se llevará a cabo un estudio paramétrico (basado en las expresiones obtenidas en la sección 3) de la influencia de la esbeltez torsional y la curvatura en la respuesta cinemática y estática de la viga, que muestra el potencial de la formulación presentada como herramienta para evaluar la respuesta de vigas curvas frente a torsión y profundizar en la comprensión del fenómeno. Finalmente, cerraremos el artículo con las conclusiones pertinentes y algunas sugerencias para desarrollos futuros. En la sección 6 se incluye una lista de los símbolos más relevantes.

2.
CONSIDERACIONES GENERALES SOBRE LAS PIEZAS CURVAS: EL ARCO Y LA VIGA CURVA

En esta primera sección del artículo nos proponemos describir el marco geométrico en el que se desarrollará el análisis, justificar la elección de un sistema de referencia específico basado en considerar una curva particular –a la que llamaremos *eje principal*– como directriz de la pieza, mostrar los valores que adoptan ciertas propiedades geométricas en esta referencia y, finalmente, exponer en qué condiciones las respuestas de arco y de viga curva se presentan desacopladas. Para ello nos basaremos en el *MVS*, que determina el modelo más elemental de viga curva.

En primer lugar, conviene reflexionar sobre el problema de la elección del sistema de referencia y de la curva directriz $\Gamma(s)$ en el caso más elemental de las piezas alargadas de sección constante. La respuesta del sólido es independiente del sistema de referencia seleccionado para formular el problema, sin embargo, el modelo matemático que se genera sí que es tributario de esta elección. Esto introduce la posibilidad de escoger el sistema de referencia de tal forma que la resolución del modelo resulte más sencilla.

En lo sucesivo denotaremos por $\tilde{\Gamma}$ y denominaremos *directriz material* de la pieza al lugar geométrico de los centros de gravedad G de las secciones transversales, reservando el símbolo Γ y la denominación *directriz principal* para el lugar geométrico de los puntos ocupados por nuevo polo O, cuyas propiedades estableceremos más adelante. Ambas curvas quedan relacionadas por sus vectores posición $\tilde{\mathbf{P}}$ y $\mathbf{P}$ mediante la fórmula $\mathbf{P} = \tilde{\mathbf{P}} + \tilde{y}_0\tilde{\mathbf{n}} + \tilde{z}_0\tilde{\mathbf{b}}$. En ella, $\tilde{\mathbf{n}}$ y $\tilde{\mathbf{b}}$ son los vectores normal y binormal del triedro intrínseco de la directriz material, mientras que $\tilde{y}_0$ y $\tilde{z}_0$ definen las coordenadas de la intersección de la directriz principal con una sección transversal genérica, referidas a la parametrización material del sólido, basada en la directriz $\tilde{\Gamma}$.

A continuación, vamos a interesarnos por el modelo más elemental de pieza alargada, formulándolo en la referencia basada en la directriz principal Γ. Según el *MVS*, sus desplazamientos generalizados son $\mathbf{u}(s)=\{u,v,w,\theta_s,\theta_y,\theta_z\}^T$ y no incluyen

el alabeo torsional. Las deformaciones generalizadas, de acuerdo con [22, fórmulas (3.1)], resultan

$$\left.\begin{array}{ll} \varepsilon_s = \dfrac{du}{ds} - \chi v & \kappa_s = \dfrac{d\theta_s}{ds} \, \chi\theta_y \\[2mm] \gamma_{sy} = \dfrac{dv}{ds} - \chi u - \theta_z & \kappa_y = \dfrac{d\theta_y}{ds} + \chi\theta_s \\[2mm] \gamma_{sz} = \dfrac{dw}{ds} + \theta_y & \kappa_z = \dfrac{d\theta_z}{ds} \end{array}\right\} \tag{1}$$

donde $\chi(s)$ es la curvatura de la directriz $\Gamma(s)$.

Agrupando en el vector $\mathbf{e}(s)=\{\varepsilon_s,\gamma_{sy},\gamma_{sz},\kappa_s,\kappa_y,\kappa_z\}^T$ las deformaciones generalizadas, la densidad lineal de energía potencial del modelo puede escribirse como

$$F(s, \mathbf{u}, \mathbf{e}) = \frac{1}{2}\,\mathbf{e}^T\mathbf{D}_{11}\,\mathbf{e} - \mathbf{u}^T\mathbf{Q} \tag{2}$$

donde $\mathbf{Q}(s)=\{q_s,q_y,q_z,m_s,m_y,m_z\}^T$ es el vector densidad lineal de carga generalizada consistente con los desplazamientos generalizados $\mathbf{u}(s)$ del *MVS*, y el operador constitutivo $\mathbf{D}_{11}$ se calcula como sigue [22, fórmula (2.34)]

$$\mathbf{D}_{11} = \int_A \mathbf{B}_1^T\mathbf{C}\mathbf{B}_1\,\mu\,dA = \int_A \mathbf{h}^T\mathbf{C}\mathbf{h}\,\frac{dA}{\mu} \tag{3}$$

El escalar $\mu=1-\chi y$ permite expresar el diferencial de volumen del sólido como $dV=\mu ds dy dz$; la matriz constitutiva $\mathbf{C}$ y el operador cinemático $\mathbf{h}(y,z)$ están definidos en [22, fórmulas (2.20) y (2.85)]. De todo ello resulta, en nuestro caso

$$\mathbf{D}_{11} = \begin{bmatrix} E\bar{A} & 0 & 0 & 0 & E\bar{S}_y & -E\bar{S}_z \\ 0 & G\bar{A} & 0 & -E\bar{S}_y & 0 & 0 \\ 0 & 0 & G\bar{A} & ES_z & 0 & 0 \\ 0 & -E\bar{S}_y & E\bar{S}_z & G\bar{I}_0 & 0 & 0 \\ E\bar{S}_y & 0 & 0 & 0 & E\bar{I}_y & -E\bar{I}_{yz} \\ -E\bar{S}_z & 0 & 0 & 0 & -E\bar{I}_{yz} & E\bar{I}_z \end{bmatrix} \tag{4}$$

con

$$\left.\begin{array}{lll} \bar{A} = \int_A \dfrac{dA}{\mu} & , \quad \bar{S}_y = \int_A z\dfrac{dA}{\mu} & , \quad \bar{S}_z = \int_A y\dfrac{dA}{\mu} \\[3mm] \bar{I}_y = \int_A z^2\dfrac{dA}{\mu} & , \quad \bar{I}_{yz} = \int_A yz\dfrac{dA}{\mu} & , \quad \bar{I}_z = \int_A y^2\dfrac{dA}{\mu} \end{array}\right\} \tag{5}$$

e $\bar{I}_0=\bar{I}_y+\bar{I}_z$. Conviene subrayar que la composición del operador $\mathbf{D}_{11}$ dada en (4) es válida cualquiera que sea la geometría de la curva directriz (plana o alabeada).

Se define la *directriz* o *eje principal* de la pieza curva mediante la propiedad siguiente

$$\bar{S}_y = \int_A z\frac{dA}{\mu} = 0 \quad , \quad \bar{S}_z = \int_A y\frac{dA}{\mu} = 0 \tag{6}$$

Por lo tanto, las coordenadas en sección transversal del polo O que lo determina, referidas al centro de gravedad de la misma, son

$$\tilde{y}_0 = \frac{\int_A \tilde{y}\,\frac{dA}{\tilde{\mu}}}{\int_A \frac{dA}{\tilde{\mu}}} \qquad , \qquad \tilde{z}_0 = \frac{\int_A \tilde{z}\,\frac{dA}{\tilde{\mu}}}{\int_A \frac{dA}{\tilde{\mu}}} \tag{7}$$

Apoyándonos ahora en la Figura 2, obtenemos las siguientes relaciones de transformación

$$\left.\begin{array}{ll} y = \tilde{y} - \tilde{y}_0 \quad , & z = \tilde{z} - \tilde{z}_0 \\[2mm] R = \tilde{R} - \tilde{y}_0 \quad , & r = \tilde{R} - \tilde{y} = R - y \end{array}\right\} \tag{8}$$

De la última se deduce además que

$$\tilde{R}\tilde{\mu} = R\mu = r \tag{9}$$

Por otra parte, las constantes estáticas recogidas en (5) merecen un estudio más detallado. En particular, la definición del escalar μ permite escribir

$$\bar{S}_z = \int_A R\,(1-\mu)\,\frac{dA}{\mu} = R\,(\bar{A} - A) \tag{10}$$

Y, como $\bar{S}_z = 0$ por (6), se cumplirá

$$\bar{A} = \int_A \frac{dA}{\mu} = A \tag{11}$$

La parametrización adoptada, en adelante *parametrización principal*, asociada a la selección de la directriz expresada por las fórmulas (7), simplifica notablemente la formulación, puesto que con ella la composición del operador constitutivo $\mathbf{D}_{11}$ resulta cuasi-diagonal y la función lagrangiana $F(s,\mathbf{u},\mathbf{e})$, definida en (2), resulta

$$\begin{aligned} F\,(s, \mathbf{u}, \mathbf{e}) &= \frac{1}{2}\ \mathbf{e}^T \mathbf{D}_{11}\,\mathbf{e} - \mathbf{u}^T \mathbf{Q} \\[2mm] &= \frac{1}{2}\left[\, EA\varepsilon_s^2 + GA\,(\gamma_{sy}^2 + \gamma_{sz}^2) + G\bar{I}_0\kappa_s^2 + E\bar{I}_y\kappa_y^2 \right.\\[2mm] &\left. - 2E\bar{I}_{yz}\kappa_y\,\kappa_z + E\bar{I}_z\kappa_z^2 \,\right] - (uq_s + vq_y + wq_z + \theta_s m_s + \theta_y m_y + \theta_z m_z) \end{aligned} \tag{12}$$

En esta expresión cada sumando corresponde a un modo de deformación del modelo (extensión, cortante, torsión y flexión), y su simple observación nos indica de forma inmediata que, en general, las flexiones están acopladas, salvo que se cancele el coeficiente $\bar{I}_{yz}$.

Hablemos ahora de vigas y arcos. *A priori*, la simple orientación de la pieza de directriz plana en el espacio parece sugerir la clasificación indicada en el título de esta sección: denominaríamos *viga curva* a aquel elemento simple cuya directriz $\Gamma\,(s)$ reside en el plano horizontal y reservaríamos el término *arco* para el caso complementario, cuando el plano de la curva directriz es vertical. Sin embargo, esto no es suficiente. Para que tenga sentido distinguir entre la respuesta de arco y la de viga curva es necesario que cada una se pueda determinar por separado, y ello depende no solo de la posición espacial de la pieza, sino también de la forma de la sección transversal. Para evaluar la influencia de esta, conviene considerar conjuntamente la fórmula de las deformaciones generalizadas (1) y la estructura
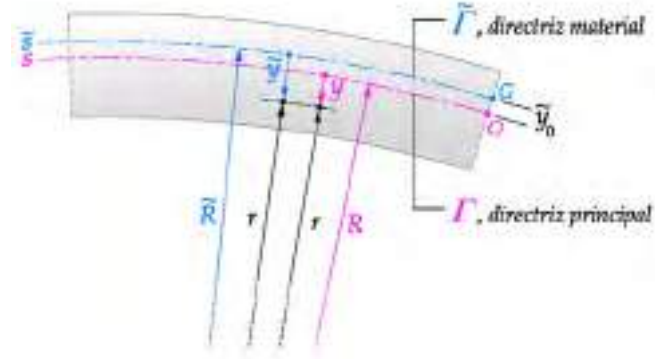
Figura 2. Sistemas de referencia material y principal de la pieza curva con directriz plana, sección por el plano osculador ($z = 0$).

de la densidad lineal de energía potencial del modelo, Ecuación (12), recordando que ambas corresponden al *MVS* y la última está asociada a la parametrización principal. Se puede observar como las componentes ε_s, γ_{sy} y κ_z son funciones lineales de los desplazamientos generalizados $\{u,v,\theta_z\}$ que se desarrollan en el plano de la directriz, mientras que γ_{sz}, κ_s y κ_y lo son de $\{w,\theta_s,\theta_y\}$, desplazamientos transversales a este plano. En consecuencia, para que el comportamiento arco se desacople de la respuesta de viga bastará que $\bar{I}_{yz}=0$, obteniendo entonces que la densidad lineal de energía potencial del arco resulta

$$\begin{aligned} F\,(s, \mathbf{u}, \mathbf{e}) &= \frac{1}{2}\ \left(EA\varepsilon_s^2 + GA\gamma_{sy}^2 + E\bar{I}_z\kappa_z^2\right) \\[2mm] &- (uq_s + vq_y + \theta_z m_z) \end{aligned} \tag{13}$$

mientras que la correspondiente a la viga curva valdrá

$$\begin{aligned} F\,(s, \mathbf{u}, \mathbf{e}) &= \frac{1}{2}\ \left(GA\gamma_{sz}^2 + G\bar{I}_0\kappa_s^2 + E\bar{I}_y\kappa_y^2\right) \\[2mm] &- (wq_z + \theta_s m_s + \theta_y m_y) \end{aligned} \tag{14}$$

La condición de desacoplamiento anterior se satisface sistemáticamente si la sección transversal de la pieza es simétrica respecto al plano $z=0$, plano osculador de la curva $\Gamma(s)$, que la contiene.

3.
LA VIGA CURVA

En este apartado nos proponemos establecer las ecuaciones que gobiernan la respuesta de una pieza de directriz plana y sección transversal simétrica respecto al plano osculador de la directriz, restringiéndonos al caso de la viga curva y teniendo en cuenta el alabeo torsional. Así pues, los grados de libertad a considerar serán $\{w,\theta_s,\theta_y,\varphi\}$, donde al desplazamiento w y los giros θ_s y θ_y propios del *MVS* se ha añadido la *intensidad de alabeo* φ. La Figura 3 muestra este tipo de pieza, así como los desplazamientos generalizados y los esfuerzos consistentes, correspondientes al *MVS*; no aparecen, pues, los desplazamientos generalizados y esfuerzos relacionados con el alabeo, de difícil representación gráfica.
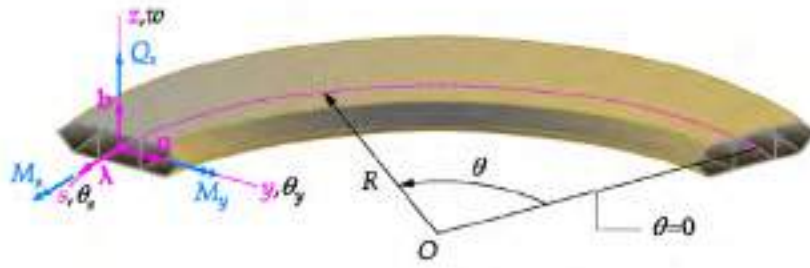
Figura 3. Sistema de referencia intrínseco, desplazamientos y esfuerzos generalizados de una viga circular.

3.1 Deducción de las ecuaciones que gobiernan el problema

En el marco de la *UBT*, la hipótesis cinemática se expresa a través de la matriz $\mathbf{h}(y,z)$ [22, pág. 25] mediante

$$\mathbf{d}^*(s, y, z) = \mathbf{h}(y, z)\, \mathbf{u}(s) \tag{15}$$

que, en nuestro caso, se desarrolla en componentes como

$$\begin{Bmatrix} u^*(s,y,z) \\ v^*(s,y,z) \\ w^*(s,y,z) \end{Bmatrix} = \begin{bmatrix} 0 & 0 & z & \hat{\omega}(y,z) \\ 0 & -\hat{z} & 0 & 0 \\ 1 & \hat{y} & 0 & 0 \end{bmatrix} \begin{Bmatrix} w(s) \\ \theta_s(s) \\ \theta_y(s) \\ \varphi(s) \end{Bmatrix} \tag{16}$$

siendo $\hat{\omega}(y,z)$ el alabeo unitario de la sección transversal, $\varphi(s)$ la intensidad de alabeo, (y_C, z_C) las coordenadas del centro de esfuerzos cortantes –nótese que $z_C = 0$ por la condición de simetría de la sección– e $\hat{y} = y - y_C$ y $\hat{z} = z - z_C$. Con estas últimas relaciones, todos los elementos del operador $\mathbf{h}(y,z)$ quedan referidos al *sistema principal* de la pieza mientras que los desplazamientos debidos a la rotación de eje longitudinal tienen su polo en el centro de esfuerzos cortantes.

En cuanto a estática, para la viga curva tendremos [22, fórmula (2.24)]

$$\mathbf{f}(s) = \int_A \mathbf{h}^{\mathrm{T}} \mathbf{t}^* dA = \int_A \begin{bmatrix} 0 & 0 & 1 \\ 0 & -\hat{z} & y \\ z & 0 & 0 \\ \hat{\omega}(y,z) & 0 & 0 \end{bmatrix} \begin{Bmatrix} \sigma_s^* \\ \tau_{sy}^* \\ \tau_{sz}^* \end{Bmatrix} dA = \begin{Bmatrix} Q_z \\ M_s \\ M_y \\ B_{\hat{\omega}} \end{Bmatrix} \tag{17}$$

que muestra como el vector de esfuerzos $\mathbf{f}(s)$ incluye las componentes de esfuerzos de flexión estándar, cortante y momento flector

$$Q_z = \int_A \tau_{sz}^* dA \quad , \quad M_y = \int_A z \sigma_s^* dA \tag{18.a}$$

y las propias de la torsión, momento torsor y bimomento, ambas referidas al centro de esfuerzos cortantes, que actúa como polo de la torsión

$$M_s = \int_A (\hat{y}\tau_{sz}^* - \hat{z}\tau_{sy}^*) dA = \int_A (\hat{y}\tau_{sz}^* - \hat{z}\tau_{sy}^*) dA - y_C Q_z \quad ,$$

$$B_{\hat{\omega}} = \int_A \hat{\omega}(y,z) \sigma_s^* dA \tag{18.b}$$

El sistema de ecuaciones diferenciales que gobierna la respuesta de la viga curva [22, ecuaciones 2.42] depende de la matriz de equilibrio $\mathbf{H}$, la matriz de acoplamiento $\hat{\mathbf{D}}_{00}$ y el operador constitutivo $\mathbf{D}_{11}$. Para establecer las matrices $\mathbf{H}$ y $\hat{\mathbf{D}}_{00}$ se requiere conocer los operadores $\mathbf{D}_{00}$, $\mathbf{D}_{01}$ y $\mathbf{D}_{11}$. [22, página 34] que quedan definidos en [22, ecuación 2.34]. A continuación procedemos a obtenerlos. Para ello se parte de los resultados generales para el cálculo de las matrices de deformación del sólido [22, ecuación (2.13)]

$$\varepsilon_s^* = \frac{1}{\mu} (u_{,s}^* - \chi v^*) \quad \Bigg\}$$

$$\gamma_{sy}^* = u_{,y}^* + \frac{1}{\mu} (v_{,s}^* + \chi u^*) \quad \Bigg\} \tag{19}$$

$$\gamma_{sz}^* = u_{,z}^* + \frac{1}{\mu} w_{,s}^*)$$

Llevando las expresiones de la Ecuación (16) a estas fórmulas se obtiene

$$\varepsilon_s^* = \frac{1}{\mu} [z(\theta_y' + \chi \theta_s) + \hat{\omega}\varphi'] \quad \Bigg\}$$

$$\gamma_{sy}^* = \frac{1}{\mu} [z(\chi\theta_y - \theta_s') + (\chi\hat{\omega} + \mu\hat{\omega}_{,y})\varphi] \quad \Bigg\} \tag{20}$$

$$\gamma_{sz}^* = \frac{1}{\mu} (w' + \mu\theta_y + \hat{y}\theta_s' + \mu\hat{\omega}_{,z}\varphi)$$

La matrices de deformación $\mathbf{B}_0$ y $\mathbf{B}_1$, que intervienen en el cálculo de $\mathbf{D}_{00}$, $\mathbf{D}_{01}$ y $\mathbf{D}_{11}$, resultan de factorizar las deformaciones anteriores, componentes del vector $\mathbf{e}^*(s,y,z)$, en $\mathbf{u}(s)$ y $\mathbf{u}'(s)$ [22, ecuación 2.12]

$$\mathbf{B}_0 = \frac{1}{\mu} \begin{bmatrix} 0 & \chi z & 0 & 0 \\ 0 & 0 & \chi z & \chi\hat{\omega} + \mu\hat{\omega}_{,y} \\ 0 & 0 & 0 & \mu\hat{\omega}_{,z} \end{bmatrix} \Bigg\}$$

$$\mathbf{B}_1 = \frac{1}{\mu} \begin{bmatrix} 0 & 0 & z & \hat{\omega} \\ 0 & -z & 0 & 0 \\ 0 & \hat{y} & 0 & 0 \end{bmatrix} \equiv \frac{1}{\mu} \mathbf{h} \Bigg\} \tag{21}$$

Los operadores constitutivos $\mathbf{D}_{rs}$ se definen mediante la expresión (2.34) de [22]. El primero de ellos, $\mathbf{D}_{00}$, resulta

$$\mathbf{D}_{00} = \int_A \mathbf{B}_0^T \mathbf{C} \mathbf{B}_0 \, \mu \, dA$$

$$= \int_A \begin{bmatrix} 0 & 0 & 0 & 0 \\ 0 & \chi^2 E z^2 & 0 & 0 \\ 0 & 0 & G(\chi^2 z^2 + \mu^2) & G[\chi z(\chi\hat{\omega} + \mu\hat{\omega}_{,y}) + \mu^2 \hat{\omega}_{,z}] \\ 0 & 0 & G[\chi z(\chi\hat{\omega} + \mu\hat{\omega}_{,y}) + \mu^2 \hat{\omega}_{,z}] & G[(\chi\hat{\omega} + \mu\hat{\omega}_{,y})^2 + (\mu\hat{\omega}_{,z})^2] \end{bmatrix} \frac{dA}{\mu}$$

$$= \begin{bmatrix} 0 & 0 & 0 & 0 \\ 0 & \chi^2 E \bar{I}_y & 0 & 0 \\ 0 & 0 & GA + \chi^2 G\bar{I}_0 & y_C GA + \chi(GW_0 + G\bar{I}_z) + \chi^2 G\bar{I}_{y\hat{\omega}} \\ 0 & 0 & y_C GA + \chi(GW_0 + G\bar{I}_z) + \chi^2 G\bar{I}_{y\hat{\omega}} & G\hat{W} + \chi G\hat{\Omega} + \chi^2 G\bar{I}_{y\hat{\omega}} \end{bmatrix}$$

(22)

donde se han introducido las constantes estáticas

$$\bar{I}_0 = \bar{I}_y + \bar{I}_z \quad con \quad \bar{I}_y = \int_A z^2 \frac{dA}{\mu} \quad , \quad \bar{I}_z = \int_A y^2 \frac{dA}{\mu}$$

$$\bar{I}_{\hat{\omega}} = \int_A \hat{\omega}^2 \frac{dA}{\mu} \quad , \quad \bar{I}_{y\hat{\omega}} = \int_A z\hat{\omega} \frac{dA}{\mu}$$

$$\hat{W} = \int_A [(\hat{\omega}_{,y})^2 + (\hat{\omega}_{,z})^2] \, dA = \int_A (\hat{z}\hat{\omega}_{,y} - \hat{y}\hat{\omega}_{,z}) \, dA$$

$$\hat{\Omega} = \int_A \{(\hat{\omega}^2)_{,y} - y[(\hat{\omega}_{,y})^2 + (\hat{\omega}_{,z})^2]\} \, dA$$

(23)

junto con

$$W_0 = \int_A (z\hat{\omega}_{,y} - y\hat{\omega}_{,z}) \, dA$$

$$= \hat{W} - (y_C^2 + z_C^2) A - \chi(y_C \bar{I}_z + z_C \bar{I}_{yz})$$

$$= \hat{W} - y_C (y_C A + \chi \bar{I}_z)$$

(24)

Análogamente, el bloque $\mathbf{D}_{01}$ es

$$\mathbf{D}_{01} = \int_A \mathbf{B}_0^T \mathbf{C} \mathbf{B}_1 \, \mu \, dA$$

$$= \int_A \begin{bmatrix} 0 & 0 & 0 & 0 \\ 0 & 0 & \chi E z^2 & \chi E z \hat{\omega} \\ G\mu & G(\mu\hat{y} - \chi z^2) & 0 & 0 \\ G\mu\hat{\omega}_{,z} & G[\mu\hat{y}\hat{\omega}_{,z} - z(\chi\hat{\omega} + \mu\hat{\omega}_{,y})] & 0 & 0 \end{bmatrix} \frac{dA}{\mu}$$

(25)

$$= \begin{bmatrix} 0 & 0 & 0 & 0 \\ 0 & 0 & \chi E \bar{I}_y & \chi E \bar{I}_{y\hat{\omega}} \\ GA & -(y_C GA) + \chi G\bar{I}_0 & 0 & 0 \\ y_C GA + \chi G\bar{I}_z & -(G\hat{W} + \chi G\bar{I}_{y\hat{\omega}}) & 0 & 0 \end{bmatrix}$$

Este resultado se ha obtenido teniendo en cuenta la siguiente propiedad del alabeo unitario (para el tipo de secciones considerado)

$$\int_A \hat{\omega}_{,y} \, dA = \int_A \hat{z} \, dA = \int_A (z - z_C) \, dA$$

$$= \int_A z \, dA - z_C A = \int_A (1 - \chi y) z \frac{dA}{\mu} = 0$$

$$\int_A \hat{\omega}_{,z} \, dA = -\int_A \hat{y} \, dA = -\int_A (y - y_C) \, dA$$

$$= y_C A - \int_A y \, dA = y_C A - \int_A (1 - \chi y) y \frac{dA}{\mu}$$

$$= y_C A + \chi \bar{I}_z$$

(26)

Finalmente, el bloque constitutivo $\mathbf{D}_{11}$ vale

$$\mathbf{D}_{11} = \int_A \mathbf{B}_1^T \mathbf{C} \mathbf{B}_1 \, \mu \, dA$$

$$= \int_A \begin{bmatrix} G & G\hat{y} & 0 & 0 \\ G\hat{y} & G(\hat{y}^2 - z^2) & 0 & 0 \\ 0 & 0 & E z^2 & E z \hat{\omega} \\ 0 & 0 & E z \hat{\omega} & E \hat{\omega}^2 \end{bmatrix} \frac{dA}{\mu}$$

(27)

$$= \begin{bmatrix} GA & -y_C GA & 0 & 0 \\ -y_C GA & G\bar{I}_0 + y_C^2 GA & 0 & 0 \\ 0 & 0 & E\bar{I}_y & E\bar{I}_{y\hat{\omega}} \\ 0 & 0 & E\bar{I}_{y\hat{\omega}} & E\bar{I}_{\hat{\omega}} \end{bmatrix}$$

Con los resultados anteriores, estamos en condiciones de calcular la matriz de equilibrio de la viga curva, [22, página 34], igual a

$$\mathbf{H} = \mathbf{D}_{01} \mathbf{D}_{11}^{-1}$$

(28)

obteniendo sucesivamente

$$\mathbf{D}_{11}^{-1} = \begin{bmatrix} \dfrac{1}{GA} + \dfrac{y_C^2}{GA} & \dfrac{y_C}{G\bar{I}_0} & 0 & 0 \\[2mm] \dfrac{y_C}{G\bar{I}_0} & \dfrac{1}{G\bar{I}_0} & 0 & 0 \\[2mm] 0 & 0 & \dfrac{1}{(1-\varepsilon)E\bar{I}_y} & \dfrac{1}{(1-\varepsilon)E\bar{I}_{y\hat{\omega}}} \\[2mm] 0 & 0 & \dfrac{1}{(1-\varepsilon)E\bar{I}_{y\hat{\omega}}} & \dfrac{1}{(1-\varepsilon)E\bar{I}_{\hat{\omega}}} \end{bmatrix}$$

(29)

donde $\varepsilon = \bar{I}_{y\acute{\omega}}^2 / \bar{I}_y \bar{I}_{\acute{\omega}}$, y

$$\mathbf{H} = \mathbf{D}_{01}\,\mathbf{D}_{11}^{-1} = \begin{bmatrix} 0 & 0 & 0 & 0 \\ 0 & 0 & \chi & 0 \\ 1-\chi y_C & -\chi & 0 & 0 \\ y_C^\ast & -\kappa_0^\ast & 0 & 0 \end{bmatrix} \tag{30}$$

con unos nuevos parámetros estáticos $y_C^\ast$, κ_0 y $\kappa_0^\ast$ definidos a continuación. El primero de ellos tiene dimensión de longitud mientras que los restantes son adimensionales.

$$\left. \begin{array}{l} y_C^\ast = (1-\kappa_0^\ast)\,y_C + \chi \bar{r}_z^2 \\[2mm] \kappa_0 = \dfrac{W_0}{\bar{I}_0} \quad,\quad \kappa_0^\ast = \dfrac{W_0 + \chi \bar{I}_{y\acute{\omega}}}{\bar{I}_0} \quad,\quad \bar{r}_z = \sqrt{\dfrac{\bar{I}_z}{A}} \end{array} \right\} \tag{31}$$

En cuanto a la matriz de acoplamiento [22, página 34], esta adopta el siguiente valor

$$\hat{\mathbf{D}}_{00} = \mathbf{D}_{00} - \mathbf{D}_{01}\,\mathbf{D}_{11}^{-1}\,\mathbf{D}_{10}$$

$$= \begin{bmatrix} 0 & 0 & 0 & 0 \\ 0 & 0 & 0 & 0 \\ 0 & 0 & 0 & 0 \\ 0 & 0 & 0 & (1-\kappa_0^\ast)G\hat{W} - y_C\,y_C^\ast\,GA + \chi G[\hat{\Omega} - (y_C^\ast \bar{I}_z + \kappa_0^\ast \bar{I}_{y\acute{\omega}})] + \chi^2\,G\bar{I}_{\acute{\omega}} \end{bmatrix} \tag{32}$$

que, de manera más compacta, escribiremos

$$\hat{\mathbf{D}}_{00} = \begin{bmatrix} 0 & 0 & 0 & 0 \\ 0 & 0 & 0 & 0 \\ 0 & 0 & 0 & 0 \\ 0 & 0 & 0 & \kappa_0^\ast GJ^\ast \end{bmatrix} \tag{33}$$

donde el valor de $J^\ast$ se deduce de la simple comparación de ambas expresiones.

Nos interesaremos a continuación por las deformaciones generalizadas $\mathbf{e}(s)$ consistentes con los esfuerzos $\mathbf{f}(s)$ presentados y evaluados estáticamente en la Ecuación (17). En la formulación general [22, página 36], estas se definen como $\mathbf{e}(s) = \mathbf{H}^T\mathbf{u} + \mathbf{u}'$ y aplicando ahora el resultado obtenido para la matriz de equilibrio –Ecuación (30)–, se llega a un conjunto de expresiones compactas para sus cuatro componentes

$$\mathbf{e}(s) = \mathbf{H}^T\mathbf{u} + \mathbf{u}'$$

$$= \begin{bmatrix} 0 & 0 & 1-\chi y_C & y_C^\ast \\ 0 & 0 & -\chi & -\kappa_0^\ast \\ 0 & \chi & 0 & 0 \\ 0 & 0 & 0 & 0 \end{bmatrix} \begin{Bmatrix} \omega \\ \theta_s \\ \theta_y \\ \varphi \end{Bmatrix} + \begin{Bmatrix} \omega' \\ \theta_s' \\ \theta_y' \\ \varphi' \end{Bmatrix} \tag{34}$$

Por lo tanto

$$\mathbf{e}(s) = \begin{Bmatrix} \gamma_{sz} \\ \kappa_s \\ \kappa_y \\ \varphi' \end{Bmatrix} = \begin{Bmatrix} w' + (1-\chi y_C)\,\theta_y + y_C^\ast\,\varphi \\ \theta_s' - \chi\theta_y - \kappa_0^\ast\,\varphi \\ \theta_y' + \chi\,\theta_s \\ \varphi' \end{Bmatrix} \tag{35}$$

Con todo ello, los esfuerzos $\mathbf{f}(s)$ se pueden expresar como [22, ecuación 2.51]

$$\mathbf{f}(s) = \mathbf{D}_{11}\,\mathbf{e}(s)$$

$$= \begin{bmatrix} GA & -y_C GA & 0 & 0 \\ -y_C GA & G\bar{I}_0 + y_C^2 GA & 0 & 0 \\ 0 & 0 & E\bar{I}_y & E\bar{I}_{y\acute{\omega}} \\ 0 & 0 & E\bar{I}_{y\acute{\omega}} & E\bar{I}_{\acute{\omega}} \end{bmatrix} \begin{Bmatrix} \gamma_{sz} \\ \kappa_s \\ \kappa_y \\ \varphi' \end{Bmatrix} = \begin{Bmatrix} Q_z \\ M_s \\ M_y \\ B_\omega \end{Bmatrix} \tag{36}$$

Estas relaciones exhiben el acoplamiento constitutivo existente entre flexión y torsión, que afecta tanto al cortante Q_z y al momento torsor M_s como al momento flector M_y y al bimomento B_ω, los primeros producidos por las tensiones tangenciales $\tau_{sy}^\ast, \tau_{sz}^\ast$ y estos últimos debidos a las tensiones normales $\sigma_s^\ast$ —ver definiciones estáticas (18)—. Finalmente, la densidad lineal de energía potencial de la viga curva vale [22, tabla II.1]

$$F(s, \mathbf{u}, \mathbf{e}) = \frac{1}{2}\,(\mathbf{e}^T\mathbf{D}_{11}\mathbf{e} + \mathbf{u}^T\hat{\mathbf{D}}_{00}\mathbf{u}) - \mathbf{u}^T\mathbf{Q}$$

$$= \frac{1}{2}\Big[GA\gamma_{sz}^2 - 2y_C GA\gamma_{sz} k_s + G\bar{I}_c k_s^2 + E\bar{I}_y k_y^2$$

$$+2E\bar{I}_{y\acute{\omega}}\,k_y\,\varphi' + E\bar{I}_{\acute{\omega}}\,(\varphi')^2 + \kappa_0^\ast GJ^\ast\dot{\varphi}^2 \Big]$$

$$- (wq_z + \theta_s m_z + \theta_y m_y + b_{\acute{\omega}}\,\varphi) \tag{37}$$

donde el vector $\mathbf{Q}(s) = \{q_z, m_s, m_y, b_\omega\}^T$ recoge las densidades lineales de cargas generalizadas distribuidas a lo largo del modelo, e $\bar{I}_C = \bar{I}_0 + y_C^2 A$.

En la formulación lineal del problema, las ecuaciones que gobiernan el equilibrio de una viga curva de directriz plana adoptan la forma siguiente [22, ecuación (2.42)]

$$\mathbf{E}'(s) = \mathbf{W}(s)\,\mathbf{E}(s) - \mathbf{F}(s) \tag{38}$$

o bien

$$\begin{Bmatrix} \mathbf{u}'(s) \\ \mathbf{f}'(s) \end{Bmatrix} = \begin{bmatrix} -\mathbf{H}^T & \mathbf{D}_{11}^{-1} \\ \hat{\mathbf{D}}_{00} & \mathbf{H} \end{bmatrix} \begin{Bmatrix} \mathbf{u}(s) \\ \mathbf{f}(s) \end{Bmatrix} - \begin{Bmatrix} \mathbf{0} \\ \mathbf{Q}(s) \end{Bmatrix} \tag{39}$$

Llevando a esta fórmula la composición de las matrices de equilibrio $\mathbf{H}(s)$ y de acoplamiento $\hat{\mathbf{D}}_{00}(s)$, se consigue una es-

critura simple del operador $\mathbf{W}(s)$, válida para analizar de forma exacta el equilibrio de vigas curvas de directriz plana $\Gamma(s)$ con forma arbitraria y sección transversal simétrica respecto al plano que contiene a $\Gamma(s)$. Esta es la siguiente

$$\mathbf{W}(s) = \begin{bmatrix} 0 & 0 & \chi y_C+1 & -y_C^* & \dfrac{1}{GA}+\dfrac{y_C^{*2}}{G\bar{I}_0} & \dfrac{y_C^*}{G\bar{I}_0} & 0 & 0 \\[2.5ex] 0 & 0 & \chi & \kappa_0^* & \dfrac{y_C^*}{G\bar{I}_0} & \dfrac{1}{G\bar{I}_0} & 0 & 0 \\[2.5ex] 0 & -\chi & 0 & 0 & 0 & 0 & \dfrac{1}{(1-\varepsilon)E\bar{I}_y} & \dfrac{1}{(1-\varepsilon)E\bar{I}_{y\dot\omega}} \\[2.5ex] 0 & 0 & 0 & 0 & 0 & 0 & \dfrac{1}{(1-\varepsilon)E\bar{I}_{y\dot\omega}} & \dfrac{1}{(1-\varepsilon)E\bar{I}_{\dot\omega}} \\[2.5ex] 0 & 0 & 0 & 0 & 0 & 0 & 0 & 0 \\[2.5ex] 0 & 0 & 0 & 0 & 0 & 0 & \chi & 0 \\[2.5ex] 0 & 0 & 0 & 0 & 1-\chi y_C & -\chi & 0 & 0 \\[2.5ex] 0 & 0 & 0 & \kappa_0^* GJ^* & y_C^* & -\kappa_0^* & 0 & 0 \end{bmatrix} \tag{40}$$

Así pues, las ecuaciones diferenciales del problema son

$$\left.\begin{aligned} \frac{dw}{ds} &= -(1-\chi y_C)\,\theta_y - y_C^*\varphi + \frac{Q_z}{GA} + y_C\,\frac{M_s+y_C Q_z}{G\bar{I}_0} \\[1.5ex] \frac{d\theta_s}{ds} &= \chi\,\theta_y + \kappa_0^*\varphi + \frac{M_s+y_C Q_z}{G\bar{I}_0} \\[1.5ex] \frac{d\theta_y}{ds} &= -\chi\,\theta_s + \frac{1}{1-\varepsilon}\left(\frac{M_y}{E\bar{I}_y} - \varepsilon\,\frac{B_{\dot\omega}}{E\bar{I}_{y\dot\omega}}\right) \\[1.5ex] \frac{d\varphi}{ds} &= \frac{1}{1-\varepsilon}\left(\frac{B_{\dot\omega}}{E\bar{I}_{\dot\omega}} - \varepsilon\,\frac{M_y}{E\bar{I}_{y\dot\omega}}\right) \\[1.5ex] \frac{dQ_z}{ds} &= -q_z \\[1.5ex] \frac{dM_s}{ds} &= \chi M_y - m_s \\[1.5ex] \frac{dM_y}{ds} &= (1-\chi y_C)Q_z - \chi M_s - m_y \\[1.5ex] \frac{dB_{\dot\omega}}{ds} &= \kappa_0^* GJ^*\varphi + y_C^* Q_z - \kappa_0^* M_s - b_{\dot\omega} \end{aligned}\right\} \tag{41}$$

3.2 Descomposición del momento torsor. Esbeltez de torsión

Resulta oportuno analizar la estructura del momento torsor M_s. Para ello, volvamos a la última ecuación del sistema (41) y sobre ella definamos el *bicortante* como

$$M_{\dot\omega} = -(B_{\dot\omega}' + b_{\dot\omega}) = \kappa_0^*(M_s - GJ^*\varphi) - y_C^* Q_z \tag{42}$$

Es sencillo comprobar, a partir de la fórmula (36) y las definiciones de γ_{sz} y κ_s facilitadas en (35), que

$$\frac{\partial F}{\partial \varphi} = B_{\dot\omega}' = -(M_{\dot\omega} + b_{\dot\omega}) \tag{43}$$

Ahora sumemos y restemos el momento torsor M_s al miembro de la derecha de la Ecuación (42)

$$M_{\dot\omega} = (\kappa_0^* - 1)\,M_s + M_s - \kappa_0^* GJ^*\varphi - y_C^* Q_z \tag{44}$$

reordenemos esta expresión para obtener

$$M_s = (1 - \kappa_0^*)\,M_s + M_{\dot\omega} + \kappa_0^* GJ^*\varphi - y_C^* Q_z \tag{45}$$

a continuación, sustituyamos y_C^* por su definición (31) y hagamos uso de las expresiones constitutivas de Q_z y M_s para llegar a

$$\begin{aligned} M_s &= (1-\kappa_0^*)\,(M_s + y_C Q_z) + M_{\dot\omega} + \kappa_0^* GJ^*\varphi + \chi r_Z^2 Q_z \\[1ex] &= (1-\kappa_0^*)\,G\bar{I}_0\kappa_s + M_{\dot\omega} + \kappa_0^* GJ^*\varphi + \chi r_Z^2 Q_z \\[1ex] &= (1-\kappa_0^* - J^*/\bar{I}_0)\,G\bar{I}_0\kappa_s + (J^*/\bar{I}_0)\,G\bar{I}_0\kappa_s \\[1ex] &\quad + M_{\dot\omega} + \kappa_0^* GJ^*\varphi + \chi r_Z^2 Q_z \\[1ex] &= (1-\kappa_0^* - J^*/I_0)\,G\bar{I}_0\kappa_s + GJ^*(\kappa_0^*\varphi + \kappa_s) + M_{\dot\omega} + \chi r_Z^2 Q_z \end{aligned} \tag{46}$$

Finalmente, introduciendo la definición de κ_s en el tercer sumando del miembro de la derecha se obtiene

$$M_s = GJ^*(\theta_s' - \chi\theta_y) + M_{\dot\omega} + (1-\kappa_0^* - J^*/\bar{I}_0)\,G\bar{I}_0\kappa_s - \chi r_Z^2 Q_z \tag{47}$$

Se comprueba de forma inmediata que esta ecuación, particularizada al caso de directriz recta, muestra cómo el momento torsor se divide en la fracción de Saint-Venant –primer sumando del término de la derecha– y el bicortante o momento torsor de alabeo –segundo sumando de la derecha–, como es característico en la torsión mixta de vigas rectas. A su vez, la curvatura introduce unas correcciones en las medidas propias de la torsión, M_s y θ_s, que se ven afectadas por los efectos de la flexión a través de las funciones Q_z y θ_y. El último sumando se cancela exactamente cuando la curvatura χ es nula.

En el caso de vigas de sección y curvatura constantes, el operador fundamental principal del sistema autónomo de ecuaciones diferenciales ordinarias asociado a **W**, que gobierna la solución general del problema de valores iniciales determinado por la ecuación de equilibrio $\mathbf{E}'(s)=\mathbf{W}\mathbf{E}(s)-\mathbf{F}(s)$ y $\mathbf{E}|_{s=0}=\mathbf{E}_0$, es

$$\mathbf{G}(s)=\exp\left[s\mathbf{W}\right] \tag{48}$$

El resultado del cálculo explícito del mismo *para torsión sin alabeo* (basta prescindir de la intensidad de alabeo φ en toda la formulación) así como la obtención de soluciones cerradas para los problemas de contorno o la expresión de la matriz de rigidez de esta misma pieza pueden consultarse en [22, páginas 119 a 121].

Volviendo al caso general de la viga curva con alabeo torsional, si admitimos que tiene sección transversal y curvatura constantes, el cálculo de los autovalores del operador **W** obtenido en (40) conduce a la ecuación característica siguiente

$$|\mathbf{W}-K\mathbf{I}|=K^2(K^2+\chi^2)^2\left[K^2-\frac{\kappa_0^*GJ^*}{(1-\varepsilon)E\bar{I}_{\acute{o}}}\right] \tag{49}$$

cuyos resultados son las raíces $K=0$ con multiplicidad dos, $K=\pm i\chi$, ambas también con multiplicidad dos, y $K=\pm\lambda_0/L$, siendo λ_0 un parámetro definido como

$$\lambda_0=L\sqrt{\frac{\kappa_0^*}{1-\varepsilon}\frac{GJ^*}{E\bar{I}_{\acute{o}}}} \tag{50}$$

al que denominaremos *esbeltez torsional*.

4.
RESULTADOS

4.1 Resultados que dependen de la sección transversal

El primer paso en el análisis de una viga curva consiste en la determinación del eje principal y de las características geométricas de la sección definidas en las expresiones (23); ambos procesos requieren realizar una serie de cálculos sobre la sección transversal.

En este ámbito, el primer paso es definir el alabeo unitario. En este trabajo hemos optado por utilizar como tal a la función de alabeo que resuelve el problema de torsión de Saint-Venant, que debe cumplir la ecuación de Laplace con condiciones de contorno de Neumann [23, ecuaciones 139 y 140]. Para hallarla hemos utilizado el programa *FlexPDE*, que facilita tanto la resolución de problemas de este estilo como la evaluación de integrales sobre su dominio de definición, dependan o no de la solución del problema. Con los medios de cálculo actuales, no tiene sentido recurrir a expresiones que aproximen dicha función de alabeo, porque los procedimientos para establecerlas [24, página 252 y s.s.] pueden resultar tan laboriosos o más que su determinación por el método de los elementos finitos. De hecho, el código de *FlexPDE* utilizado apenas ocupa un par de páginas y su ejecución dura menos de un segundo (Con *FlexPDE 6.36s*, en un ordenador con proce-

sador *Intel i7-6700* a 3.40 GHz dotado de sistema operativo *Windows 10 Enterprise*).

Hemos analizado tres secciones, una cerrada, rectangular hueca, de dimensiones exteriores 50×25 cm y espesor 1 cm, y dos abiertas, una en U, resultado de eliminar de la anterior el alma izquierda, y otra en I, obtenida trasladando el alma de esta última al eje de simetría de las alas. Las dimensiones de la sección rectangular inicial son similares a las de los tubos estructurales de mayor tamaño que se pueden encontrar en el mercado; además, la proporción entre las dimensiones exteriores es semejante a la de una sección de puente en cajón —excluidas las alas—.

La Figura 4 muestra el alabeo unitario calculado en cada una de ellas, representado con la misma escala cromática en todas. Se observa que, como es bien conocido, este resulta mucho mayor en las secciones abiertas.

A continuación se presentan una serie de gráficas en las que se comparan los parámetros geométricos de estas secciones calculados para diferentes valores del radio de curvatura; se han considerado 14 de ellos, variando entre 2.5 m y 5120 m. En todas las gráficas la escala es lineal en ordenadas y logarítmica en abscisas, y en ellas se representan de color oscuro los resultados de la sección cerrada, con un tono intermedio los de la U y de color más claro los de la doble T.

En primer lugar, se analiza la distancia entre el centro de gravedad de la sección y el polo principal, o lo que es lo mismo, la relación entre el radio de curvatura $\tilde{R}$ del eje material y el radio de curvatura R del eje principal. La Figura 5 muestra el cociente $R/\tilde{R}$ frente a $\tilde{R}$. Se observa que ambos radios son prácticamente iguales en todos los casos. La mayor diferencia, que se da para el menor valor de $\tilde{R}$, es del orden del 5‰; para valores mayores resultan indistinguibles.

Seguidamente se estudian los cocientes entre los momentos de inercia $\bar{I}_y$ e $\bar{I}_z$ de la viga curva, que dependen de la curvatura a través de μ –Ecuación (23)–, y los valores correspondientes $\bar{I}_y$ e $\bar{I}_z$ en una viga recta de la misma sección, donde no interviene este parámetro. También se analiza la relación entre el módulo de alabeo $\bar{I}_{\acute{o}}$ de la viga curva, que depende de la curvatura, y el de la viga recta de igual sección, $\bar{I}_{\acute{o}}$, que no lo hace. La Figura 6 muestra los cocientes entre los momentos de inercia y la Figura 7 los correspondientes a los módulos de alabeo. Ambas agrupan a la izquierda las secciones en cajón y en I, en las que el centro de gravedad y el centro de esfuerzos cortantes coinciden, y presentan a la derecha la sección en U, en la que están separados. En el primer caso los tres parámetros son casi idénticos sea cual sea el radio de curvatura, pues las diferencias apenas alcanzan el 3‰; en el segundo, la diferencia es algo mayor, pero sigue siendo inferior al 1% salvo para el menor de los radios procesados, de solo cinco veces la anchura de la pieza. Así pues, las diferencias son siempre muy pequeñas, y que sean solo muy pequeñas o casi imperceptibles no depende de que la sección sea abierta o cerrada, sino de que el centro de gravedad y el de esfuerzos cortantes estén próximos o alejados.

La Figura 8 muestra los valores del parámetro $\bar{I}_{y\acute{o}}$ para el conjunto de casos estudiado. No se pueden presentar normalizados por el valor correspondiente a la viga recta porque este es nulo. La gráfica muestra claramente que $\bar{I}_{y\acute{o}}$ tiende a cero cuando el radio de curvatura crece, pero los valores son significativos para un amplio rango de curvaturas. Ahora lo que influye en el resultado es que la sección sea abierta o cerrada
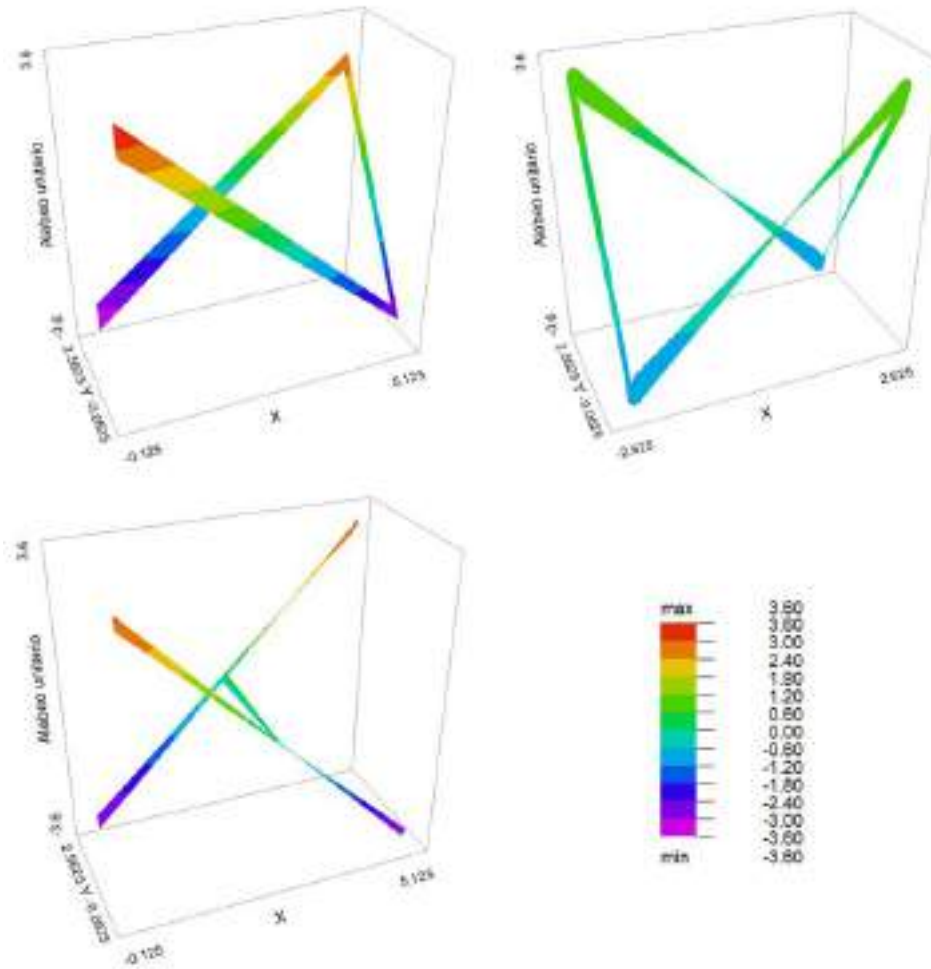
Figura 4. Representación del alabeo unitario en las secciones analizadas.

y no la distancia entre los centros de gravedad y de esfuerzos cortantes. En secciones cerradas el valor absoluto es menor, y el signo cambia respecto al de las secciones abiertas.

El parámetro $\hat{W}$ no depende de la curvatura. Adopta el valor 26 452 cm⁴ en la sección rectangular cerrada, 272 372 cm⁴ en la U y 36 216 cm⁴ en la **I**. Así pues, en él influye más la distancia entre los centros de gravedad y de esfuerzos cortantes que el hecho de ser abierta o cerrada la sección, y su orden de magnitud es mayor cuando dichos puntos están alejados que cuando están próximos.

En cuanto a la constante $\hat{\Omega}$, Figura 9, depende del radio de curvatura y su valor es varios órdenes de magnitud menor en secciones donde el centro de gravedad y el de esfuerzos cortantes están próximos que en aquellas en que están separados. Además, la gráfica $\hat{\Omega} - \tilde{R}$ tiene una asíntota horizontal en ambos casos, pero en el primero corresponde a $\hat{\Omega} = 0$ y en el segundo a un valor finito diferente de cero, del orden de 2 900 000 cm⁵ en nuestro caso. Que las secciones sean abiertas o cerradas no influye en este resultado.

La coordenada y_C del centro de esfuerzos cortantes en la referencia principal, Figura 10, depende de la curvatura y tiende al valor de la coordenada $\tilde{y}_C$ de dicho punto respecto al centro de gravedad en todos los casos. En contraposición a lo que ocurría con los radios R y $\tilde{R}$, las diferencias entre y_C e $\tilde{y}_C$ son
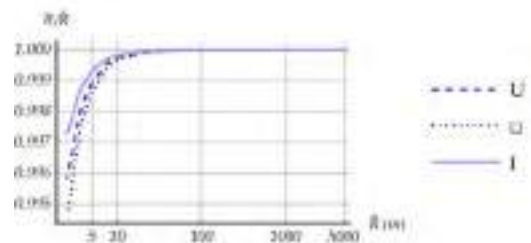
Figura 5. Relación entre el radio de curvatura de la directriz principal y el de la directriz material en los tres tipos de sección estudiados.

más significativas para un rango amplio de radios de curvatura; no obstante, las mayores diferencias, que se dan para radios pequeños, son inferiores al 1% de la anchura de la sección en los casos en que los centros de gravedad y de esfuerzos cortantes coinciden, y del orden de 2.3% de $\tilde{y}_C$ cuando no lo hacen.

Por último, en la Figura 11 se presenta la comparación del parámetro J^* con el módulo de torsión J, con el que está claramente relacionado. En el caso de la sección cerrada el cociente entre ambos es inferior al 0.8‰ para cualquier curvatura. En el de las secciones abiertas la diferencia es mayor, pero como el
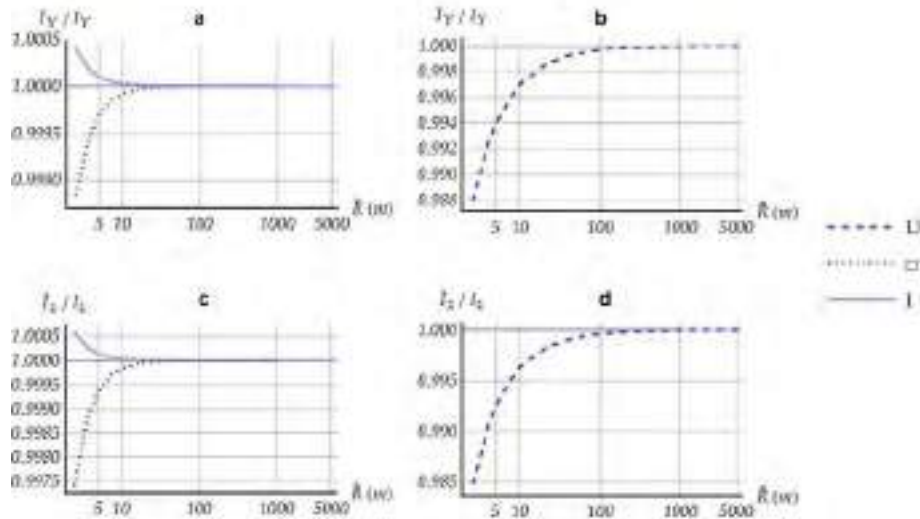
Figura 6. Relación entre los momentos de inercia de la viga curva y los de la viga recta. (a) y (c) secciones en las que el centro de gravedad y el de esfuerzos cortantes coinciden; (b) y (d) sección en la que no lo hacen.
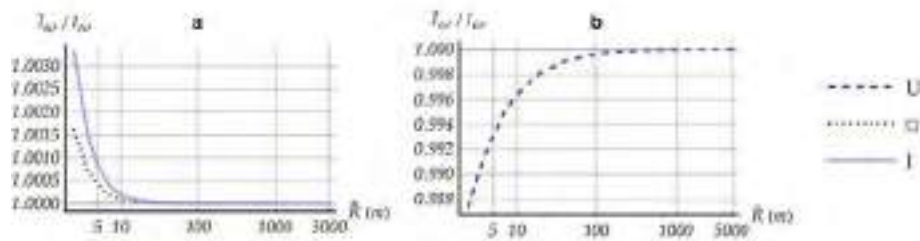
Figura 7. Relación entre el módulo de alabeo de la viga curva y el de la viga recta. (a) secciones en las que el centro de gravedad y el de esfuerzos cortantes coinciden; (b) sección en la que no lo hacen.
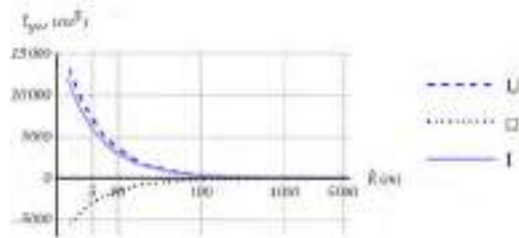
Figura 8. Evolución del valor del parámetro $\bar{I}_{y\omega}$.

módulo de torsión de este tipo de secciones es muy pequeño es razonable pensar que el término J^*, o GJ^*, será despreciable frente a otros términos en las ecuaciones en las que intervenga –fundamentalmente, la última del sistema (41) y la Ecuación (2.23)–.

En resumen, hemos comprobado que el radio de curvatura de la directriz principal puede aproximarse por el de la directriz material en prácticamente todos los casos; que sucede lo mismo con los momentos de inercia y el módulo de alabeo de la viga curva $\bar{I}_y$, $\bar{I}_z$ e $\bar{I}_{y\omega}$ y la viga recta; y que también se puede proceder así con el módulo de torsión J^*, porque las diferencias son despreciables en secciones cerradas y el valor absoluto muy bajo en secciones abiertas. Las similitudes o diferencias en $\hat{\Omega}$ son irrelevantes, puesto que esta constante solo interviene a en la definición de J^*, cuya variación ya se ha comentado.

4.2 Comparación de la esbeltez torsional en vigas de sección abierta y cerrada

En esta sección vamos a comparar el valor de la esbeltez torsional λ_0 para la sección en **U** y para la sección en cajón. Para ello obtenemos los valores de la misma según la Ecuación (50) para distintos valores de la longitud y de la curvatura medida en el centroide. En la Figura 12 se representan los valores de la esbeltez para ambas secciones. Es interesante observar que en la sección abierta los valores de la esbeltez correspondiente a una misma longitud y curvatura son dos órdenes de magnitud inferiores a los valores que corresponden a la sección en cajón. Por ejemplo, si comparamos la esbeltez correspondiente a una viga recta de longitud 10 m, la viga con sección en U tiene una esbeltez $\lambda_0 = 0.21$ y la viga con sección cerrada $\lambda_0 = 10.937$. La viga de sección abierta de mayor longitud y curvatura (30 m, 1/10 m^{-1}) tiene una esbeltez torsional $\lambda_0 = 8.081$, y la viga de sección cerrada más larga y curva (2 m, 1/2.5 m^{-1}) $\lambda_0 = 22.004$, a pesar de ser 15 veces más corta. Por otra parte, los valores de la esbeltez son bastante insensibles a la curvatura, especialmente en el caso de la sección en cajón.

4.3 Desplazamientos generalizados y esfuerzos para distintas curvaturas

Ahora vamos a presentar grupos de soluciones del sistema de ecuaciones (41) para las dos secciones consideradas. Para ello
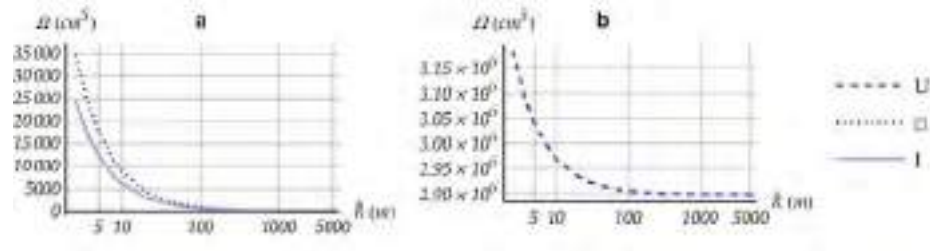
Figura 9. Evolución del valor del parámetro $\hat{\Omega}$. (a) secciones en las que el centro de gravedad y el de esfuerzos cortantes coinciden; (b) sección en la que no lo hacen.
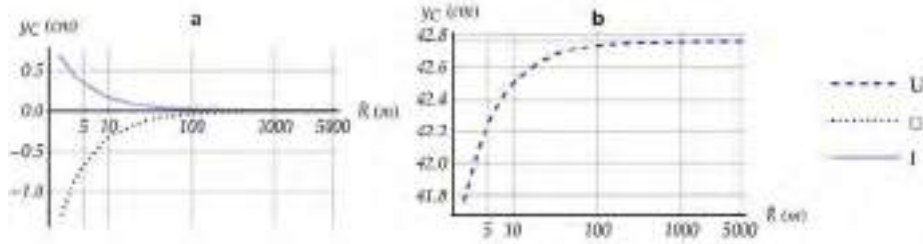
Figura 10. Evolución del valor de y_C, coordenada del centro de esfuerzos cortantes respecto al polo principal.
(a) secciones en las que el centro de gravedad y el de esfuerzos cortantes coinciden; (b) sección en la que no lo hacen.
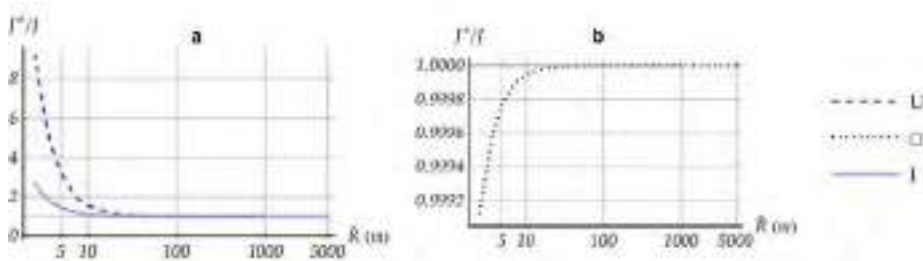
Figura 11. Comparación del parámetro J^* con el módulo de torsión J. (a) secciones abiertas; (b) sección cerrada.

planteamos la solución del problema genérico de una viga curva de longitud l dada y curvatura χ variable, empotrada en ambos extremos. El empotramiento considerado implica que todos los grados de libertad del modelo (incluida la intensidad de alabeo φ) son nulos. La viga se somete en todos los casos a una carga uniforme $q_z = 100$ kN/m y a un par torsor uniforme $m_s = 1$ kN m/m.

4.3.1 Sección en U

Para esta sección se escoge una longitud de viga $l = 15$ m y se analiza una secuencia de curvaturas (referidas al centroide de la sección) que comprende desde la viga recta hasta una apertura muy cercana a la de una semicircunferencia. En todos los casos, la esbeltez torsional tiene valores bajos. Las curvaturas, aperturas α_0 y esbelteces torsionales asociadas λ_0 se recogen en la Tabla 1:

TABLA 1
Curvaturas, aperturas y esbelteces empleadas en el análisis de la viga con sección en U.

χ (m^{-1})	0	1/60	1/40	1/10
α_0 (rad)	0	0.03π	0.12π	0.48π
λ_0	3.20	3.21	3.26	4.04

Los resultados normalizados de las variables estáticas y cinemáticas para la sección en U se representan en las Figuras

13 y 14. En la Figura 13 se observa cómo la flecha normalizada aumenta considerablemente con la curvatura, como es esperable, y lo mismo sucede con el giro de flexión. El giro de torsión cambia de sentido para curvaturas bajas ya que el efecto torsional de la carga vertical dominante supera al de la acción torsora distribuida; con curvaturas más altas el giro de torsión presenta varios cambios de signo. La intensidad de alabeo exhibe un comportamiento semejante, cambiando de sentido con curvaturas bajas, y aumentando el número de ondas con curvaturas mayores.

Por lo que respecta a las variables estáticas normalizadas (Figura 14), el cortante es prácticamente idéntico para todos los valores de la curvatura. El momento flector no tiene una dependencia muy marcada de esta, y mantiene la forma del diagrama. Sin embargo, el momento torsor deja de ser una función lineal en cuanto la curvatura crece, y el bimomento, como sucedía con la intensidad de alabeo, tiene un desarrollo marcadamente diferente y valores extremos muy superiores cuando la viga deja de ser recta.

4.3.2 Sección en cajón

En este caso se analiza una viga de longitud $l = 2$ m con la misma secuencia de curvaturas que en el caso de la sección en U, a la que corresponden las aperturas y esbelteces torsionales
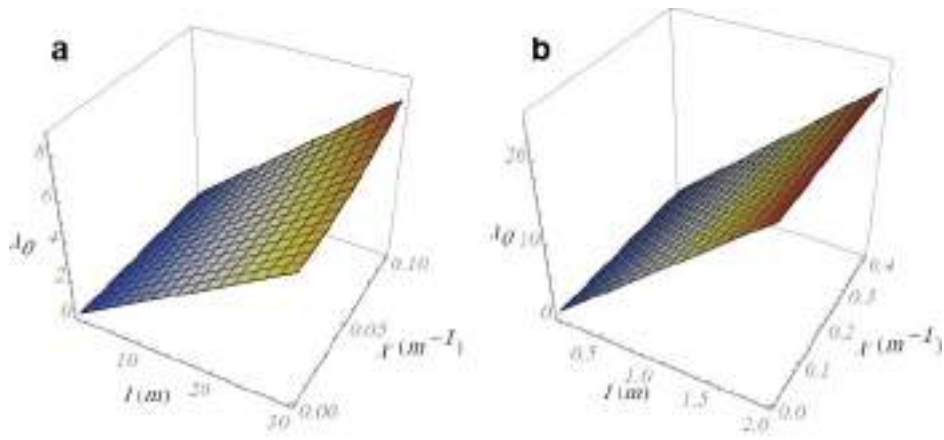
Figura 12. Esbeltez torsional en función de la longitud de la viga y de la curvatura. (a) sección en U; (b) sección en cajón.
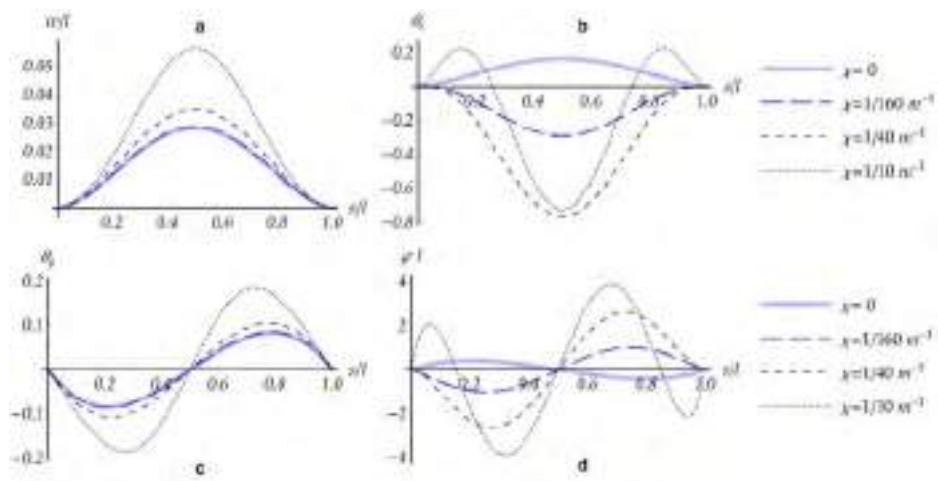
Figura 13. Variables cinemáticas normalizadas para distintas curvaturas en una viga biempotrada de sección abierta sometida a carga y par torsor uniformes. (a) desplazamiento vertical normalizado; (b) giro de flexión; (c) giro de torsión; (d) intensidad de alabeo normalizada.
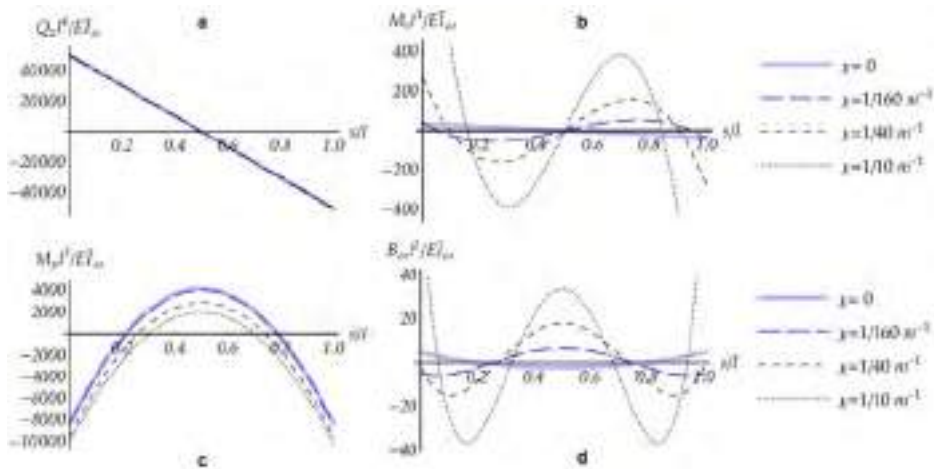
Figura 14. Variables estáticas normalizadas para distintas curvaturas en una viga biempotrada de sección abierta sometida a carga y par torsor uniformes. (a) esfuerzo cortante normalizado; (b) momento torsor normalizado; (c) momento flector normalizado; (d) bimomento normalizado.
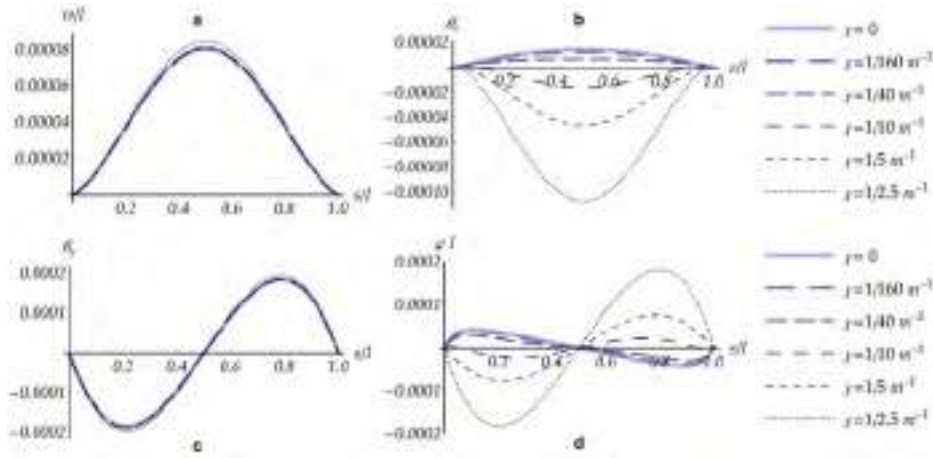
Figura 15. Variables cinemáticas normalizadas para distintas curvaturas en una viga biempotrada de sección en cajón sometida a carga y par torsor uniformes. (a) desplazamiento vertical normalizado; (b) giro de flexión; (c) giro de torsión; (d) intensidad de alabeo normalizada.
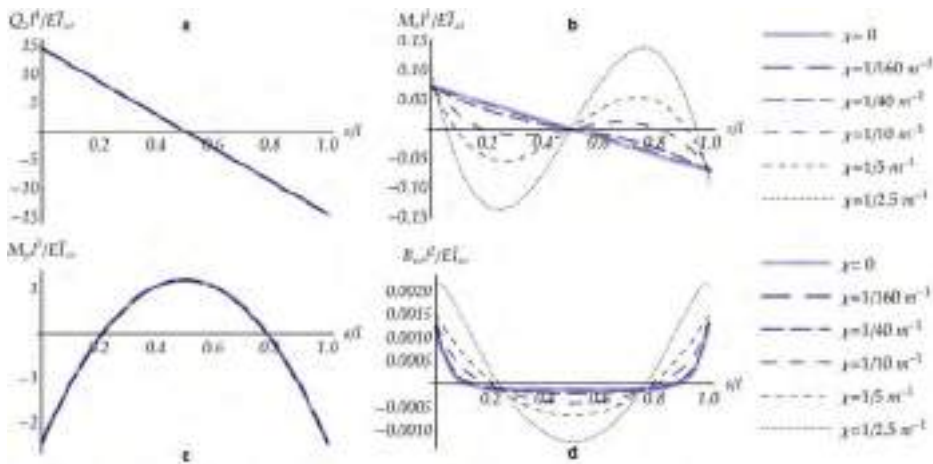
Figura 16. Variables estáticas normalizadas para distintas curvaturas en una viga biempotrada de sección en cajón sometida a carga y par torsor uniformes. (a) esfuerzo cortante normalizado; (b) momento torsor normalizado; (c) momento flector normalizado; (d) bimomento normalizado.

recogidas en la siguiente tabla:

TABLA 2
Curvaturas, aperturas y esbelteces empleadas en el análisis de la viga con sección cerrada.

$\chi(\mathrm{m}^{-1})$	0	1/60	1/40	1/10	1/5	1/2.5
α_0 (rad)	0	0.004π	0.016π	0.064π	0.127π	0.255π
λ_0	21.875	21.875	21.875	21.883	21.907	22.004

En la Figura 15 se observa que, en la pieza cerrada analizada, la flecha y el giro de flexión normalizados no dependen prácticamente de la curvatura. El giro de torsión y la intensidad de alabeo sí están fuertemente influidas por la misma, y cambian de sentido a medida que aumenta la curvatura por la misma razón que en la pieza abierta.

En cuanto a los esfuerzos normalizados (Figura 16), el cortante y el momento flector tampoco se modifican en la práctica con la curvatura. Por el contrario, los valores extremos del momento torsor y del bimomento crecen apreciablemente a medida que lo hace la curvatura.

4.4 Influencia de la esbeltez torsional y de la curvatura en la respuesta

En esta sección vamos a emplear la descomposición del torsor introducida en la Sección 3 con objeto de evaluar la influencia de la esbeltez torsional y la curvatura en la respuesta estática de la viga. Para cada una de las secciones estudiadas (abierta y cerrada) representamos, a partir de la descomposición introducida en la Ecuación (47), las siguientes fracciones del torsor total:

El momento torsor de Saint-Venant:

$$GJ^* \left(\theta'_s - \chi\theta_y\right) \tag{51}$$

El bicortante o momento torsor de alabeo:

$$M_{\dot{\omega}} = (\kappa_0^{\star} - 1)\, M_s + M_s - \kappa_0^{\star} GJ^{\star}\varphi - y_C^{\star} Q_z \tag{52}$$

La corrección dependiente de la deformación generalizada de torsión:

$$(1 - \kappa_0^{\star} - J^{*}/\bar{I}_0)\, G\bar{I}_0 \kappa_s \tag{53}$$

La corrección dependiente del cortante:

$$\chi\, \bar{r}_Z^2\, Q_z \tag{54}$$

En la representación gráfica de las funciones que se explica a continuación, se ha empleado en todos los casos el siguiente criterio para la leyenda de las gráficas:

- La Curva 1 representa el momento torsor total.
- La Curva 2 representa la suma del momento torsor de Saint-Venant más el torsor de alabeo, más la corrección asociada a la deformación de torsión.
- La Curva 3 representa la suma del momento torsor de Saint-Venant más el torsor de alabeo.
- La Curva 4 representa el momento torsor de Saint-Venant.

En todas las curvas se ha representado valores normalizados (adimensionales). La parte sombreada del diagrama corresponde a la suma del torsor de alabeo (bicortante) más los dos términos correctores. En el caso de curvatura nula, estos últimos se anulan y los diagramas obtenidos se corresponden con la descomposición esperada del torsor en la parte de Saint-Venant y la parte debida al alabeo.

4.4.1 Sección en U

En la Figura 17 se representa la descomposición (normalizada) del torsor en la viga biempotrada con sección abierta de 1 m de longitud en el caso de la viga recta (izquierda) y con una curvatura 1/10 m^{-1} (derecha). Las esbelteces torsionales que corresponden a estos dos casos son, respectivamente, $\lambda_0 = 0.214$, y $\lambda_0 = 0.270$. Para estos valores tan bajos de la esbeltez, como era de esperar, el torsor de Saint-Venant es despreciable, y prácticamente la totalidad del torsor es consecuencia del alabeo de la sección. Para la viga curva, el valor del bicortante supera al torsor total, y entran en juego los términos correctores, que en este caso no son despreciables.

La Figura 18 recoge el caso de la viga de 30 m de longitud, de nuevo recta o con curvatura 1/10 m^{-1}. Las esbelteces torsionales asociadas son, respectivamente, $\lambda_0 = 6.407$, y $\lambda_0 = 8.081$. En este rango de valores de la esbeltez, el torsor de Saint-Venant es prácticamente nulo en las secciones de empotramiento, y representa una fracción apreciable del torsor total en secciones suficientemente alejadas de los extremos. Esta proporción se mantiene en el caso curvo, en el que el torsor total ya no tiene una distribución lineal.

4.4.2 Sección en cajón

Las Figuras 19 y 20 reflejan la descomposición del torsor en el caso de una viga biempotrada con sección en cajón. Para mostrar valores suficientemente diferentes de la esbeltez torsional, se ha estudiado una pieza muy corta de medio metro de longitud (Figura 19), y otra más larga de 2 m (Figura 20), en los casos de curvatura nula y curvatura 1/2.5 m^{-1}. En la pieza corta, las esbelteces torsionales son $\lambda_0 = 5.469$ (viga recta), y $\lambda_0 = 5.501$ (viga curva). En la viga de 2 m de longitud las esbelteces crecen hasta $\lambda_0 = 21.875$ (viga recta), y $\lambda_0 = 22.004$ (viga curva).
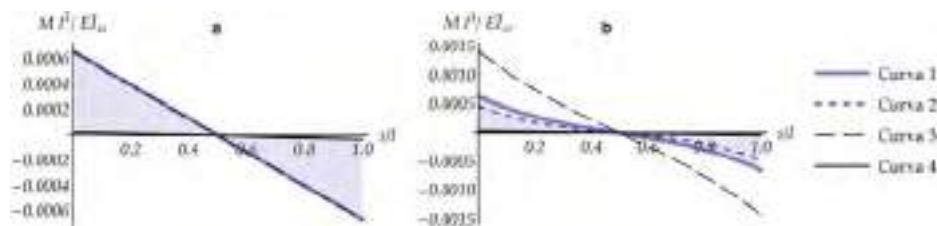
Figura 17. Descomposición del momento torsor normalizado en la viga biempotrada con sección abierta de 1 m de longitud. (a) viga recta; (b) curvatura 1/10 m^{-1}. Curva 1: Torsor total; Curva 2: Torsor de Saint-Venant, más torsor de alabeo, más corrección asociada a la deformación de torsión; Curva 3: Torsor de Saint-Venant, más torsor de alabeo; Curva 4: Torsor de Saint-Venant. El sombreado representa la parte del torsor debida al alabeo y a las correcciones asociadas a la curvatura.
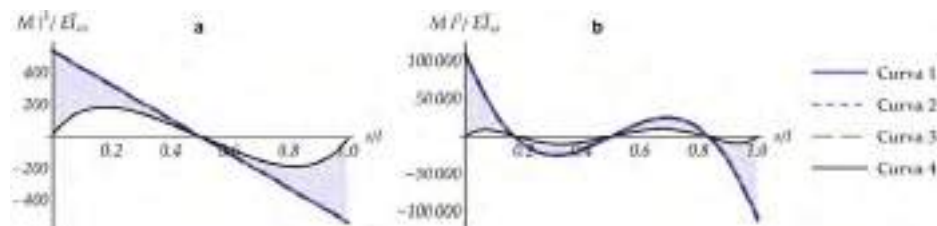
Figura 18. Descomposición del momento torsor normalizado en la viga biempotrada con sección abierta de 30 m de longitud. (a) viga recta; (b) curvatura 1/10 m^{-1}. Curva 1: Torsor total; Curva 2: Torsor de Saint-Venant, más torsor de alabeo, más corrección asociada a la deformación de torsión; Curva 3: Torsor de Saint-Venant, más torsor de alabeo; Curva 4: Torsor de Saint-Venant. El sombreado representa la parte del torsor debida al alabeo y a las correcciones asociadas a la curvatura.
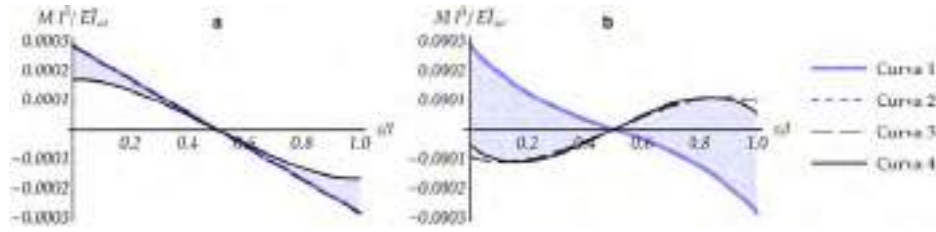
Figura 19. Descomposición del momento torsor normalizado en la viga biempotrada con sección cerrada de 0.5 m de longitud. (a) viga recta; (b) curvatura 1/2.5 m^{-1}. Curva 1: Torsor total; Curva 2: Torsor de Saint-Venant, más torsor de alabeo, más corrección asociada a la deformación de torsión; Curva 3: Torsor de Saint-Venant, más torsor de alabeo; Curva 4: Torsor de Saint-Venant. El sombreado representa la parte del torsor debida al alabeo y a las correcciones asociadas a la curvatura.
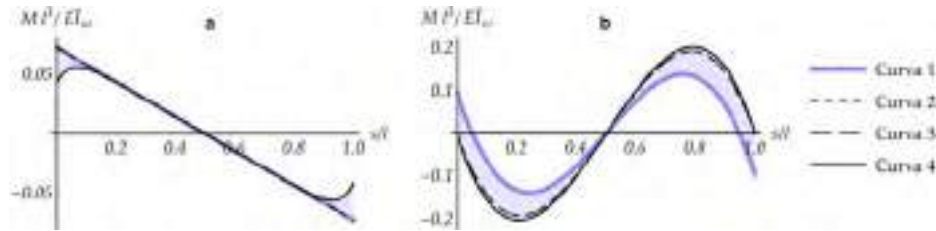
Figura 20. Descomposición del momento torsor normalizado en la viga biempotrada con sección cerrada de 2.0 m de longitud. (a) viga recta; (b) curvatura 1/2.5 m^{-1}. Curva 1: Torsor total; Curva 2: Torsor de Saint-Venant, más torsor de alabeo, más corrección asociada a la deformación de torsión; Curva 3: Torsor de Saint-Venant, más torsor de alabeo; Curva 4: Torsor de Saint-Venant. El sombreado representa la parte del torsor debida al alabeo y a las correcciones asociadas a la curvatura.
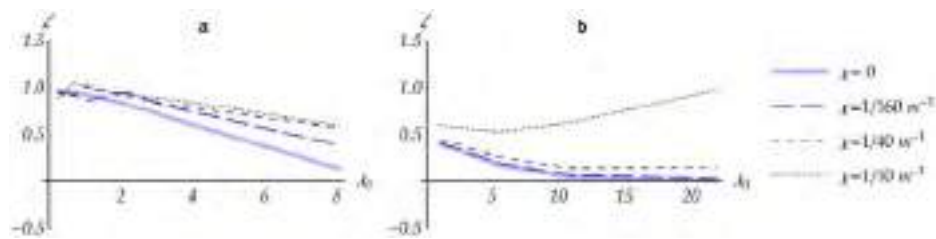
Figura 21. Relación entre el bicortante corregido y el torsor total, evaluados en $s/l = 0.3$, en función de la esbeltez torsional, para distintos valores de la curvatura. (a) viga con sección en U; (b) viga con sección en cajón

En la viga recta de menor esbeltez, el comportamiento es parecido al caso de sección abierta, salvo por el hecho de que en el empotramiento, el torsor de Saint-Venant no tiende a ser nulo. En la viga recta de mayor esbeltez, como era esperable, el bicortante es prácticamente nulo salvo en secciones muy próximas a los extremos, y su valor es en todo caso pequeño.

En los casos de sección cerrada con curvatura (diagramas de la parte derecha en las Figuras 19 y 20) sucede algo que no se había observado en la pieza recta: en valor absoluto, el torsor de Saint-Venant supera al torsor total; el bicortante y los términos correctores actúan entonces en sentido contrario al primero para que la suma iguale al torsor total.

4.4.3 Síntesis de resultados

Para concluir la sección de resultados hemos analizado la relación ζ entre valores absolutos del bicortante corregido y del torsor total en función de la esbeltez torsional, para distintas curvaturas. Entendemos por bicortante corregido la diferencia entre el torsor total y el torsor de Saint-Venant.

$$\zeta = \frac{|M_s - GJ^*(\theta_s' - \chi\theta_y)|}{|M_s|} \tag{55}$$

Esta relación es indicativa del mecanismo por el que se resiste la torsión: cuando tiende a 0 la torsión se resiste como torsión de Saint-Venant, y cuando tiende a 1, la torsión se resiste mediante alabeo de la sección. Los resultados se recogen en la Figura 21.

En ella se observa que en el rango de esbelteces pequeñas (sección en U y pieza corta) la relación ζ, evaluada en la sección $s = 0.3l$, es cercana a 1 (lo que indica que la torsión se resiste por alabeo), y que en ese caso el aumento de la curvatura

produce fluctuaciones en ella. En la viga larga con sección abierta (esbelteces torsionales del orden de 8) ζ llega a ser muy bajo en la viga recta, pero la curvatura incrementa la fracción de torsor resistida por alabeo. La viga con sección cerrada muy corta (esbelteces torsionales del orden de 5) ζ presenta ratios en el entorno de 0.5, pero en este caso el comportamiento es divergente: a medida que aumenta la longitud de la viga, en el caso recto o de curvatura baja ζ decrece rápidamente, y la torsión es de Saint-Venant para esbelteces superiores a 10, pero si la curvatura es alta, una fracción importante del torsor se resiste por otros mecanismos.

La Figura 21 sintetiza por tanto el comportamiento de vigas curvas de sección abierta y cerrada en función de su esbeltez torsional y de su curvatura.

5.
CONCLUSIONES Y DESARROLLOS FUTUROS

Dedicaremos las próximas líneas a subrayar los aspectos más relevantes del análisis de piezas curvas expuesto en este trabajo y las conclusiones que de él se extraen.

- El ámbito del estudio se ha limitado a piezas con *directriz plana*, que son las únicas que pueden proporcionar sistemas autónomos. Esto no merma su interés, ya que esta condición se cumple en la mayoría de las estructuras de ingeniería civil, y en particular en los puentes.
- Se han establecido y analizado las *condiciones de desacoplamiento* de las respuestas arco y viga curva. Incluso para el modelo más elemental, el *MVS*, esto solo lo garantiza la directriz plana. Por el mismo motivo se ha adoptado un segunda restricción, que la sección sea simétrica respecto al plano osculador de la directriz; a falta de profundizar en este aspecto, esperamos que suavizando esta condición se puedan obtener soluciones suficientemente aproximadas. Es una de las líneas por las que continuará este trabajo.
- Se han obtenido las ecuaciones generales de la viga plana con curvatura variable, Ecuaciones (41), que evidencian el acoplamiento torsión-flexión. La formulación es aplicable a cualquier tipo de sección transversal de la viga que cumpla el requisito de simetría asociado al desacoplamiento de las respuestas, sea abierta o cerrada.
- Se ha justificado que, para el tipo de piezas considerado en el estudio, se pueden identificar la directriz material y la directriz principal.
- Así mismo, se ha mostrado que, para tales piezas, los parámetros $\bar{I}_y$, $\bar{I}_z$ e $\bar{I}_\omega$ que incorporan la curvatura en su definición, se pueden sustituir por los momentos de inercia y el módulo de alabeo de la pieza recta prácticamente sin error cuando el centro de gravedad y el de esfuerzos cortantes están muy próximos, y con un error pequeño cuando no lo están. Además, se ha argumentado que el parámetro J^* se puede aproximar por el módulo de torsión de la pieza recta cuando la sección es cerrada. La deducción de las condiciones en las que se podría adoptar un valor de y_C e $\bar{I}_{y\omega}$ independiente de la curvatura, lo cual simplificaría notablemente el análisis de piezas de curvatura variable, queda pendiente para desarrollos posteriores.
- Se ha identificado la esbeltez torsional como parámetro que gobierna la solución del sistema de ecuaciones diferenciales de la viga curva.
- El valor de la esbeltez depende fundamentalmente de la forma de la sección transversal y de la longitud de la viga, y en mucha menor medida de la curvatura. Esto último es especialmente cierto en secciones cerradas, en las que la esbeltez es prácticamente independiente de la curvatura.
- Se ha propuesto una descomposición del torsor total en una fracción asimilable al torsor de Sain-Venant, otra que denominamos bicortante, que coincide con el torsor de alabeo en la pieza recta, y otras dos fracciones correctoras, dependientes de la deformación generalizada de torsión y del cortante, que tienden a cero con la curvatura.
- A partir de esta descomposición, se ha estudiado la relación entre la torsión resistida por alabeo y la torsión total en función de la curvatura y de la esbeltez. Los resultados se han expresado en forma gráfica y muestran cómo, al contrario que en la viga recta, en vigas curvas ambos tipos de torsión son relevantes incluso con esbelteces altas.

Por último, el cómputo de la distorsión de la sección transversal, que Manterola también abordó para la viga recta en [1], podría llevarse a cabo en la viga curva con el mismo esquema general que el desarrollado para la torsión. Bastaría ampliar la hipótesis cinemática (16), incorporando al vector de desplazamientos generalizados del modelo dos componentes adicionales: la intensidad de distorsión $\gamma_D(s)$ y la intensidad de alabeo de distorsión $\varphi_D(s)$, conjugadas con un patrón de alabeo de distorsión $\omega_D(y,z)$, tal y como se muestra en [15].

6.
LISTA DE SÍMBOLOS

SÍMBOLOS GENERALES

$\tilde{\Gamma}$	Curva directriz material de la pieza alargada (lugar geométrico de los centros de gravedad de las secciones)
$\tilde{\mathbf{P}}$	Vector posición de los puntos de la directriz material
$\tilde{y}_0$, $\tilde{z}_0$	Coordenadas del eje principal en la sección transversal, referidas al centro de gravedad
Γ	Curva directriz principal de la pieza alargada
s	Longitud de arco sobre la directriz principal
$\chi(s)$	Curvatura de la directriz principal
$\mathbf{P}$	Vector posición de la directriz principal
y, z	Coordenadas en la sección transversal, referidas al eje principal
μ	Determinante del tensor métrico del espacio viga, igual a $1-\chi y$

SÍMBOLOS RELACIONADOS CON LA TEORÍA UNIFICADA

$\mathbf{d}^*(s,y,z)$	Vector de desplazamientos del sólido tridimensional, de tres componentes
$\mathbf{u}(s)$	Vector de desplazamientos generalizados del modelo unidimensional
$\mathbf{h}(y,z)$	Operador cinemático característico del modelo propuesto. Relaciona los desplazamientos generalizados del modelo con los del sólido

$\mathbf{e}^*(s,y,z)$ Vector de deformaciones del sólido tridimensional, de seis componentes

$\mathbf{e}(s)$ Vector de deformaciones generalizadas del modelo unidimensional

$\mathbf{B}_r$ Matrices de deformación (Relacionan las deformaciones generalizadas del modelo con las del sólido.)

$\mathbf{Q}(s)$ Vector de densidades lineales de carga (se aplica al modelo unidimensional)

$F(s,\mathbf{u},\mathbf{e})$ Densidad lineal de energía potencial del modelo unidimensional

$\mathbf{C}$ Operador constitutivo del sólido

$\mathbf{D}_{rs}$ Operadores constitutivos del modelo unidimensional

$\mathbf{f}(s)$ Vector de esfuerzos del modelo unidimensional

$\mathbf{H}(s)$ Operador de equilibrio del modelo unidimensional

$\hat{\mathbf{D}}_{00}$ Operador de acoplamiento del modelo unidimensional

$\mathbf{E}(s)$ Vector estado del modelo. Agrupa los desplazamientos y esfuerzos, incógnitas del problema

$\mathbf{W}(s)$ Operador Wronskiano del modelo. Relaciona el vector estado con su primera derivada

$\mathbf{G}(s)$ Operador fundamental principal. Resuelve el problema de equilibrio homogéneo y permite construir la solución del problema de valores iniciales asociado a $\mathbf{W}$ así como resolver los problemas de contorno de la pieza de curva

SÍMBOLOS RELACIONADOS CON EL MODELO DE VIGA CURVA

y_C Coordenada del centro de torsión (referida al eje principal)

$\hat{y}$, $\hat{z}$ Coordenadas en la sección transversal referidas al centro de torsión

$\hat{\omega}(y,z)$ Alabeo unitario o patrón de alabeo de la sección transversal

$w(s)$ Desplazamiento transversal de los puntos de la directriz

$\theta_s(s)$ Rotación de eje tangente a la directriz de las secciones transversales

$\theta_y(s)$ Rotación de flexión de las secciones transversales

$\varphi(s)$ Intensidad de alabeo

$Q_z(s)$ Esfuerzo cortante

$M_s(s)$ Momento torsor

$M_y(s)$ Momento flector

$B_{\hat{\omega}}(s)$ Bimomento

$M_{\hat{\omega}}(s)$ Bicortante o momento torsor de alabeo

$\bar{A}$ Área de la sección transversal

$\bar{I}_y$, $\bar{I}_z$, $\bar{I}_{yz}$ Momentos de inercia y producto de inercia referidos al eje principal

$\bar{I}_0$ Momento polar de inercia con respecto al eje principal

$\bar{I}_{\hat{\omega}}$, $\bar{I}_{y\hat{\omega}}$ Módulo de alabeo y producto de alabeo de la sección

$\hat{W}$, $\hat{\Omega}$ Nuevas constantes estáticas seccionales referidas al centro de torsión

W_0 Resultado de referir la constante al eje principal

κ_0^*, y_C^* Nuevos parámetros dependientes de la curvatura

κ_0^*, J^* Módulo de torsión corregido por efecto de la curvatura

λ_0 Esbeltez de torsión de la viga curva

Bibliografía

[1] Manterola, J. (1976) *La sección abierta y cerrada bajo solicitación excéntrica*. Hormigón - Puentes II, A.F.C.E., Monografía nº 15

[2] Manterola, J. (1977) *Cálculo de tableros por el método del emparrillado*, Hormigón y Acero, núm. 122, pp. 93-149

[3] Manterola, J. (1977), *Análisis de tableros rectos de puentes por métodos armónicos*, I.E.T.C.C., Monografía nº 343

[4] Vlassov, B.Z., *Pièces longues en voiles minces*, Eyrolles (1962)

[5] Kollbrunner, C.F.; Basler,K., *Torsion in structures. An engineering approach*, Springer (1969)

[6] Kirchhoff, G., (1859) *Ueber das Gleichgewicht und die Bewegung eines unendlich dünnen elastischen Stabes*. J. für die reine und Angew. Math.; núm. 56, pp. 285–313.

[7] Winkler, E. (1858) *Formänderung und Festigkeit gekrümmter Körper, insbesondere der Ringe*. Civilingenieur; vol. 4, pp. 232-246.

[8] Timoshenko, S.P. *Resistencia de Materiales*. Espasa Calpe (1967).

[9] Courbon, J. *Tratado de Resistencia de Materiales*, (2ª ed.). Aguilar (1968).

[10] Anderson, C.G. (1959) *Flexural Stresses in Curved Beams of I- and Box-section*. Proc. Inst. Mech. Eng.; vol. 163 núm. 1, pp. 295–306.

[11] Samartín, A., González de Cangas, J.R. *Teoría elemental de vigas alabeadas. Aplicación a la viga balcón circular*. Universidad de Santander. ETSI de Caminos, Canales y Puertos. (1980)

[12] Gimena, L., Gimena, F.N., Gonzaga, P. (2008) *Structural analysis of a curved beam element defined in global coordinates*, Engineering Structures, vol. 30, pp. 3355-3364

[13] Barretta R., Barretta A. (2010) *Shear stresses in elastic beams: an intrinsic approach*, European Journal of Mechanics A/Solids, vol. 29, pp. 400-409

[14] Romano, G., Barretta, A., Barretta, R. (2012) *On torsion and shear of Saint-Venant beams*, European Journal of Mechanics A/Solids, vol. 35, pp. 47-60

[15] Yamada, Y.; Ezawa, Y. (1977) *On curved finite elements for the analysis of circular arches*. Int. J. Numer. Methods Eng.; vol. 11, núm.11, pp.1635–1651.

[16] Lee, P-G.; Sin, H-C. (1994) *Locking-free curved beam element based on curvature*. Int. J. Numer. Methods Eng.; vol. 37, núm. 6, pp. 989–1007.

[17] Choit, J.; Lim, J. (1995) *General curved beam elements based on the assumed strain fields*. Comput. Struct.; vol. 55, núm. 3, pp. 379–86.

[18] Raveendranath, P.; Singh, G.; Venkateswara Rao, G. (2001) *A three-noded shear-flexible curved beam element based on coupled displacement field interpolations*. Int. J. Numer. Methods Eng.; vol. 51, núm. 1, pp. 85–101.

[19] Reissner, E. (1981) *On finite deformations of space-curved beams*. ZAMP Zeitschrift für Angew. Math. und Phys.; vol. 32, núm. 6, pp. 734–44.

[20] Simó, J.C. (1985) *A finite strain beam formulation. The three-dimensional dynamic problem. Part I*. Comput. Methods Appl. Mech. Eng.; vol. 49, núm. 1, pp. 55–70.

[21] Simó, J.C.; Vu-Quoc, L. (1991) *A Geometrically-exact rod model incorporating shear and torsion-warping deformation*. Int. J. Solids Struct.; vol. 27, núm. 3, pp. 371–93.

[22] Monleón, S. *Teoría unificada de elementos estructurales esbeltos*. Editorial de la Universidad Politécnica de Valencia (2017)

[23] Timoshenko, S. y Goodier, J.N. *Teoría de la Elasticidad*. Urmo (1972)

[24] Sáez Benito, J.M. *Cálculo matricial de estructuras formadas por piezas rectas*. Fondo editorial de ingeniería naval (1975)

Search for the true structural solution

En la búsqueda de la verdadera solución estructural

Jiri Strasky[a]

[a] Professor. DSc. Technical Director and Partner. Strasky, Husty and Partners, Ltd. (Brno, Czech Republic).

ABSTRACT

For a long time, I have been admiring the design work of the engineering firm Carlos Fernádez Casado, S.L., Madrid and his president Prof. Javier Manterola Armisén. His structures express the unity of function and form as well as unity of structural and architectural solution. I always wanted to work similarly. However, since I am living in different social, historical, technological and physical environments, my structures are different. Here I present several structures on which examples my continuous search for the true structural solution will be demonstrated. The presented structures were designed by engineering staff of the design firm Strasky, Husty and Partners, ltd., Brno, Czech Republic. The presented structures utilize different architectural and structural forms that are inherent in the constraints of the site and are economical and structurally efficient. They were well accepted both the public and professional.

RESUMEN

Durante mucho tiempo, he estado admirando el trabajo de la oficina de proyectos Carlos Fernádez Casado, S.L. y su presidente Prof. Javier Manterola Armisén. Sus estructuras expresan la unidad de función y forma, así como la unión de la solución estructural y arquitectónica. Siempre quise trabajar de manera similar. Sin embargo, como vivo en un entorno social, histórico, tecnológico y físico diferente, mis estructuras son diferentes. En este artículo les presento varias estructuras en las que se demostrará mi continua búsqueda de la verdadera solución estructural. Las presentes estructuras fueron diseñadas por ingenieros de la empresa de proyectos Strasky, Husty y Partners, Ltd., Brno, República Checa. Utilizan diferentes formas arquitectónicas y estructurales que son inherentes a las limitaciones del lugar y son económica y estructuralmente eficientes. Fueron bien aceptadas tanto por el usuario como por los profesionales.

1.

INTRODUCTION

For a long time, I have been admiring the design work of the engineering firm Carlos Fernádez Casado, s.l., Madrid and his president Prof. Javier Manterola Armisén. He designs structures which architecture is developed from true structural solutions that simply and clearly express the flow of internal forces through their static system. He develops new architectural and structural forms making use of the latest technological and scientific innovations to achieve the most appropriate solutions for each individual case. His structures express the unity of function and form as well as unity of structural and architectural solution.

What is more, he designs bridges that are developed from the social and cultural history of Spain, from Spanish tradition of understanding of the plastic richness of concrete and the strength of steel. Furthermore, his structures are personal and express his personal attitude to work and life.

I always wanted to work similarly. However, since I am living in different social, historical, technological and physical environments, my structures are different. In Spain, I had several

---

Figure 1. Bridge across the Lazny Creek Valley.

opportunities to present our design philosophy, our structures and our approach to design [1] and [2]. Therefore, I will present here several new structures on which examples my continuous search for the true structural solution will be demonstrated. The presented structures were designed by engineering staff of the design firm Strasky, Husty and Partners, ltd., Brno, Czech Republic

2.
VIADUCTS WITH PROGRESSIVELY ERECTED DECKS

Bridge structures formed by concrete or steel box girders with large overhangs supported by struts represent an optimum solution for crossings of deep valleys. These bridges are esthetically pleasing and structurally very efficient. Their economy can be enhanced by a progressive erection of their decks. This is illustrated on a construction of several viaducts built in the Slovak and Czech Republic.

2.1 Concrete Viaducts

Thirty years ago, a cable stayed bridge across the River Elbe near a city of Podebrady was erected. Its 31.80 m wide deck is formed by a spine girder with large overhangs supported by not mutually connected precast slab struts [3]. The one cell box girder assembled from precast segments was constructed first, then the struts were erected, and the overhangs were cast in simple formwork that was supported by these struts. After that similar arrangement was used in a construction of the Vrsovice cable stayed bridge built in Prague and in several bridges designed by others.

Recently similar approach has been used in construction of several long viaducts that have been built in Slovakia - see Figures 1 and 2. These bridges have span lengths up to 69 m, their widths are up to 28.70 m. The spine girders were cast span by-span in a formwork suspended on a special overhead gantry with 'organic' prestressing system (OPS) which eliminates the deflection of the gantry - see Figure 3. To reduce the self-weight of the spine girder as much as possible, the girders are very narrow. Therefore, the transverse projection of the overhangs up to 11.00 m.

The first structure of this kind was a 975 m long viaduct across the Hostovsky Creek built on the Expressway R1 near a city of Nitra. The bridge of the width of 25.66 m has 17 spans of lengths from 33.0 to 69.0 m. The depth of the girder varies from 4.00 to 2.60 m.

Two bridges of similar arrangement were being built on a motorway D1 section Fricovce – Svinia near a city of Presov. These bridges built across the Lazny (see Figure 1) and Stefanovsky Creek Valley have total lengths of 269 m and 182 m; typical span length is 45 m. Both motorway directions are carried by one bridge of a total width of 29.5 m. The depth of the girder is 2.60 m. Since the bridge decks are frame connected with H shaped piers, the bridges form semi-integral structural systems.

Another two bridges of similar arrangement were also built on a motorway D1 section Janovce – Jablonov near a city of Levoca. The bridges across the Lodina (see Figure 2) and Doliansky Creek Valley have total lengths of 367 m and 414 m; typical span length is 65 m. Both motorway directions are carried by one bridge of the total width of 28.70 m. The depth of the girder is from 4.00 to 2.60 m. Since the bridge decks

Figure 2. Bridge across the Lodina Creek Valley.

Figure 3. Movable scaffolding - Bridge across the Lodina Creek Valley.

are hinge connected with twin piers, the bridges form semi-integral structural systems.

The spine girder of all bridges was progressively cast span–by-span in a formwork suspended on overhead gantries. The girders were cast with short overhanging cantilevers. The decks of all bridges are longitudinally prestressed by internal bonded tendons situated within the basic cross section and by external non-bonded tendons situated inside the central box. The bonded tendons are coupled in each construction joint. External cables are anchored at pier diaphragms and are deviated at pier and span deviators.

In the transverse direction the deck slab is prestressed by tendons composed of strands installed in flat ducts spaced 1.50 m. During erection the struts are suspended on two prestressing bars anchored at outer cantilevers of the basic cross section - see Figures 4 and 5. The struts of a nominal width of 3.00 or 2.50 m are supported by short bottom corbels of the box girder. The cast-in-place deck slab was cast in the formwork supported by already erected precast struts. After the transverse prestressing of the deck slab is applied, the longitudinal external cables are post-tensioned.

The structural solution was developed on a basis of very detailed static and dynamic analyses. The first structure, the Viaduct across the Hostovsky Creek Valley, has been carefully monitored during construction, in depth loading tests and during service. The measurements confirmed the static loading assumptions and showed a very good agreement between the measured and the expected behaviour.
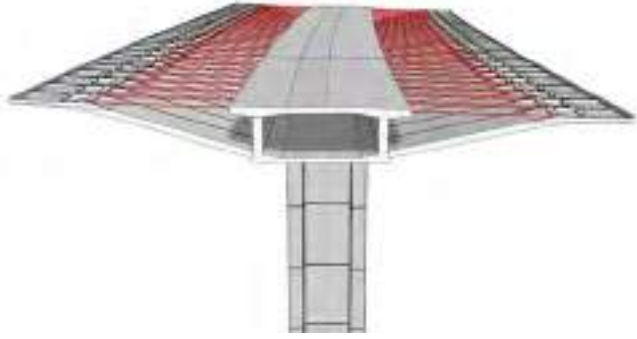
Figure 4. Progressive erection of the deck.

Figure 5. Precast struts - Bridge across the Lodina Creek Valley.

Figure 6. Bridge across the Kremlice Creek Valley.
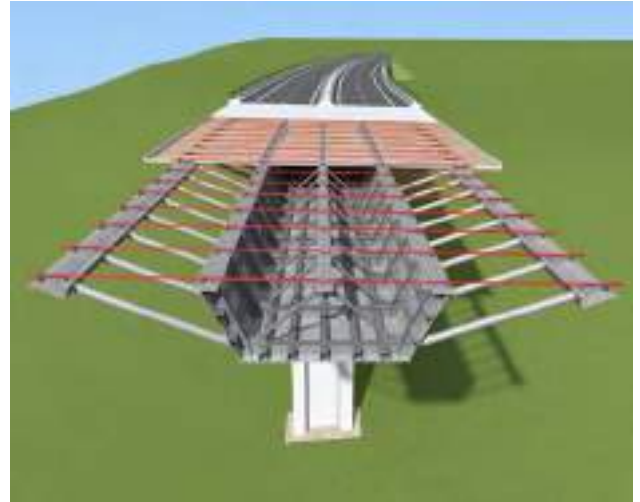
Figure 7. Progressive erection of the deck.

Figure 8. Steel structure - Bridge across the Kremlice Creek Valley.

Figure 9. Progressive erection of the deck - Bridge across the Kremlice Creek Valley.

2.2 Composite Viaducts

Progressive erection of the deck was also utilized in construction of two composite viaducts that were built on the highway I/11 in the North Moravia, Czech Republic - see Figure 6. The first viaduct, the Bridge across the Hrabynka Creek Valley of a total length of 330.0 m, consists of a 6 span continous girder of lengths from 39.0 to 66.0 m, the second one, the Bridge across the Kremlice Creek Valley of a total length of 528.0 m, consists of a 11 span continous girder of lengths from 33.0 to 57.0 m. While the Bridge 206 has a straight axis, the Bridge 207 includes a 900 m radius horizontal curve plus an horizontal agreement.

Both directions of the highway are carried by carried by single deck composed of a steel girder and a 25.5 m wide concrete deck slab – see Figure 7. The steel girders of the
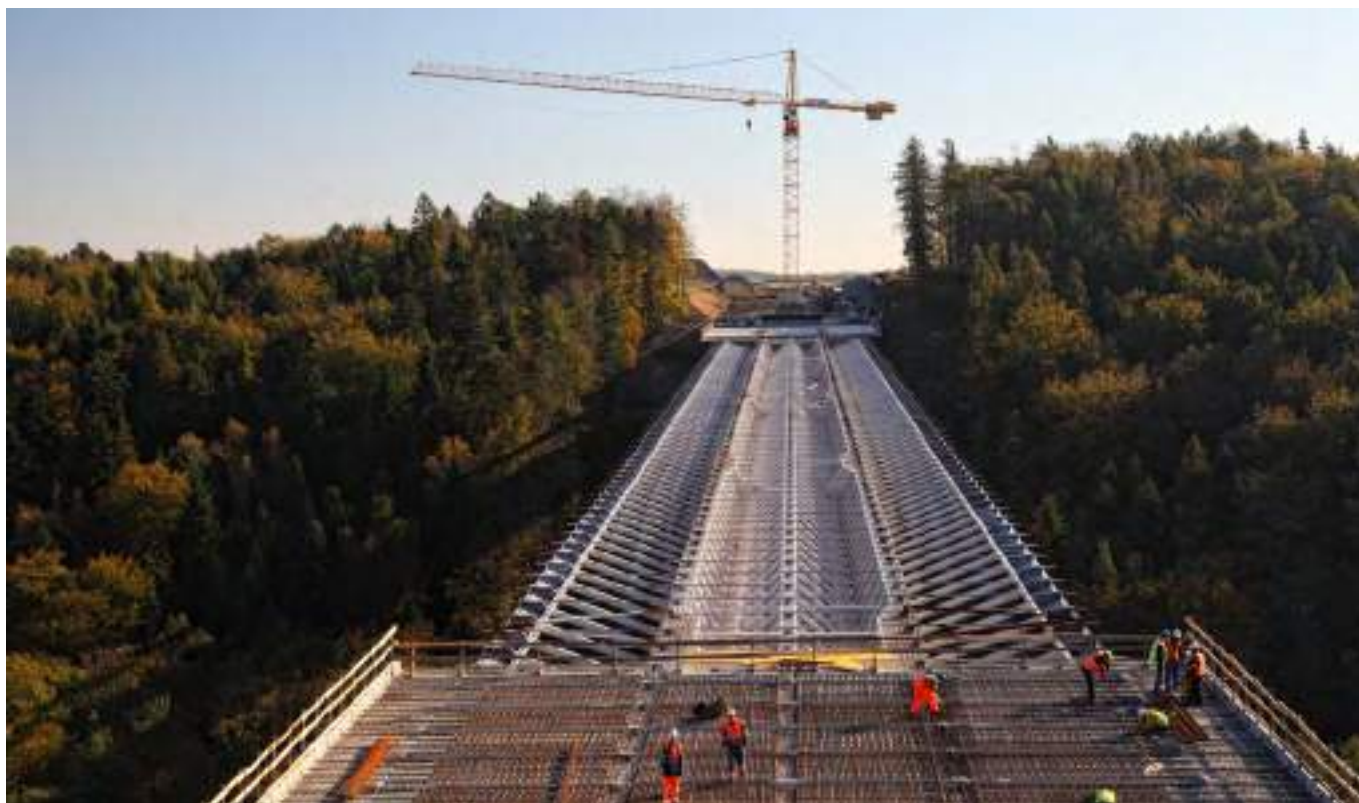
Figure 10. Progressive casting of the deck - Bridge across the Kremlice Creek Valley.

trough cross section assembled of top and bottom flanges and inclined webs are supplemented by central stringer and two edge stringers. While the central stringer has I cross section, the edge stringers have V shape with smooth surface that simplify the bridge maintenance. At distance of 3.0 m the stringers are supported by diagonal pipes attached to the girder's bottom corners. The shape of the structure is secured by top transverse ties anchored at the top flanges and at the edge and central stringers – see Figure 8. The deck slab is composite of precast slab members and additionally cast deck slab. The precast members of thickness of 100 mm are stiffened by steel trusses welded from reinforcing bars. Their function both, for erection and service load, was verified by loading tests done at a Brno University of Technology.

Both bridges were incrementally assembled beyond the abutments and consequently launched into their final position. The steel structure of the first bridge was divided into 20 segments of lengths from 13.0 to 21.3 m. The steel structure was incrementally launched with precast members; only a part of the structure of the length of 66 m beyond the launching nose was formed by the steel section. When launching was completed, remaining precast members were erected and the deck slab was progressively cast.

The steel structure of the second bridge was divided into 25 segments of lengths from 13.0 to 29.0 m. Due to the complex bridge geometry the steel structure is assembled from two parts and it was launched from both abutments. At first, the part of the steel structure close to the abutment 1 was incrementally assembled and launched, and then the part of the structure close to abutment 12 was assembled and launched. Due to the variable plan curvature the launched

structure was temporarily supported by pier transverse steel girders that allowed a transverse movement of the deck. To reduce the weight of the launched structure, the steel structure was launched without precast members. After connection of both parts, the precast members were progressively erected, and the deck slab was cast – see Figure 9 and 10.

3.
SEMI-INTEGRAL CANTILEVER BRIDGES

Recently we have designed three semi-integral cantilever bridges with decks supported on twin twin piers. All these bridges were built on the motorway D3 in Slovakia.

3.1 Bridges Valy and Rieka, Motorway D3, Slovakia

These bridges were built across the deep valleys on the section Svrcinovec – Skalite see Figure 11. The Bridge 'Valy' is a 591 m long continous structure consisting of nine spans with lenghts ranging from 30 to 92 m. The bridge Rieka of the total length of 500 m is formed by a continuous structure of eight spans is a 500 m long continous structure consisting of eight spans with lenghts ranging from 25 to 92 m. The deck of both bridges consist of by box girders of a variable depth from 2.70 to 5.00 m that were segmentally cast in balanced cantilevers starting at piers m - see Figure 12.

The slender piers that are monolitically coonnected to the deck consist of by twin walls which bottom portions are mutually connected by longitudinal walls. The piers height is up to 76 m. The bearings are situated only on short side piers

Figure 11. Bridge Valy.

Figure 12. External continuity cable.

Figure 13. Cantilever construction of the Bridge Valy.

3.2 Bridge across the River Vah's Reservoir Hricov, Motorway D3, Slovakia

In December 2017 a 1.50 km long viaduct across the River Vah's Reservoir Hricov, on the Motorway D3, Slovakia was opened. The viaduct consists of a continous structure of span lengths from 30.50 to 110.00 m. The central spans bridging the River Vah consist of a box girder of a variable depth from 3.00 to 6.00 m that were segmentally cast in balanced cantilevers - see Figures 14 and 15; the remaining spans have a double tee cross section of a constant depth of 3.00 m - see Figure 16. These spans were cast span-by-span on stationary or movable scaffoldings. The bridge forms a semi-integral structure with expansion joints situated only at the abutments.

The cantilever spans are supported by twin piers that consist of two transversally inclined columns directly supporting the box girder's webs; the approach spans are indirectly supported by single elliptical columns. Although these supports have a different static function, their shape is consistent – see Figure 17.

and abutments. The horizontal distance of the twin walls and height of the connecting wall were determined by a parametric study in which a bridge stability during the progressive erection of the bridge and a flexibility of the integral structural systems were compared.

The deck is post-tensioned by cantilever tendons situated in the deck slab, span tendons situated in the bottom slab and by external continuity tendons situated inside of the box section - see Figure 13. The prestressing tendons balance not only bending moments, but also shear stresses. Therefore, the box girders' webs thickness is only 350 mm.

Figure 14. Cantilever construction of the Bridge across the River Vah's Reservoir.

Figure 15. Deck of the main spans of the Bridge across the River Vah's Reservoir.

Figure 17. Piers of the Bridge across the River Vah's Reservoir.

Figure 16. Deck of the approach spans of the Bridge across the River Vah's Reservoir.

4.
CABLE-SUPPORTED BRIDGES

According to the nature of the obstacle and local conditions, classical cable -stayed, extradosed and suspension structures are designed. Some of them are described below.

4.1 Bridge across the Odra River and Antosovice Lake, Czech Republic

Near the city of Ostrava the motorway D1 crosses the River Odra and Antosovice Lake on a twin bridge of a total length of 589 m. Due to a limited clearance, the deck of the structure had to be as slender as possible. Since the bridge is situated in a nice recreation area, it was necessary to design a structure of high aesthetic value that can become a symbol of the new freeway. Therefore, a cable stayed structure suspended on one single pylon was accepted - see Figure 18. The bridge crosses the river

Figure 18. Bridge across the Odra River.

Figure 19. Deck of the viaducts - Bridge across the Odra River.

in a skew angle of 54°. The horizontal alignment comprises a 1500 m radius horizontal curve followed by a transition while the vertical alignment is a crest elevation with radius of 20000 m.

The span length varies between 24.5 to 105.0 m. The main span bridging the Odra River is suspended on a 46.8 m high single

pylon. Since the stay cables have a symmetrical arrangement, the back stays are anchored in two adjacent spans situated on the land between the river and lake. The stay cables have a semi-radial arrangement; in the deck they are anchored at distance of 6.07 m, at the pylon they are anchored at a distance of 1.20 m.

The decks are formed by two cell box girders 2.20 m

Figure 20. Deck of the suspended spans - Bridge across the Odra River.

Figure 21. Bridge across the Railway Station at Bohumin.

Figure 22. Structure of the Bridge across the Railway Station at Bohumin.

deep without traditional overhangs. The bottom slab of both cells is inclined, and it is curved in the middle of the girder - see Figure 19. In the suspended spans the box girders are mutually connected by a top slab cast between the girders and by individual struts situated at distance of 6.07 m. The stay cables are anchored at anchor blocks situated at the connected slab. The struts connect the curved bottom of the girders and together with the inclined slabs create a simple truss system transferring the force from the stays into the webs. Between the stays' anchors there are circular openings at the connected slab. All piers have an elliptical cross section of the width of 4.10 m and depth of 1.60 m - see Figure 20.

The bridge deck was cast span-by-span in two formworks suspended on two movable scaffoldings. With respect to the span length of the movable scaffoldings, temporary piers had to be built in the suspended spans. As soon as the spans adjacent to the pylon were cast, the pylon's steel core was erected, and concrete fill and cover were progressively cast.

Simultaneously, the concrete struts between the girders were erected and top slab between the girders was cast and transversally prestressed. After that, the stay cables were erected and tensioned. Then the temporary piers were removed.

4.2 Bridge across the Railway Station at Bohumin, Czech Republic

For the crossing of the railway station in a city of Bohumin, a structure of a minimum structural depth had to be designed. Since the bridge is located close to historic center, the new bridge should be as modest as possible. Therefore, an extradosed structure suspended on low pylons was built – see Figure 21.

The bridge is 140.30 m long distributed in three spans
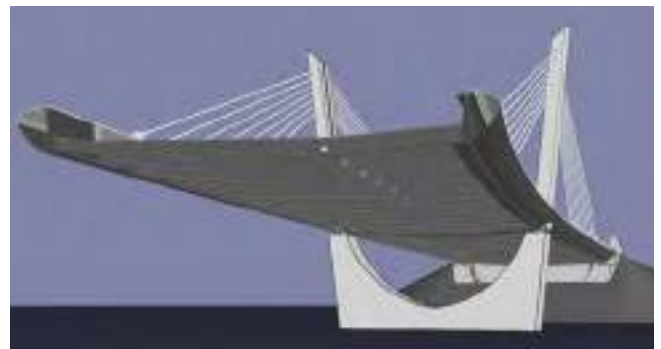
of length of 30.0+70.0+30.0 m that are suspended on transversally inclined low pylons situated above intermediate supports. The bridge axis is in a plan curvature with a radius of 256 m. The deck is formed by two edge box girders that are mutually connected by floor beams and a composite deck slab – see Figure 22. The deck's steel structure was incrementally assembled beyond an abutment and consequently launched into its final position.

4.3 Bridge across the River Ebro, Spain

Together with the Spanish firm Tec-Cuatro, from Barcelona, we won a competition for the design of the new bridge across the Rio Ebro. The bridge replaces a ferry that connected the small cities Deltebre – Sant Jaume D'Enveja situated close to the river's estuary into the Mediterranean Sea. The client required a signature structure that, however, corresponds to a scale of these decent cities. The bridge crosses the river in a skew angle and it is in a crest elevation. The bridge forms a self-anchored suspension structure of three spans of lengths 69.00+ 112.00 + 69.00 m - see Figure 23.

The 19.30 m wide deck is suspended on four suspension cables situated in the bridge axis. The torsionally stiff deck is consist of a four-cell box. The central web of a variable depth that protrudes above the deck slab and substitute suspenders of the classical suspension structures naturally divides a local highway from pedestrian and cyclist routes. At a distance of 3.00 m the steel structure is stiffened by transverse cross beams that support the composite deck slab. At the abutments

Figure 23. Bridge across the River Ebro.

Figure 24. Lifting of the deck of the Bridge across the River Ebro.

the deck is stiffened by the end cross beams transferring the load from the bearings into the central webs.

The main suspension cables are consist of four BBRV cables anchored at the end diaphragms and are deviated at the saddles of the low pylons. For the construction of the side spans and piers, artificial peninsulas were consecutively created on both river banks. They served for drilling of 46m long piles, casting the footings and construction of the piers. Then the steel structure forming the side spans and cantilevers protruding into the main span were erected. After that the pylons were erected, the pylons' saddles were connected with the central walls by steel pipes forming the stays. In this way a cable-stayed structure was created.

The whole central portion of the main span being 61.40 m long and 500 tons heavywas assembled on one bank and consequently floated and lifted into its final position – see Figure 24. When the central portion was connected to the already assembled structure, the suspension cables were pulled through the pipes and were partially tensioned. In this way the weight of the steel structure was transferred from the steel pipes to the suspension cables and the cable stayed structure was transformed into a self-anchored suspension structure. Consequently, the deck slab was progressively cast, and stresses in suspension cables were adjusted. The construction was finalized by loading tests. The structure was tested for five positions of the live load that creates maximum bending and torsion.

4.4   Pedestrian Bridge across the motorway D1, Czech Republic

The bridge that crosses the motorway D1 near a city of Bohumin is used both by pedestrians and bicycles - see Figure 25. The bridge deck of two spans of 54.94 and 58.29 m is in a plan curvature with a radius of 220 m. The bridge is suspended on a single mast situated in the area between the freeway and local roads.

Figure 25. Pedestrian Bridge across the motorway D1.

Figure 27. Wildlife Overpasses, Czech Republic.

Figure 26. Deck of the Pedestrian Bridge across the motorway D1.

Figure 28. Wildlife Overpasses, Czech Republic.

The bridge deck is fixed into the end abutments consisting of front inclined walls and rear walls. Due to heavy bicycle traffic the city of Bohumin has required to separate the pedestrian and bicycle pathways. Therefore, the deck is consists of a central spine girder with nonsymmetrical cantilevers carrying the pedestrians and bicycles. To balance the transverse load, the shorter cantilever is solid, while the longer is consists of a slender slab stiffened by transverse ribs - see Figure 26. The mast is consists of two inclined columns of two cell box sections that are tied by top and bottom steel plates connecting the boxes' central webs.

5.
ARCH BRIDGES

An arch by its own shape naturally expresses an effort to bridge the obstacle. For the dead load a correctly designed arch

is stressed primary by compression stresses. Therefore, it can be light and transparent. Recently we participated in a design of several arch bridges built in the Czech Republic and in the USA. The most interesting bridges are described below.

5.1 Wildlife Overpasses, Czech Republic

For motorway wildlife crossings, a new structure consists of two continuous shell arches that are supported by an intermediate support situated in the motorway median have been developed – see Figure 27. The shell structure is continuously widened in the plan and smoothly link up the side embankments - see Figure 28. To enable design these structures also in areas with poor geotechnical conditions, a self-anchored structural system that stresses the footings only by vertical forces has been developed. The arch horizontal force is resisted by prestressed ties (stress ribbons) that are situated above the shells.

Eliminating the abutments and substituting the wings by a continuously widened shell allows to design structures naturally connected with surroundings. So far two structures of this type have been built.

5.2 Willamette River Bridge, Eugene, Oregon, USA

A successful realization of the Redmond Arch Bridge has helped getting a project of another arch bridge that was built in a city of Eugene, Oregon, USA. The interstate freeway I-5 crosses the Willamette River, a local highway, a railroad and a junction ramp on north bound and south bound bridges

Figure 29. Willamette River Bridge.

Figure 30. Willamette River Bridge.

Figure 31. Pedestrian Bridge across the Olse River.

of lengths of 604.9 m and 536.1 m. These bridges replace original bridges built in fifties of the last century.

The main bridgeconsisting of two arch spans of length 118.9 and 126.8 m – see Figure 29. The deck that is formed by two girders and deck slab is stiffened by precast cross beams; the arches consist of two ribs without any bracing – see Figure 30. The approach bridges are multi-cell box girders of a variable depth that has the same perimeter as the arch deck. The substructure has a similar architectural and structural arrangement that the arch columns.

The bridge was erected progressively. At first, the arch ribs with the crown precast cross beams were cast. After the jacking, the midspan joints were cast. Then the columns were erected and longitudinal girders with the transverse cross beams are cast. After that the deck slab was cast.

5.3 Pedestrian Bridge across the Olse River connecting the Czech and Polish Tesin

The 95.40 m long bridge across the border River Olse that connects the Czech an Polish cities of Tesin includes an horizontal curve with a radius of 100 m. The bridge has four spans of lengths from 13 to 45 m. The deck consists of a slender box girder of a non-symmetrical streamline cross section that is stiffened by one side inclined arch in the main span – see Figure 31. The deck is fixed into the end abutments and is supported by elastomer pads on intermediate piers. To balance the torsional
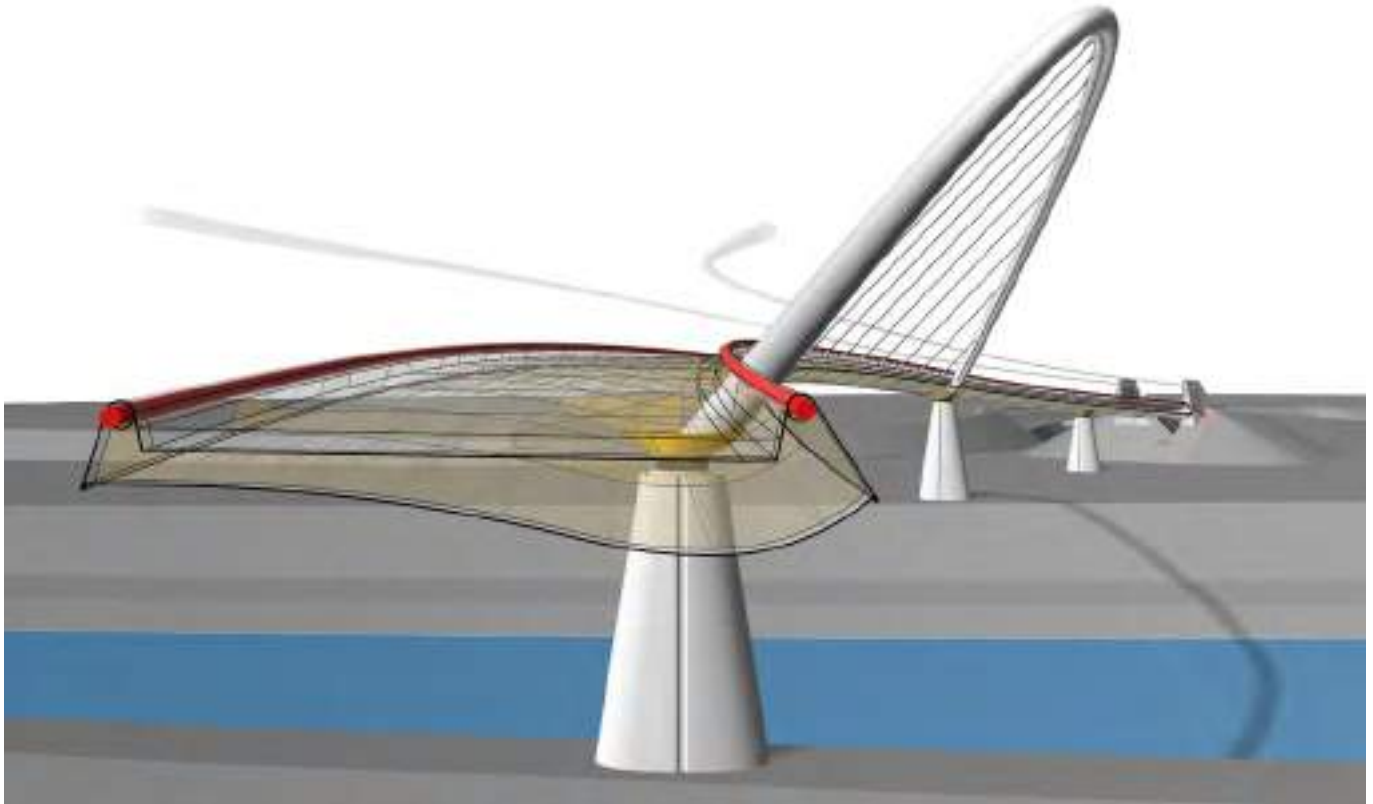
Figure 32. Structure of the Pedestrian Bridge across the Olse River.

Figure 33. Brno-Komarov Pedestrian Bridge.

moment due to the dead load, the deck is prestressed by radial cables situated at edge curbs – see Figure 32. Both, the girder and the arch are composite of steel and concrete.

5.4 Pedestrian Bridge across the Svratka River in Brno-Komarov

In Komarov district, a city, of Brno suburb, another arch structure has been built. The pedestrian bridge connects new sport facilities situated on both banks of the river. The bridge

consists of by a spine girder that is suspended on a central arch of a span of 58.5 m – see Figure 33. The arch force is resisted by a prestressed concrete deck that is integrated with the end diaphragms supported by drilled piles.

5.5 Minto Island Pedestrian Bridge across the Willamette River in Salem, Oregon, USA

We also participated in a design of the Minto Island Pedestrian Bridge that was completed this spring in a city of Salem,

Figure 34. Minto Island Pedestrian Bridge.

Figure 35. Svratka River Pedestrian Bridge.

Oregon, USA. The bridge that crosses the Willamette River consists of a continuous girder of 5 spans ranging from 15.24 to 93.88 m. The main span consists of a stress-ribbon deck that is suspended on two inclined arches of the 'butterfly' arrangement – see Figure 34. The stress-ribbon deck is assembled from precast segments and a composite deck slab. The arch force is resisted by prestressed concrete deck.

5.6 Pedestrian Bridge across the Svratka River in Brno, Czech Republic

This pedestrian bridge connects a newly develope business area with the old city center. It consists of a self-anchored stress ribbon & arch structure – see Figure 35. Both, the stress ribbon and the arch are assembled of precast segments made of high strength concrete and were erected without any temporary towers. Smooth curves that are characteristic for stress ribbon structures allowed a soft connection of the bridge deck with both banks.

the main arch span is 42.90 m and its rise 2.65 m, leading to a rise to span ratio of 1/16.19.. The arch consists of two branches that have a variable mutual distance and merge at the arch springs. The 43.50 m long stress-ribbon is assembled of segments of length of 1.5 m. In the middle portion of the bridge the stress ribbon is supported by low spandrel walls

of variable depth. At midspan the arch and stress ribbon are mutually connected by 2x3 steel dowels that transfer the shear forces from the ribbon into the arch. The stress ribbon is carried and prestressed by four internal tendons of 12 0.6" dia monostrands grouted in PE ducts. In the transverse direction the segments have variable depth with a curved soffit.

6.
CONCLUSIONS

The presented structures utilize different architectural and structural forms that are inherent in the constraints of the site and are economical and structurally efficient. They were well accepted both the public and professional.

References

[1] Strasky, J.: Bridges designed by Strasky, Husty and Partners. Puentes "La vida de los puentes", San Sebastian, Spain 2005.

[2] Strasky, J.: Puentes proyectados por Strasky, Husty and Partners (Parte I), (Parte II), Cemento Hormigón 2006, No. 887 (pp. 78-90) and 888 (pp.78-90), ISSN 0008-8919, 2006, Madrid.

[3] Strasky, J.: Design and construction of cable-stayed bridges in the Czech Republic. PCI JOURNAL, November.

Birth, development and future of the extradosed bridge
Nacimiento, desarrollo y futuro de los puentes extradosados

Akio Kasuga[a]

[a] *Ph.D. Chief Technology Officer. Technical Director. Sumimoto Mitsui construction. (Tokyo, Japan).*

ABSTRACT

The extradosed bridge ideas dates back to 1988, when Mathivat presented the concept. Since then, this structural type has been used worldwide. The first extradosed bridge was the Odawara Blueway Bridge completed in Japan in 1994. Although the principle was originated in France, it is fair to say that the bridge would not have spread, so far and so quickly around the world, without Japan's efforts to put the principle into practice. In this paper, the progress of the extradosed bridge from its birth to the today state of the art is analysed. Finally some thoughts on the future trends on design of this structural type are presented.

© 2019 Asociación Española de Ingeniería Estructural (ACHE). Published by Cinter Divulgación Técnica S.L.L. All rights reserved.

KEYWORDS: Extradosed bridge, butterfly web, multi-span bridge, hybrid bridge, cable anchorage.

RESUMEN

El primer concepto de puente extradosado fue presentado por Mathivat en 1988. Desde entonces este tipo estructural se ha construido por todo el mundo, siendo su primera realización el Puente Odawara Blueway terminado en Japón en 1994. Aunque la idea original surge en Francia, es justo decir que el desarrollo y la construcción de los puentes extradosados no habría llegado tan lejos y tan rápidamente sin los esfuerzos de Japón para poner en práctica el principio. En este artículo, se describe el progreso de los puentes extradosados desde su nacimiento hasta el estado actual de su técnica, así como una reflexión sobre las futuras tendencias del proyecto de este tipo estructural.

© 2019 Asociación Española de Ingeniería Estructural (ACHE). Publicado por Cinter Divulgación Técnica S.L.L. Todos los derechos reservados.

PALABRAS CLAVE: Puente extradosado, alma en mariposa, puente multivano, puente híbrido, anclaje de cables.

1.
INTRODUCTION

The world's first extradosed bridge, the Odawara Blueway Bridge (Figure 1), was completed in 1994, and I had the honor of working on its design and construction. In the twenty-something years since then, I have remained involved with extradosed bridges, including giving keynote speeches at international conferences, serving on conference committees, writing articles, and contributing to books. All in all, about half of my career as a bridge engineer has been intertwined with the advance of the extradosed bridge. That has given me a privileged view of the birth and development of this new structural form.

The extradosed bridge dates back to 1988, when Mathivat [1] first laid open his ideas, and has since spread worldwide, beginning with the Odawara Blueway Bridge. Although the principle originated in France, it is fair to say that the bridge would not have spread so far and so quickly around the world without Japan's efforts to put the principle into practice. The first extradosed bridge to be completed in France was the Saint-Remy-de-Maurienne Bridge over the A43 (1997). An extradosed bridge has since been constructed in French territo-

* Persona de contacto / *Corresponding author.*
Correo electrónico: Akio Kasuga: Aakasuga@smcon.co.jp

Figure 1. Odawara Blueway Bridge

Figure 2. Saddle anchorage of extradosed cables
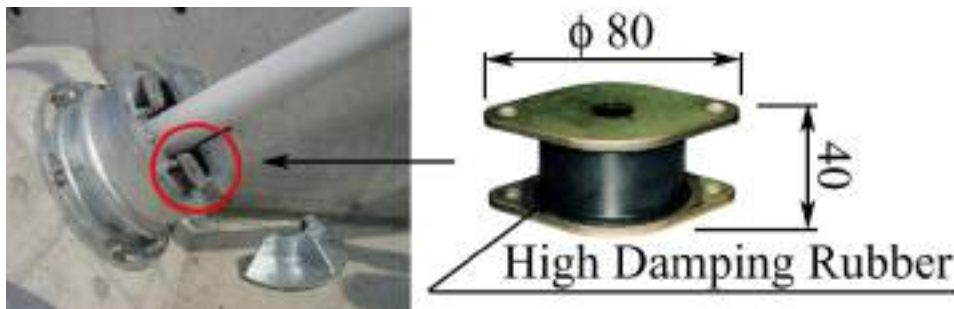
Figure 3. High damping rubber damper

ry on Réunion Island, but there are still no full-scale examples in mainland France.

When Mathivat's ideas first appeared in FIP Notes, Japanese readers paid little attention to them, seeing them as little different from the cable-stayed bridges that were already in service. Nevertheless, when construction of the Odawara Blueway Bridge commenced, the site proved a constant attraction to engineers, receiving over 3,000 visits in total. Considered in the context of the subsequent development of extradosed bridges, this represents a tribute to the expressway company for its bold decision to adopt an extradosed bridge design for the Odawara Blueway Bridge. In this paper, I would like to outline the progress of the extradosed bridge from birth to development, and present my views regarding directions for further development.

2.
ODAWARA BLUEWAY BRIDGE

Designing the world's first extradosed bridge, the Odawara Blueway Bridge, involved tackling a host of difficult issues. The first challenge was the design of the saddle for the cables on the pylons, which was being used for the first time on a concrete bridge. Detail design had to find a solution for securing the cables that could cope with a difference in tension on either side of the pylon in an earthquake. Secondly, the struc-

tural grounds behind adopting an allowable stress of $0.6f_{pu}$ for the cables had to be demonstrated. That meant clarifying how the cables differed from those of cable-stayed bridges, which were designed with a maximum stress of $0.4f_{pu}$. Thirdly, there was the challenge of having to control vibration in the cables, because lowering the safety factor for the cables reduced their fatigue strength. To achieve that, a new cable damping system had to be developed.

The key point of the saddle design was the detail design that took replacement of cables into account. By making the holes in the saddle keyhole-shaped, a cable being replaced could be shifted to one side so as not to interfere with the new cable. Also, we used on-site fabrication for the body of the anchorage that keeps the saddles in place in an earthquake, and devised a solution for securing the cables by wedging a bifurcated taper plate between the anchor and the pylon (Figure 2). We then verified the appropriateness of this new anchor structure by testing it with full-size models [2]. At the time, there were no saddle systems like this anywhere in the world, so we had no develop the technology from scratch with no examples for reference.

For the cable damping system, the systems in use at the time were either viscous dampers or oil dampers. I was working on this issue, and attempting to find a way to utilize high-damping rubber, which involved the rapid development of a high-damping rubber damper. After establishing a design methodology [3], a high-damping rubber damper that was sufficiently compact to fit inside the cable end was designed
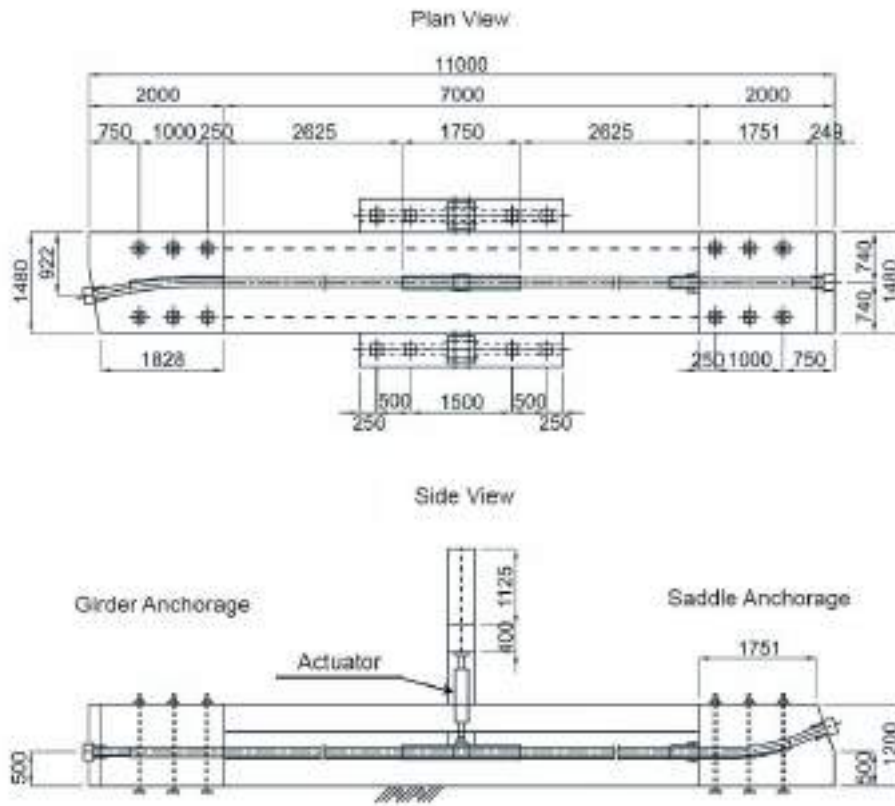
Figure 4. Cable bending fatigue test setup

(Figure 3). The Odawara Blueway Bridge adopts the premise of using a damping system to damp vibration of the cables, and because the cables are bent when anchored at both the saddle and deck anchorage, design had to take into account fatigue within the allowable range of vibration amplitude. We used the cable bending fatigue test [4] shown in Figure 4, which was probably the first time such a test had been performed. Once the cables start to vibrate, they reach 2 million oscillations in a very short time. Consequently, we considered that dangerous vibrations could be avoided by managing the fatigue limit, or in other words, by clarifying and managing the allowable amplitude. In a major inspection of the cables after 14 years in service, neither the cables nor the rubber dampers showed any signs of potentially problematic symptoms.

3.
CABLE ANCHORAGE STRUCTURES ON PYLONS

Following Mathivat's proposals, saddles were used on the first extradosed bridges. However, news reached Japan of fatigue tests on cable-stay bridge saddles in the US revealing strand fracture issues. The problem appeared to be due to fretting fatigue resulting from very small relative movements causing bare strands to rub against one another. We promptly conducted fretting fatigue tests [5], and set an upper limit, 50 N/mm², for variations of cable tension in the saddle (Figure 5). This has
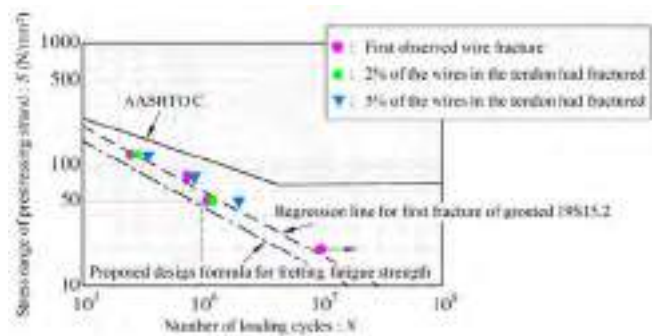
Figure 5. Fretting fatigue test results

been incorporated into Japan Prestressed Concrete Institute (JPCI) standards [6]. The tests were performed on uncoated strands, so a higher limit applies to epoxy-coated strands, which have greater resistance to fretting fatigue. The research concerning strand fretting fatigue, like that concerning cable bending fatigue, was a world first.

In fretting fatigue, the fatigue characteristics are greatly influenced by the contact pressure, which varies according to the number of overlapping layers of strands bent at the saddle. At the time, the only saddle systems available in Japan were for 19S15 or 27S15 cables, which have 19 or 27 strands. and that was a significant constraint on extradosed bridge design. Also, the studies on fretting fatigue had only covered cables with up

Figure 6. Ibigawa Bridge

Figure 8. Shimmeisei Bridge
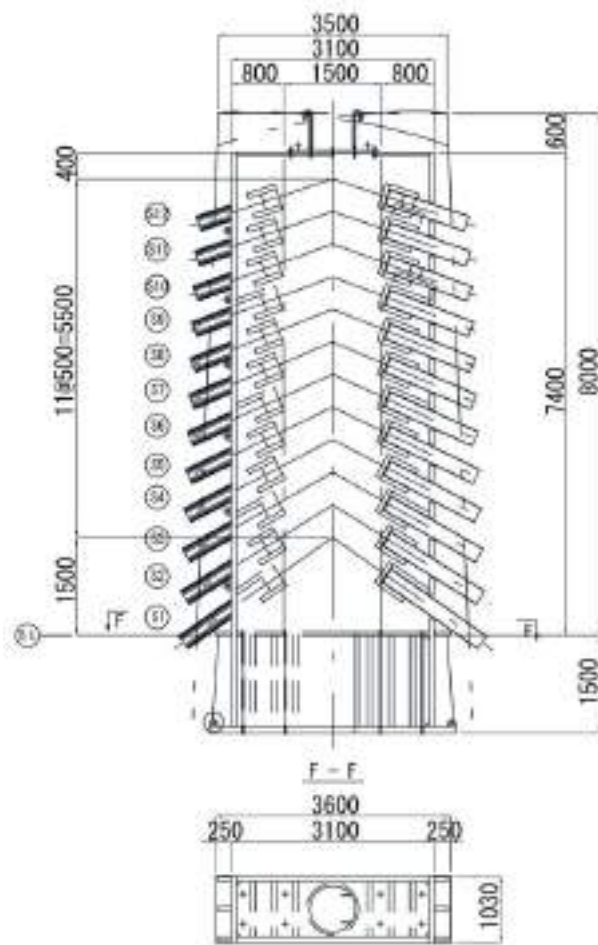
Figure 7. Steel anchorage box of extradosed cables
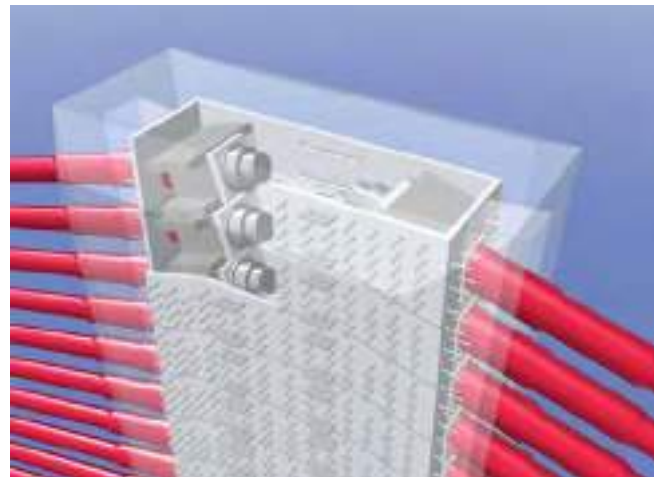
Figure 9. Composite extradosed cable anchorage system

Figure 10. Separated steel box anchorage

to 27 strands, so if wanted to use cables with more strands, we would have had to conduct a new set of fretting fatigue tests. Consequently, we had reached the limit of what was feasible with the saddles that were available.

In the Ibigawa Bridge (Figure 6), the design called for factory-made cables using wires, so a saddle was not an option.

From that point, steel box structures (Figure 7) became available as an alternative to saddles for anchoring the cables on the pylons. Later, for the Shimmeisai Bridge (Figure 8), we used steel boxes because the capacity of the extradosed cables exceeded 27S15, ruling out saddles. This brought the problem of the overall steel box structure being too heavy. For the Ibi

River Bridge, we had been able to use a large floating crane for erection, but here we had to find a land-based solution. Eventually, we designed a structure with separate steel boxes for individual cables and stacked the boxes without welding or bolting them together before integrating the structure with concrete (Figures 9 and 10). Setting the tolerance for the gap between the metal surfaces of the boxes to 0.5 mm, this creates a composite structure in which the concrete carries the full load of the vertical component of the cable forces, while the horizontal components is borne by the steel plates. The intervening concrete is not placed until after the overdosed cables are completed, so none of the horizontal components of the forces acts on the concrete.
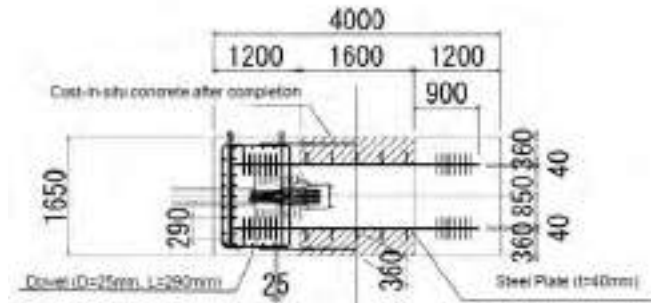
Figure 13. New composite cable anchorage system

Figure 11. Single steel plate type

Figure 14. DSI system

Figure 12. Extradosed cable anchorage with single plate of Mukogawa Bridge

Figure 15. Nonthaburi Bridge (Thailand)

If a bridge requires narrow pylons, making it difficult to use a steel box structure, an anchorage structure based on a single steel plate (Figure 11) can be used, as in the Mukogawa Bridge (Figure 12). The steel plate is fabricated with holes for dowel reinforcements, producing a simple structure that needs no welding at all, enabling a reduction in cost. To further reduce

costs, it is possible to use a composite structure with a concrete anchorage beam as shown in Figure 13. This structure has already been tested and verified, and is now ready for practical application.

Major enhancements were made to saddle designs after the issue of fretting fatigue arose, and saddle systems have now been developed that can handle large-capacity cables. Figure 14 shows an example with built-up steel sections in the saddle. With this German system, the cables are anchored directly to the steel, which completely eliminates fretting fatigue in the cables [7]. The main disadvantage of this sort of design is that the anchorages are exposed, so care is required with aesthetic and rust-protection considerations. We used this saddle system for the Nonthaburi Bridge (Figure 15), the first extradosed bridge in Thailand.

Figure 16. VSL system

Figure 17. Distribution ratio of vertical load VS stress change due to live load

Figure 18. Allowable stress versus stress change owing to live loads by JPCI and SETRA
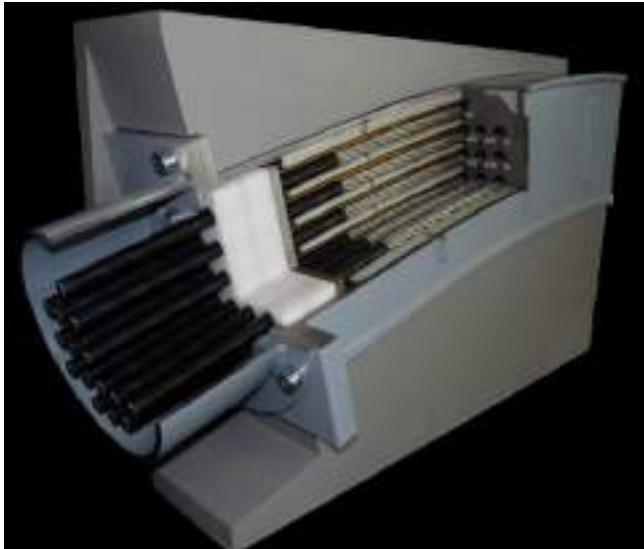
Another approach is to avoid bundling strands together, instead arranging each strand independently to minimize fretting fatigue. Figure 16 shows a typical Swiss system of this type [8]. It has undergone large-scale fatigue testing at the Technical University of Berlin [9], and uses teardrop-shaped holes to ensure that the strands are securely retained, enhancing frictional forces. For countries in seismic zones like Japan, there is the question of the extent to which that friction could be relied upon, and consideration would also have to be given to the issue of how to achieve consistency during construction.

Personally, based on maintenance and cost considerations, I prefer anchorage structures to saddle systems on the pylons. And when constructing bridges in a seismic zone, it is always important to gain a full understanding of the seismic performance of any systems or components originally designed for use in areas with few concerns regarding earthquakes. The Odawara Blueway Bridge project was the first in the world to develop a saddle for a full-scale concrete bridge. The expertise accumulated on that project has been of great help in the further development of saddle systems. And now there is also much more variation in the anchorage structures that can be used for anchoring extradosed cables to pylons, providing bridge engineers with brouder of options.

4.

THE DIFFERENCE BETWEEN EXTRADOSED AND CABLE-STAYED BRIDGES

Ever since the Odawara Blueway Bridge project, I have frequently been asked how an extradosed bridge differs from a cable-stayed bridge. Mathivat's proposal only explained that he was using the same factor of safety as for regular external cables of the relatively small influence of fatigue. That is reasonable, but it leaves open the questions of what the limits are, and under what conditions $0.6f_{pu}$ can be used. Finding the answers required a substantial investment of time and effort.
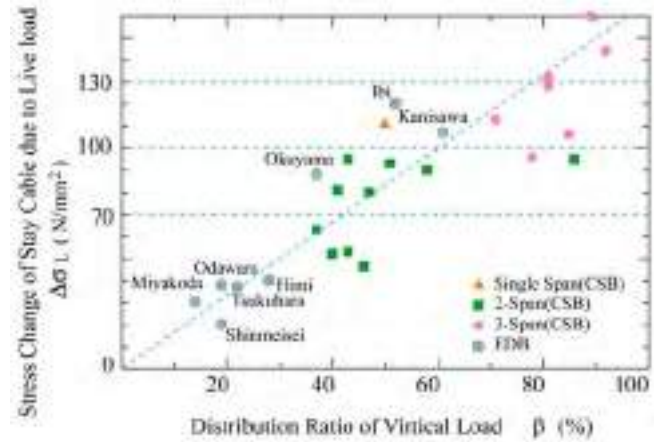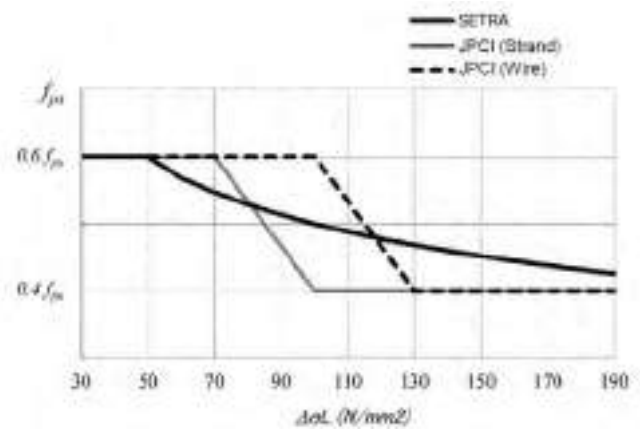
The first issue is the definition of a cable-stayed bridge and extradosed bridge. The cable-stayed bridge was already covered by current standards, which stipulated an allowable stress for the cables of $0.4f_{pu}$ in Japan. I decided to think of cable-stayed bridge and extradosed bridge as part of a continuum rather than having a clear borderline between them, and proceeded to investigate and verify the safety factor by focusing on the proportion of live load carried by the cables [10]. Figure 17 shows the results of that investigation. The distribution ratio of vertical load β and the stress change in the stay cables due to live load can be seen to be correlated, which means that the latter can be used as a design parameter. For cable-stayed bridges, β is in the region of 80–100%, as the cables carry nearly all the live load. In contrast, for extradosed bridges, β is in the region of 10–20%, with the main girder carrying most of the live load. There is a clear difference between the two types of bridge, but no clear boundary between them. Consequently, engineers are free to determine the proportions carried by the cables and by the main girder. The concept of the extradosed bridge provides a link between cable-stayed bridges and girder bridges, and is a structural form with a broad range of applicability. Figure 18 shows the standards adopted by JPCI (Japan)
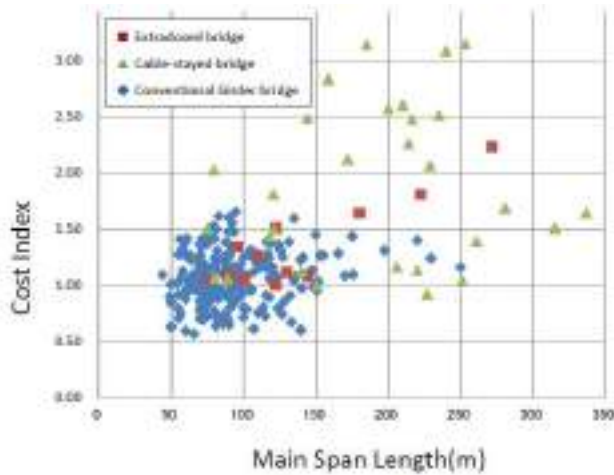
Figure 19. Comparison of cost index in Japan

and SETRA (France). These standards differ as to whether the transition should be straight-line or curved, but the basic approach is the same.

The Japanese standards have one more feature, in that they define the allowable stress in terms of stress variation. This has the advantage of enabling engineers to consider the limit separately for each individual cable. In other words, the allowable stress can differ from cable to cable. Consequently, engineers can assume a low level of allowable stress where there is a large stress variation, or a high level when there is a small stress variation. This permits the adoption of efficient designs that were not possible under conventional standards that determined a single allowable stress for the whole bridge. Furthermore, this design philosophy can be applied to cable-stayed steel bridges as well as to concrete bridges. In each case, what matters is the proportions of live load carried by the cables and the girder. The JPCI standards take the stance that there is no borderline between cable-stayed and extradosed bridges. Today, bridge engineers around the world are increasingly accepting this philosophy.

Another point worth mentioning is the difference in construction cost. Figure 19 shows a comparison of cost index for a number of cable-stayed bridges, girder bridges, and extradosed bridges. The base for the index is the cost for a girder bridge with a 100m span (cost index set to 1.0). Structurally, extradosed bridges fall between girder bridges and cable-stayed bridges, and this chart shows that, broadly speaking, a similar relationship applies to cost considerations. The chart only takes the superstructure into account, so the main factor keeping down the extradosed bridge cost is probably the ability to use lower pylons and simpler cable systems.

5.

COMPOSITE GIRDER EXTRADOSED BRIDGES

Composite bridges are structures that combine steel and concrete, selecting the material to suit the characteristics required for each part of the bridge. In Japan, where there are frequent earthquakes, reducing girder weight brings a range of bene-

fits, and this has been a driving force behind the remarkable pace of development over the past twenty years. Reducing the weight of the superstructure is the key to innovation in long span bridges supported by cables. The reason is that this approach enables stiffness to be increased without increasing girder weight.

The corrugated steel web bridge dates back to 1965 when Shimada proposed that corrugated steel plate may be used in the web of main girders [11]. However, it was a long time before this marvelous concept was realized in an actual bridge. That was in 1984, when a composite bridge using this approach was completed in France, far away from the birthplace of the idea. By replacing the concrete web with corrugated steel plate, a corrugated steel web bridge enables the weight of the main girder to be reduced by around 10 to 15%. An example of corrugated steel webs used in an extradosed bridge includes the Himi Bridge [12] (Figure 20). The Himi Bridge is particularly interesting as it was the world's first use of a corrugated steel web in a cable supported structure. There are another three examples of corrugated steel web extradosed bridges in Japan.

Moreover, there is one example of the extradosed bridge, the Fudo Bridge, utilizing composite truss techniques but replacing just the web with a steel pipe truss, as can be seen in Figure 21. In addition, as a means of reducing axial forces acting on the truss nodes, it is possible to use a hybrid structure combining a concrete box girder with a space truss as shown in Figure 22.

Figure 20. Himi Bridge

Figure 21. Fudo Bridge
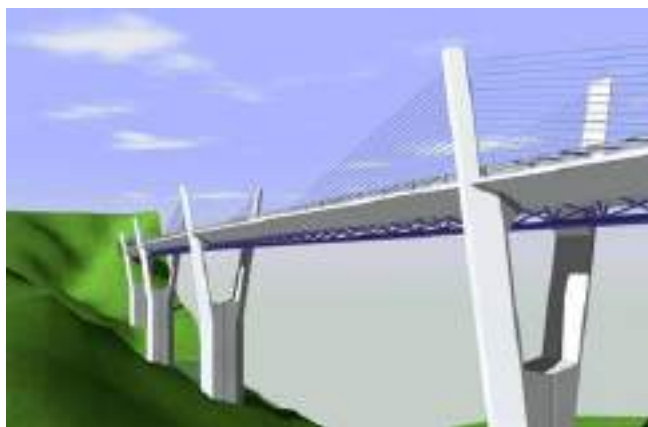
Figure 22. Hybrid combining concrete and space truss
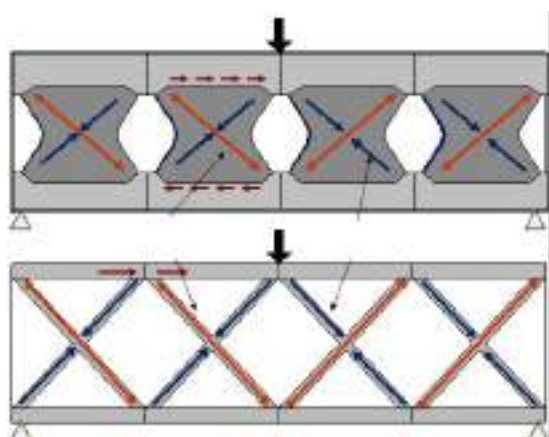
Figure 23. Behavior of butterfly web bridge
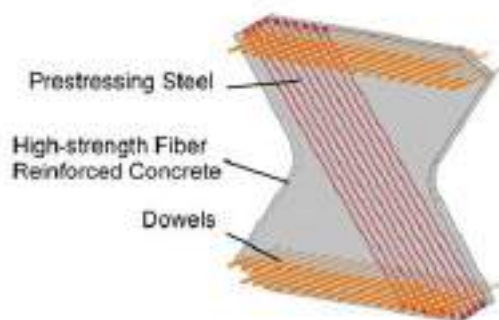
Figure 24. Butterfly web panel

6.

BUTTERFLY WEB FOR LARGE SPAN EXTRADOSED BRIDGES

6.1 Butterfly web bridge

The butterfly web [13] is a new structure with butterfly-shaped web members having the following characteristics.

(1) The web is configured with butterfly-shaped panels placed independently and not joined continuously. The shape limits the orientation of compression and tension in the panel due to shear forces, meaning that the structure is similar to a double warren truss (Figure 23).

(2) The butterfly web uses 80 MPa steel fibre reinforced concrete, and has prestressing steel oriented in the direction that tensile forces act (Figure 24), limiting the occurrence of cracks. It does not use steel reinforcements, relying instead on steel fibers and prestressing to achieve the required strength.

(3) Transmission of shear forces between the butterfly web and deck slabs is achieved by the joint between the slab concrete and dowels embedded in the panel.

Many corrugated steel web bridges and steel truss web bridges have been built in Japan. These bridges had rational structures and excellent structural characteristics, but at the same time, they required complex machining of steel members, on-site welding, or other special skills for fabrication or construction. In contrast, as the butterfly web is a precast product, all that is needed to construct a girder is to combine the web with the slabs on site. The prestressing steel oriented in the same direction as the tensile forces in the web is pre-tensioned at the factory, so there is no need to work on the butterfly web at the construction site. The potential weight reduction of the main girder is similar to that of a corrugated steel web bridge, achieving about a 10% to 15% reduction compared to a conventional box girder section. Consequently, the length of segments that can be constructed using a form traveler can be 50% longer because of light weight of the girder.

A butterfly web bridge, which uses butterfly-shaped panels instead of a double warren truss, is a new structure that has both the corrugated steel web bridge's advantage of being able to simplify the joints with the concrete slabs, and the truss bridge's advantage of not needing on-site work to make joints between the butterfly-shaped panels that carry the shear forces.

One of these solutions for long span extradosed bridges was used in an innovative project that was completed in 2017. The Mukogawa Bridge, shown in Figure 25 and Figure 26, is an extradosed bridge using butterfly web technology. This is a 5-span continuous rigid frame bridge with a span length of 100 m. The tallest piers are 81.2 m, and they were designed for rapid construction. The cross section incorporates four butterfly webs, and the extradosed cables are located in the center of the cross section. The main girder is constructed by free cantilevering, with individual segments having a length of 6.0 m and incorporating two butterfly web panels parallel to the longitudinal direction. After setting panels, the concrete deck is cast in place. The reduction in superstructure weight achieved enables a substantial reduction in pier thickness and the size of foundations.

6.2 Large span extradosed bridge

Conventional explanation of the extradosed bridge used to be that it was a structure that filled the gap between girder bridges and cable-stayed bridges for spans of up to 250 m. However, the use of a butterfly web structure now enables main girder stiffness to be increased without an increase in weight, making it feasible to construct extradosed bridges with span lengths in around 500 m. Moreover, the openings in a butterfly web girder account for 30% of the area of an equivalent full web girder, leading to greater wind stability.

Figure 25. Mukogawa Bridge
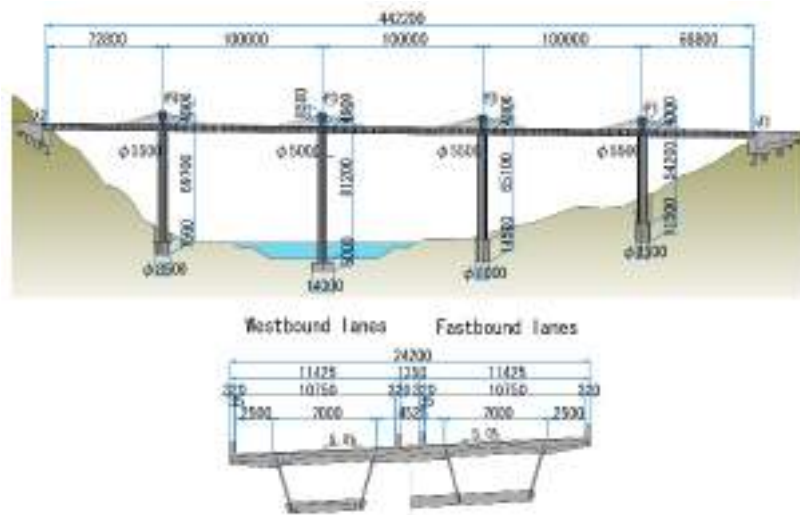
Figure 26. General view of Mukogawa Bridge
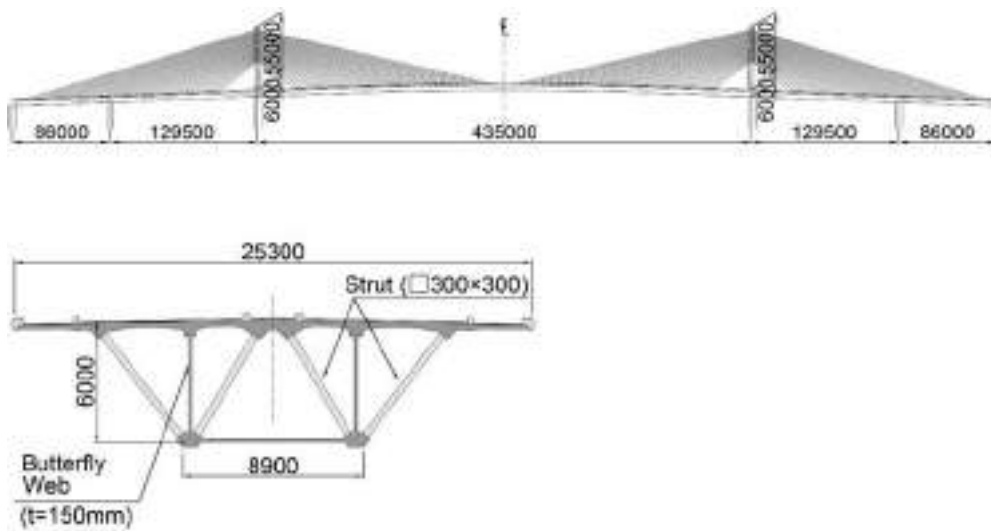
Figure 27. Extradosed Type (a) General view (b) Cross section
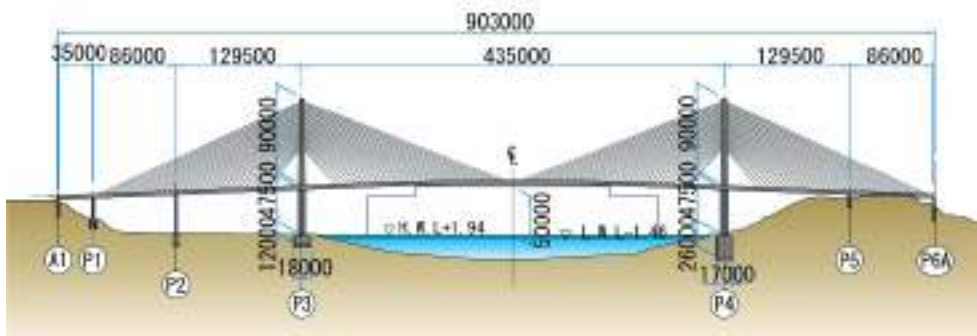
(a)
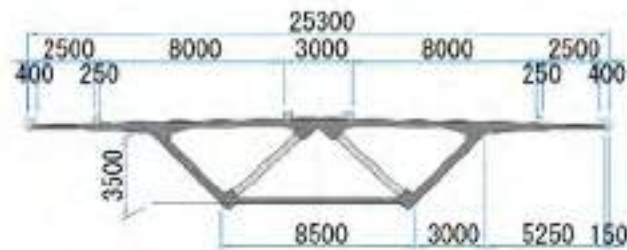
(b)

Figure 28. Cable-stayed type (Bai-Chai Bridge, 2006) (a) General view (b) Cross section
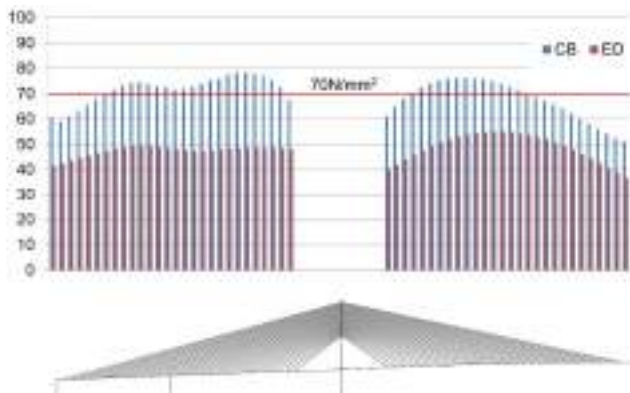
Figure 29. Stay cable stress change due to live load
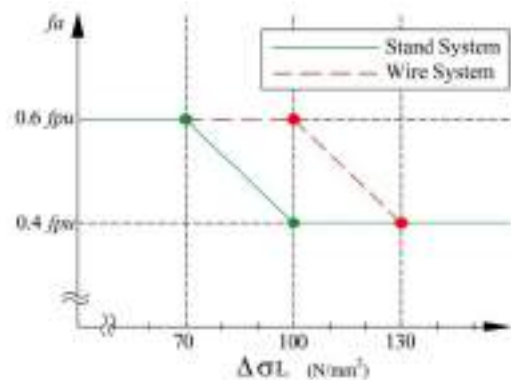
Figure 30. Allowable stay cable stress VS stress change owing to live loads

An extradosed bridge with a central span of 435 m as shown in Figure 27 [14] is considered, and it has lower pylons, about 60% of the height of the towers for the cable-stayed bridge, Bai-Chai Bridge (Figure 28). The girder height is 6.0 m in the extradosed type, using a single plane of stay cables and struts inside the box girder. The extradosed bridge uses a butterfly web to counter the increase in weight due to the larger girder height. Consequently, the superstructure weight is unchanged compared with conventional cable-stayed bridges, but the stiffness of the main girder is doubled. Figure 29 shows the variation in stay tension due to live loads. The JPCI standards in Japan (Figure 30) permit a maximum allowable stress of $0.6f_{pu}$ for stay cables, even for this sort of long span extradosed bridge. The number of cables required is about 20% more than for the cable-stayed bridge, but because the weight reduction technology has produced a stiffer main girder without an increase in weight, the pylons can be shorter, which makes this structure very competitive in earthquake-prone Japan. Table 1 shows a comparison of the material quantities for the two configurations. The amount of concrete for the extradosed bridge using butterfly webs is almost the same, despite having a deeper girder. And because the safety factor can be lowered with the use of an extradosed bridge, the weight of stay cables is similar to that of the cable-stayed bridge, even with a shorter pylons. This

TABLE 1
Comparison of material quantities (Three spans).

			CB	ED
Concrete	Girder	m³	13200	13400
	Tower	m³	2200	1400
Rebar		ton	3190	2751
Prestressing steel		ton	220	195
Stay cable		ton	1040	1042
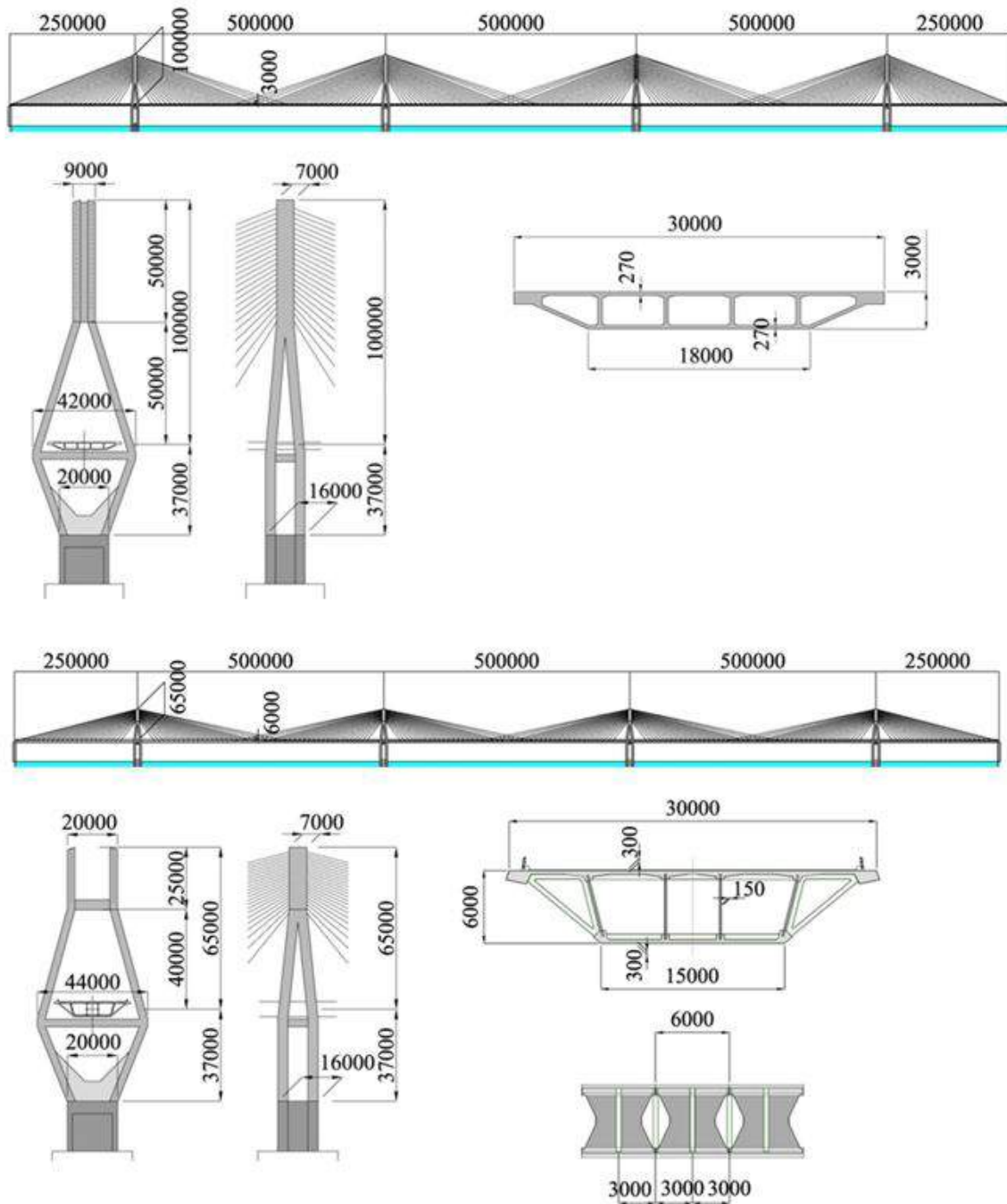
Figure 31. 500-m Five-span bridge. (a) Cable-stayed type and (b) Extradosed type

demonstrates that a long span extradosed bridge with reduced weight main girder is feasible.

6.3 Multi-span large extradosed bridge

The benefits of butterfly web are particularly clear with long span multi-span bridges, which tend to have a lower overall stiffness. Increasing the stiffness of the main girder enables the bridge to be designed with lower pylons, enhancing seismic performance and suppressing cable stress variation.

The models used for this comparative study are a cable-stayed bridge and an extradosed bridge composed of five continuous spans with a central span of 500 m (Figure 31). In order to raise the overall stiffness of the multi-span cable supported structure, overlapping cables are distributed at the middle of the span, and the stiffness of the bridge piers and pylons is increased. Moreover, highly stiff butterfly webs with a 6.0 m depth are used for the extradosed bridge. Using these two structures, stay cable stress variations at the serviceability limit state was compared, and the structural feasibility of the proposed continuous long span extradosed bridge is verified [15].

Figure 32 shows a comparison of the stress variations in stay cables due to live loads. According to the JPCI standards (Figure 30), up to $0.6f_{pu}$, the limit value for stay cable tension,
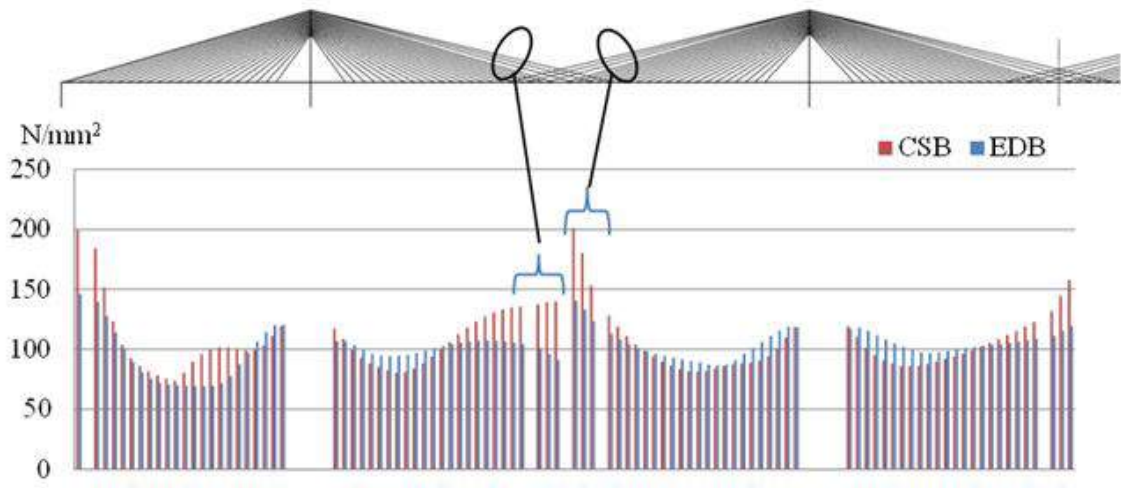
Figure 32. Stay cable stress variations owing to live loads
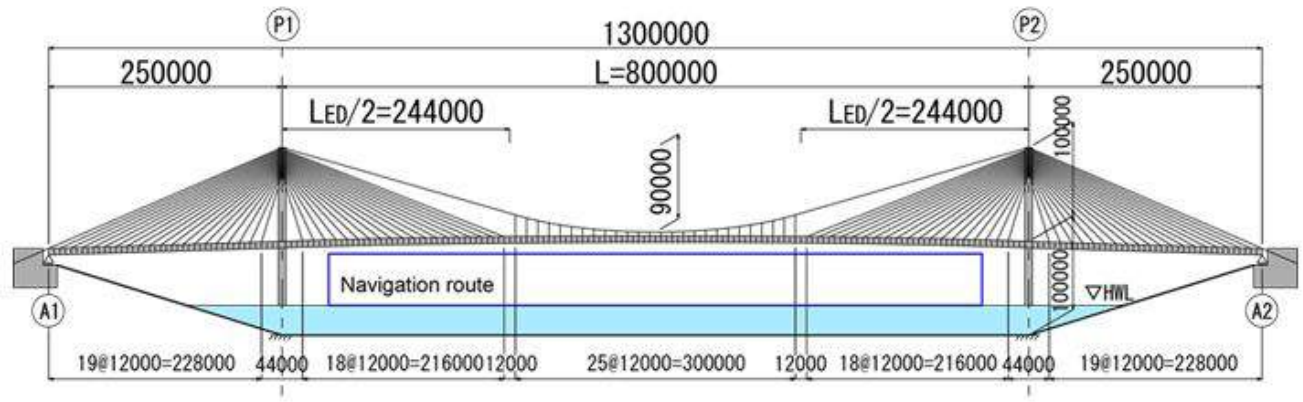
Figure 33. Hybrid of extradosed and suspension bridge with 800m span

is allowed for road bridges as long as the stay cable stress variation is 70 N/mm^2 or less. However, it was confirmed that almost all of the cable stress variation exceeds 70 N/mm^2 except some cables of the side span because multi-span structures are very flexible. Table 2 shows a comparison of the material quantities for the two configurations. The amount of concrete for the extradosed bridge using butterfly webs is lighter, despite having a deeper girder. Moreover, the material required for the pylons was reduced. However, there is no big difference of the weight of stay cables in the multi-span structures.

6.4 Large span hybrid design for future generations of bridges

The first idea of hybrid structure in the Brooklyn Bridge which combines the suspension system with the stays to achieve more efficient structural system has been noticed [16]. However, these hybrid structures are generally adopted with higher towers, in stress which consequently, the angular change of the main suspension cable at the tower saddle could be larger and

causes increasing secondary stresses in the main cable to lead the cable becomes more critical in fatigue.

Therefore, to deal with the secondary stresses in main suspension cable and as well as to enhance the aerodynamic stability of the hybrid structure, we aim to develop a long span concrete box girder bridge which is a hybrid between an extradosed structure and a suspension structure. By using a deeper girder, the hybrid structure is expected to be stiffer and at the same time, the angular change of the main suspension cable will be smaller due to their short towers.

Furthermore, in order to reduce the weight of the girder,

TABLE 2
Comparison of material quantities (Five spans).

			CB	ED
Concrete	Girder	m^3	48900	43700
	Pylon	m^3	18500	1400
Rebar		ton	15960	2751
Prestressing steel		ton	259	261
Stay cable		ton	6030	6300

Figure 34. 800m span hybrid bridge

the butterfly web girder in which the webs were replaced by thin panels with a butterfly-wing shaped was adopted. In past studies, butterfly web has an open section of around 30% and can reduce the weight of the superstructure from 10% to 20%. It is also expected that its wind resistance is appropriate, due to its special openings, and maintenance is easier because of brightness in the girder.

As a case study, a hybrid of extradosed and suspension bridge with 800 m span of concrete butterfly web girder was suggested (Figure 33) [17]. The bridge basically consists of a main span 800 m long and effective width of 30 m respectively. Stiffening girder is a structural element subjected directly to the live load and transfer the vertical load globally to the main tower through the cable system. For the extradosed bridge, by making the girder deeper, the stiffness of the girder increases so that the load distribution ratio for the cable is smaller and makes the material consumption effectively. The towers are considered to be 100 m in height as well as the girder is set to 7 m deep with 150 mm butterfly web.

In a hybrid structure system, some important issues have been raised, such as the discontinuity of the system and how to optimize the span of the extradosed area to achieve an economical efficiency as well. The hybrid systems with three different extradosed-to-span ratios, 79%, 61% and 43% respectively, are examined and investigated their structural behaviors. Herein, the extradosed-to-span ratio is the ratio of extradosed span (L_{ED}) to main span (L). After a parametric study, it was confirmed that this new type structure of hybrid bridge was able to be soundly designed. Moreover, it was found that the system with extradosed-to-span ratio of 61% used the least materials than the others (Figure 34).

7
CONCLUSIONS

When the construction of the Odawara Blueway Bridge was reported in the *Engineering News Record*, using the unfamiliar term "extradosed" coined by a French engineer, one editor jokingly asked in its editorials if regular cables would now have to be called "intradosed" [18]. Now, however, extradosed bridges have become so familiar to the community that no-one makes such comments any more. I am delighted that extradosed bridges have progressed to such an extent. My only regret is that I was unable to meet Jacques Mathivat before he passed away in 2012. There are lots of questions that I wanted to ask

him about the structural form that he introduced, and I would have been very keen to hear his thoughts on the projects that I have been involved in.

My story of the extradosed bridge began with Mathivat's theory and the Odawara Blueway Bridge. I have now been involved with extradosed bridges for a substantial proportion of my career as a bridge engineer, and have always felt a close affinity for the structure as it took form and developed. And it is a great satisfaction to have been able to propose an evolution that addresses the challenge of longer spans, further extending the applicability of the extradosed bridge.

Just as partially prestressed concrete concept acts as a link between reinforced concrete and prestressed concrete, the extradosed bridge has linked the cable-stayed bridge and the girder bridge. In doing so, it has greatly expanded the degree of freedom available for designs. That sense of freedom is surely one of the reasons why bridge engineers around the world continue to construct extradosed bridges.

References

[1] Mathivat, J. Recent Development in Prestressed Concrete Bridges. *FIP notes*: pp15-21. 1988/2.

[2] Kimizu, T, et al, Research on Saddle System of Odawara Blueway Bridge, Prestressed Concrete, JPCA, 1994. (in Japanese)

[3] Kasuga, A, et al. Testing of High Damping Rubber Damper for Stay Cables, EASEC-5, Australia, pp243-246, 1995

[4] Onodera, I, et al, Bending Fatigue Test for Stay Cable System of Odawara Blueway Bridge, JPCA Symposium 1995. (in Japanese)

[5] Fujita, M, et al, Fretting Fatigue Characteristics in the Curved Layout of Large-capacity Prestressing Strands, 15th US-Japan Bridge Engineering Workshop, Tsukuba, 1999

[6] JPCI. November 2000. *Specifications for design and construction of prestressed concrete cable-stayed bridges and extradosed bridges*: Japan Prestressed Concrete Institute.

[7] https://www.dywidag-systems.com/emea/products/stay-cable-systems/dynar-link-anchor-box-system.html

[8] http://www.vsl.com/business-lines/systems-and-technologies/stay-cable-systems.html

[9] Schlaich, M, Abdalsamad, A, Annan, R, Fatigue and Tensile Tests of a 55 Strands Saddle System, *Proceedings of 3rd fib International Congress 2010*, *Washington DC*.

[10] Ogawa, A, Kasuga, A, Extradosed Bridges in Japan, FIP Note, pp11-15, 1998/2.

[11] Shimada S. Dec. 1965. Shear Strength of Steel Plate Girders with Folded Web Plate (Ripple Web Girders). *Journals of the Japan Society of Civil Engineers* No.124: 1-10. (in Japanese)

[12] Maeda Y., et al. 2002. Design and Construction of the Himi Bridge – Extradosed Bridge with Corrugated Steel Web. 1st fib Congress 2002 Session1: 95-100. Osaka

[13] Kasuga, A., et al. 2010. Study of a bridge with a new structural system using ultra high strength fiber reinforced concrete. *Proceedings of 3rd fib Congress*: Washington DC.

[14] Kasuga, A., et al. 2015. Study on 500m span extradosed bridges. fib Symposium Copenhagen.

[15] Kasuga, A. Multi-span extradosed bridge, Multi-Span Large Bridge, pp67-82, 2015.

[16] Gimsing, N. J. et al. 2012, Cable supported bridges, John-Wiley, West Sussex, UK.

[17] Salpisoth, H. et al. 2017, Study on the design of an extradosed and suspension hybrid bridge with 800m span of butterfly web girder, *fib Symposium, Maastricht*.

[18] Engineering News Record, McGraw-Hill Construction Weekly, p90, February 21, 1994.

Cable stay bridge

Puentes atirantados

Naeem Hussain[a]

[a] Structural Engineer. Director. Global Bridge Leader. ARUP. (Hong Kong, China).

ABSTRACT

This paper presents the typological and conceptual evolution of cable stayed bridges from the Kings Meadow Bridge of 1817, to the recent Third Bosphorus Bridge 2017. The paper highlighted the breakthrough in understanding cable stay bridge structural behaviour of E. Torroja in 1926 with the Tempul Aqueduct, and the relevance of the Dischinger's publication 'Suspension for very heavy loads' published in 1949 where the design basis for stay cables were analysed for the first time.

The paper also remarks the significance of the Dusseldorf North Bridge, designed by Leonhardt where the special structural analyses issues of cable stay bridges was essentially solved. The text includes the specific aspects related to multispan cable stayed bridges as well as those particular issues Finally, some thoughts on the limits of this typology and its future development are presented, among which the use of new materials is indicated.

© 2019 Asociación Española de Ingeniería Estructural (ACHE). Published by Cinter Divulgación Técnica S.L.L. All rights reserved.

KEYWORDS: Cable stayed, stay, typology, conceptual design, aesthetic.

RESUMEN

En este artículo se presenta la evolución tipológica y conceptual de los puentes atirantados desde el Kings Meadow Bridge de 1817, hasta el reciente Tercer Puente del Bósforo 2017. El artículo destaca la aportación fundamental de Eduardo Torroja en 1926 en la comprensión del funcionamiento de esta tipología, con el acueducto de Tempul y el salto posterior cualitativo dado por Dischinger en 1949 con su publicación "Suspensión de cargas pesadas", en el que explicó por primera vez las pautas para el diseño de tirantes.

El artículo también destaca el Puente Norte de Dusseldorf North proyectado por Leonhardt en el que ya se resuelven los aspectos especiales del análisis estructural de esta tipología. En el texto, se incluyen además, los aspectos específicos de los puentes atirantados multivanos y aquellas cuestiones particulares correspondientes a las últimas realizaciones en las que ya se han superado ya los 1000 de luz. Por último se presentan unas reflexiones sobre los límites de esta tipología y su desarrollo futuro, entre los se indican el uso de nuevos materiales.

© 2019 Asociación Española de Ingeniería Estructural (ACHE). Publicado por Cinter Divulgación Técnica S.L.L. Todos los derechos reservados.

PALABRAS CLAVE: Puente atirantado, tirante, tipología, diseño conceptual, estética.

1.
INTRODUCTION

The concept of supporting a girder with taught cables goes back a long way, but the first proven bridge with inclined stays was Kings Meadow Bridge in England, designed by James Redpath and John Brown and constructed in 1817. However at that time the structural action was not fully understood in that the stays have to be tensioned and the forces in the stays tuned to pick up the girder load directly. Failures of these type of bridges in the early 1800's put a damper on development of stay cable cable bridges.

The break through in understanding cable stay bridge structural behaviour came in 1926 with the Tempul Aqueduct designed by Eduardo Torroja. However it was not till after the Second World War, when cable stay bridge technology flowered with Dischinger's publication 'Suspension for very heavy loads' published in 1949. In it Dischinger for the first time gives the design basis for stay cables.

Figure 1. Stromsund Bridge, Sweden.

Figure 2. Knie Bridge, Dusseldorf, Germany.

The first modern concrete cable-stay bridge is the Donziere-Montragon Bridge in France that was completed in 1952. It was designed by Albert Caquot who stressed the high strength steel tendons to support the stiff concrete roadway and anchored the stay cables in the deck which induced compressive stresses in the deck.

The Stromsund Bridge, which represents a leap in the development of cable stay bridges, was constructed in Sweden in 1956 and is generally looked upon as the first modern cable stay steel bridge, because the concrete deck slab distributes only local wheel loads and is not composite with the steel beam, Figure 1. The concrete slab does not participate in carrying the overall main girder bending moments and normal forces and hence Stromsund Bridge is considered as a steel bridge. Dischinger advised on the design of Strosmund Bridge.

The development of lightweight steel orthotropic decks allowed cable stay bridges with slender steel decks to be constructed. The Dusseldorf bridge family of three cable stay bridges, whose planning commenced in 1952, are a significant and early application of the use of orthotropic decks. Their

Figure 3. Oberkassel Bridge, Dusseldorf, Germany.

Figure 4. St. Nazaire Bridge, France.

design, fabrication and construction initiated the development of cable stay bridges worldwide. The three bridges, Dusseldorf North Bridge, Knie Bridge, and Oberkassel Bridge were designed during 1953 and 1954 and completed in 1957, 1969 and 1976 respectively, Figures 2 & 3. The chief designer for the North Bridge and Knie Bridge was Fritz Leonhardt and for the Oberkassel Bridge the designer was Hans Grassl.

The special structural analyses issues of cable stay bridges was essentially solved with the design of the Dusseldorf North Bridge: such as the development of their influence lines including stress influence lines; non-linear effects from compression with bending in the deck; the free selection of the run of moments under permanent loads; and the structural analyses of the free-cantilevering construction. The structural issues of the buckling of the free-standing towers, loaded and elastically supported by the stay cables were resolved.

The span range of Dusseldorf bridge family was modest in the range of 260-319 m, and the number of stays used were also modest, a maximum of four primarily because of the limitations of doing analyses by hand. The advent of computers has had a significant effect on computation powers, which meant that cable stay bridges with a large number of stays could be analysed.

The first bridge to break the 400 m span barrier is the two tower St. Nazaire Bridge across the River Loire in France with a span of 404 m, which was completed in 1975. The steel box girder deck is continuous over the three stayed spans and has an aerodynamically shaped cross-section, Figure 4.

Cable stay bridges with concrete decks were also being developed and with the construction of the 235 m main span Maracaibo Bridge in 1962, Figure 5, designed by Riccardo Morandi, they tend to now form the preferred economical system

Figure 5. Maracaibo Bridge, Venezuela.

Figure 6. Brotonne Bridge, France.

Figure 7. Barrios de Luna Bridge, Spain

Figure 8. Alex Fraser Bridge, Vancouver, Canada.

for spans in the range of 200-300 m, especially in developing countries where concrete construction is more economic than steel construction.

Brotonne Bridge in Normandy France, Figure 6, designed by Jean Muller and completed in 1977, has a unique main span single cell box girder with inclined webs. The box was constructed using precast webs and in situ concrete for the rest. All elements of the box girder are post-tensioned, the webs, top slab, bottom slab and the inclined ties.

In the 1980's concrete deck spans in excess of 400 m were realised. Spanish designers and constructors have usually been in the fore-front in the use of concrete. Javier Manterola and Carlos Fernando Casados designed the concrete box girder deck Barrios de Luna Bridge in Spain with a record span of 440 m which was completed in 1983, Figure 7, and was the longest span for any type of cable stay bridge at that time. With back spans of 99 m, the span ratio of backspan to main span is only 0.23 compared to the usual ratio of 0.4. This required unique heavy 35 m long concrete abutments on both sides as counterweights. The decks are monolithic with the abutments and there is a longitudinal movement joint at midspan to cater for temperature variations and shrinkage and creep.

Steel concrete - composite bridges also began to be used increasingly due to their economy and constructability. Compared to steel bridges, savings are achieved because concrete can carry compression forces more economically than steel, and a concrete deck slab is more economic than an orthotropic deck. Also compared to concrete bridges less cable steel and smaller foundations are required. A typical composite deck consists of longitudinal steel I-section or boxes along the edges and transverse I-section girders with a composite insitu or precast concrete deck slab. The deck can be constructed in small units with steel main and cross girders and precast road slabs erected with light lifting equipment.

The next increase in span length of whatever deck type came in 1986, with the construction of the composite ladder deck Alex Fraser Bridge in Vancouver with an H-tower and span of 465m, Figure 8. The designers were Peter Buckland and Peter Taylor who used steel I-section girders along the edges with transverse I-section girders and composite deck slab, which are typical for composite decks.

The 500 m span barrier was broken in 1991 with the construction of the 530 m main span Skarsundet Bridge at Trondheim in Norway. This is still the longest concrete cable stayed span in the world. The concrete towers have a box girder cross-section, and the main girder has an aerodynamically advantageous triangular box cross-section which is solid in the relatively short backspans to provide counterweight, Figure 9.

The 600 m span barrier was broken in 1993 with the construction of the 602 m span Yang Pu Bridge in Shanghai, China, Figure 10. The main span comprises of two edge steel box girders connected with steel transverse girders and a concrete deck slab. The bridge was designed by the Shanghai Municipal Design Institute (SMEDI) under the direction of Lin Yuan Pei.

The major significant jump in span length came in 1995 with the completion of the Normandy Bridge in France, the lead engineer for which was Michel Virlegeoux. The bridge has a span of 856m and concrete A-frame towers, Figure 11. The main span comprises of a central 624 m orthotropic box

Figure 9. Skarsundet Bridge, Trondheim, Norway.

Figure 10. Yang Pu Bridge, Shanghai, China.

girder, with the outer 116m on each side being an extension of the concrete box girder backspans. An innovation in this bridge is the deck which is embedded with the towers and with a pronounced curved vertical profile. The effects of the temperature variation are catered for by the vertical deflection of the curved deck.

Normandy Bridge was followed soon after by the 890 m span Tatara bridge in Japan with a diamond shaped tower and a steel orthotropic box girder deck, which was completed in

1999, Figure 12. The bridge was designed by the consultant Chodai. Steel towers have been used to minimise load on the foundations and hence reduce their size.

The bridges mentioned above were single deck road bridges. It was realised that cable stay bridges with a deep deck could provide the necessary stiffness for railway bridges and that cable stay bridges could be designed and constucted to carry both rail and road. The Kap Shui Mun Bridge in Hong Kong, completed in 1997 with a span of 430 m has a compos-

Figure 11. Normandy Bridge, France.

Figure 12. Tatara Bridge, Japan.

Figure 13. Kap Shui Mun Bridge, Hong Kong.

Figure 14. Oresund Crossing, Denmark & Sweden.

Figure 15. Sutong Bridge, China.

ite box girder deck and H-shaped towers carries six lanes road traffic at the top level and two lanes of road and two mass transit rail tracks at the lower level, Figure 13.

A contemporary to Kap Shui Mun Bridge is the Oresund Crossing between Denmark and Sweden which was completed in 2000 and has a composite truss deck that carries four lanes plus two hardshoulders road traffic at the top level and two heavy rail tracks at the lower level, Figure 14. Oresund Crossing with a span of 490m has free standing towers similar in principle to the Dusseldorf Bridge Family of the 1950's and is a departure from the heavier looking A, H and Diamond shaped towers that were becoming the norm for cable stay bridges. It held the world record for the longest span cable stayed rail bridge span at its opening. The competition winning concept design was led by Jorgen Nissen of Arup.

Since the 1990's by far the major development in cable stay bridges has taken place in the Far East particularly in China with its necessary push on economic development, that has required the crossing of very wide rivers and estuaries with road and rail bridges to reduce journey times and enable efficient transportation of goods and people. Major fundamental research in all aspects of bridge design and construction has and is being carried out in Chinese universities.

At the the turn of the 20th century two major cable stay bridges with spans in excess of 1000 m were constructed in China. Sutong Bridge in mainland China with a span of 1088 m was completed in 2008, Figure 15, followed a year later in 2009 by the 1018 m span Stonecutters Bridge in Hong Kong China, Figure 16.

Sutong Bridge which carries six lanes of traffic crosses the Yangtze river near Shanghai and has a single orthotropic steel box girder, A-shaped towers and two outer cable stay planes giving a high torsional resistance and good aerodynamic stability. The 300 m high concrete box shaped towers have the simple shape of a straight A, which in the Chinese culture reflects the harmony between heaven and earth. The bridge was designed by China Highway Planning and Design Institute (HPDI).

Figure 16. Stonecutters Bridge, Hong Kong.

Figure 17. Russki Bridge, Vladivostok, Russia.

Figure 18. Tiangxingzhou Bridge, Wuhan, China.

Stonecutters Bridge by contrast is particularly unique. It is situated in Hong Kong Harbour which is encompassed with tall buildings in a hilly terrain. At 300 m it has the highest hollow circular monopole bridge towers in the world, which visually blend with the tall buildings and do not compete with them. There is a world first stainless steel-concrete composite section in the upper part of the tower, and the deck which carries six lanes of traffic comprises two separated streamlined steel ortho-tropic box girders, which is ideally suited to cope with turbulent and high speed typhoon winds, Figure 16. The concept design of the bridge was done by Ian Firth, with the detail design being done under the leadership of Naeem Hussain of Arup.

The trend in longer spans has continued with the comple-tion in 2012 of the Russki bridge in Vladivostok in Far East Russia with a span of 1104 m, which is currently the longest cable stayed span in the world. It has an orthotropic deck and kinked A-shaped towers. Figure 17.

Since the turn of the century long and very long span cable stay bridges for combined road and rail have been developed

and constructed in China. The Tiangxingzhou double deck cable stay bridge with a main span of 504 m for high speed rail across the Yangtze River in Wuhan has been completed in 2009, Figure 18. It carries 6 lanes of road traffic at the top and 4 railway tracks at lower level. The bridge was designed under the leadership of Gao Zhongyu of China Railway Major Bridge Reconnaissance Design Institute Co., Ltd (BRDI)

The Pingtan Strait Sea Crossing in Fujian Province, has three navigation channel bridges, all cable stayed composite double deck for road and railway with main spans of 532 m, 364 m and 336 m. The bridges are currently under construc-tion and will be completed in 2019, Figure 19. It carries 6 lanes of road traffic at the top and 2 railway tracks at lower level. The bridges were designed under the leadership of Fan Lilong of China Railway Construction Bridge Engineering Group.

The longest span combined road railway cable stayed bridge will be the 1092 m mainspan Hutong Bridge near Shanghai, which is scheduled for completion in September 2019, Figure 20. It carries 6 lanes of road traffic at the top and

Figure 19. Pintan Strait Crossing, Fujian, China.

Figure 20. Hutong Bridge, Shanghai, China.

4 railway tracks at lower level. The bridge was designed under the leadership of Gao Zhongyu of China Railway Major Bridge Reconnaissance Design Institute Co., Ltd (BRDI).

The project linking Hainan Island to the mainland in Southern China is the Qiongzhou Strait Sea Crossing currently under planning for which bridge and tunnel options are being considered. Prof. XIANG Haifan of Tongji University has suggested a 3-tower cable stayed bridge with either 2x1300 m or 2x800 m main spans.

For longer crossings or locations with unique site conditions, multiple span cable stay bridges have been used. As is well known the load transfer of a three span cable stayed bridge from the main spans to the anchor pier or abutment runs from the forestay cables via the tower head into the backstay cables which are anchored to holding down piers and anchor piers. For multiple span cable stay bridges, the backstays, which restrain the horizontal deflection of the tower head, are missing. The issue then is how to restrain the excessive horizontal deflection of the tower head due to live loads which also results in large vertical deflection of the deck. A number

of solutions, also well known, are possible to restrain the excesive deflections as shown in Figure 21.

The first solution is to have anchor piers in every second span of multiple span cable stay bridges. Another possibility for restraining the tower head is by means of various cable arrangement. The first one is to connect the top of the towers with horizontal cables which itself is anchored at the outer tie-down piers. A second solution is to tie the tower head by cables anchored to the junction of the side towers and main girder at deck level. A third solution is to overlap the stay cables in the adjacent spans, in which live loads in one of the main spans produces compression (unloading) in the stays of the adjacent spans.

The Second Orinico Bridge has a central anchor pier that is an A-frame in the longitudinal direction which not only restrains the tower head but also caters for the longitudinal rail braking loads, Figure 22.

Ting Kau Bridge Bridge in Hong Kong, with six lanes of traffic and two hard shoulders was designed by Jorg Schlaich. It has three slim monopole towers with composite ladder deck
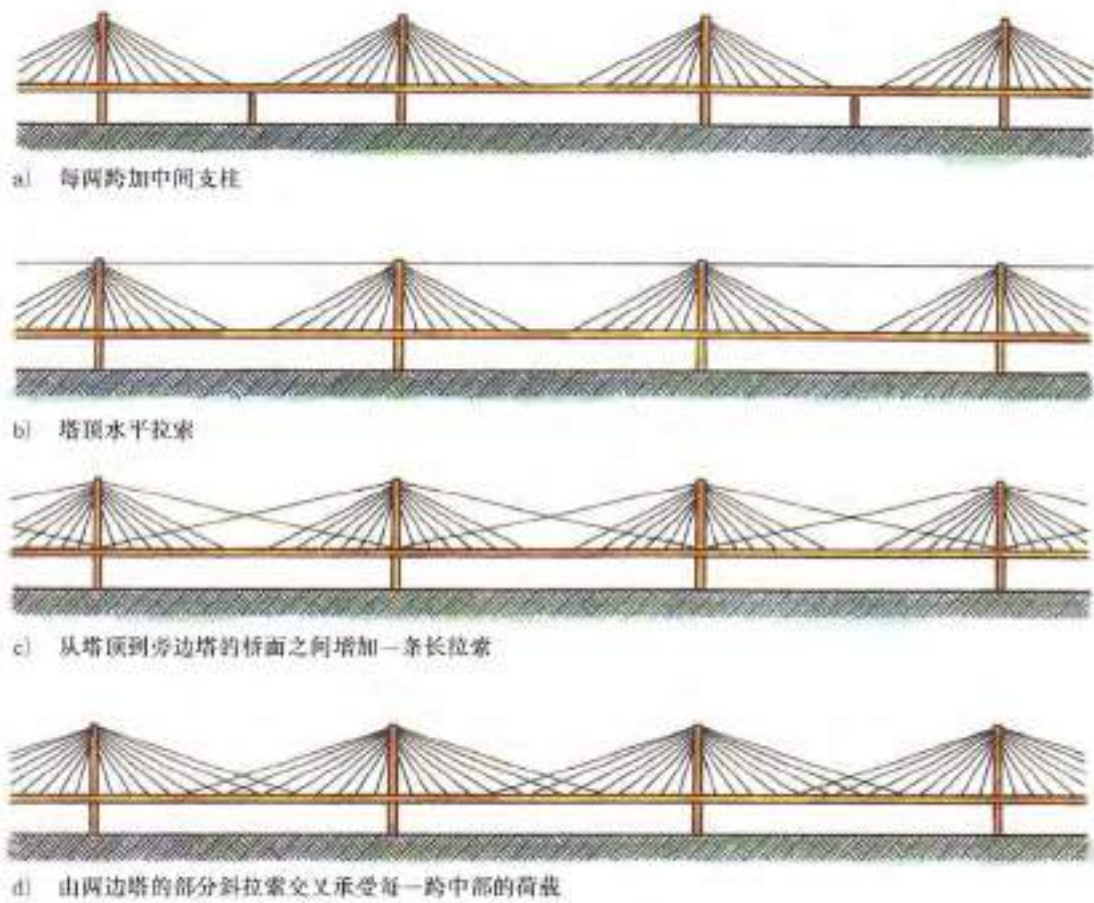
Figure 21. Restraining of tower head of multi-span cable stayed bridges.

Figure 22. Orinico Bridge, Venezuela.

Figure 23. Ting Kau Bridge, Hong Kong.

Figure 24. Queensferry Crossing, Scotland.

and spans of 448 m and 475 m. The restraining of the central tower is ensured by providing stabilising cables between the top of the tower and the junction of the side towers and deck, Figure 23.

Queensferry Crossing in Scotland, with four lanes of traffic and two hard shoulders has three slim monopole towers with composite box girder deck and spans of 650 m. The restraining of the central tower is ensured by crossing the stay cables at midspan of the adjacent spans, Figure 24. The concept design was done by Naeem Hussain and the bridge was completed in 2017.

Another way of overcoming the problem of restraining the deflection of the intermediate towers is to stiffen the towers themselves. This can be done by using A-towers in the longitudinal direction or using pyramid shaped towers.

The stunning Millau Viaduct in France with spans of 342 m and an orthotropic deck has multiple towers. The restraining of the towers in the longitudinal direction is ensured by use of A- towers above deck level in the longitudinal direction that provide the necessary stiffness, Figure 25. The bridge was designed by Michel Virlegeoux.

Figure 25. Millau Viaduct, France.

Figure 26. Rion Anterion Bridge, Greece.

Figure 27. Yavuz Sultan Bridge, Istanbul, Turkey.

Rion Anterion Bridge in Greece with four towers and composite ladder deck with spans of 560 m is located in a high seismic zone. The restraining of the towers in the longitudinal direction is achieved with use of pyramid towers above deck level that provide the necessary stiffness. The towers are founded on caissons in deep water which rest on a gravel mat on top of the sea bed, reinforced with pile inclusions. In the case of a major seismic event the stone mats act as seismic fuses in that the towers can move on the mats and dissipate energy, Figure 26.

What is the future of cable-stayed bridges? In 1986 there were about 150 major cable-stayed bridges in the world and their number has increased to more than 1000. For many locations it is likely to be the preferred bridge type in the range of 200 – 1200 m with decks being in concrete, composite and steel depending upon the span length. Theoretical studies have shown that cable-stayed bidges could be economic up to spans of 1500 m, but the main constraint on larger spans is likely to be the stay cables as their stiffness will be lower with longer lengths and they will be susceptible to oscilla-

tions. Special dampers will be required both at the top and bottom of the stay cables combined with use of tuned mass dampers for the girders to limit parametric stay cable oscillations. Carbon fibre stay cables may be used.

Another major development is the use of hybrid cable-stayed plus suspension bridges. The Third Bosporus Bridge (Yavuz Selim Bridge) for road and rail with a span of 1450 m and completed in 2017 is a major breakthrough in use of hybrid solutions for very long span combined road and rail bridges, Figure 27.

The future development of cable-stayed bridges will continue to take place with possible use of composite materials and construction ingenuity being deployed on a world wide basis.

References

[1] Holger Svensson, Cable-Stayed Bridges, 40 Years of Experience Worldwide, Wiley-Blackwell, Ernst & Sohn

[2] Niels J. Gimsing, Cable Supported Bridges, Concept & Design, Wiley

New trends in typology: hybrid bridges, a field for innovation in structural engineering

Nuevas tendencias en tipología: puentes híbridos, un campo para la innovación en la ingeniería estructural

José Romo[a]

[a] Structural Engineer. CEO. FHECOR Ingenieros Consultores SA (Spain)

ABSTRACT

One of the fundamental characteristics of Javier Manterola's attitude towards design is innovation. His search for innovative solutions has led him to refine the canonical structural types to the limit. Furthermore, he has also contributed to the development of more complex structural solutions that could be said to constitute hybrid structures, on which this article deals.

This paper will show that hybrid bridges are not a contemporary invention, since their more or less conscious constant use in engineering through its history. For the author hybrid structure could be recognized as one of the obvious fields for creativity and innovation in structural engineering and the works of Javier Manterola are good examples of that design's approach.

© 2019 Asociación Española de Ingeniería Estructural (ACHE). Published by Cinter Divulgación Técnica S.L.L. All rights reserved.

KEYWORDS: Hybrid, extradosed, suspension, cable stayed, truss.

RESUMEN

Una de las características fundamentales de la actitud de Javier Manterola hacia el proyecto es la innovación. Su búsqueda de soluciones innovadoras le ha llevado a refinar los tipos estructurales canónicos hasta el límite. Además, su trabajo también incluye el desarrollo de soluciones estructurales más complejas que podrían decirse que constituyen estructuras híbridas, sobre las cuales trata este artículo.

Como se explica en el artículo, los puentes híbridos no son una invención contemporánea ya que su uso, más o menos consciente, es constante en la ingeniería a lo largo de su historia. Para el autor, la estructura híbrida podría ser reconocida como uno de los campos obvios para la creatividad y la innovación en la ingeniería estructural, siendo los trabajos de Javier Manterola el mejor paradigma de su uso.

© 2019 Asociación Española de Ingeniería Estructural (ACHE). Publicado por Cinter Divulgación Técnica S.L.L. Todos los derechos reservados.

PALABRAS CLAVE: Híbrido, extradosado, colgante, atirantado, celosía.

1.
INTRODUCTION

One of the fundamental characteristics of Javier Manterola's attitude towards the design is innovation. His search for innovative solutions has led him to refine the canonical structural types to the limit. Furthermore, he has also contributed to the development of more complex structural solutions that

could be said to constitute hybrid structures, on which this article deals.

This paper will show that hybrid bridges are not a contemporary invention, since their more or less conscious constant use in engineering through its history. For the author hybrid structure could be recognized as one of the obvious fields for creativity and innovation in structural engineering and the

---

* Persona de contacto / *Corresponding author.*
Email - Correo electrónico: José Romo: jrm@fhecor.es

works of Javier Manterola are good examples of that design's approach.

It can be affirmed that the use of systems beyond the canonical types is common in the design of structures for buildings, because of their complexity. However, the use of combined structural systems is no so common in bridges, even though the departure from the canonical is fully justified. The aim of this paper is to contribute to the diffusion of these bridges, in which without leaving the structural rigor, several resistant systems are combined, in order to adapt to specific problems particularities.

2.
DEFINITION OF HYBRID STRUCTURES

Hybrid structures are those in which two or more different structural systems which work together coexisting or overlapping. Perhaps to understand this definition better, it is necessary to understand the opposite of the hybrid, that is, the structural types we might call canonical. The canonical types correspond to the most known structural solutions. Among these solutions are: the beam, the frame, the arch, the cable stayed bridge or the suspension bridge. In all these systems the main flow of forces is well known and is easy to understand and visualize by a connoisseur of structural engineering: in this types of bridges the structural system is very clear. It could be said that the structural science is in a state that has allowed distilling these concepts or canonical solutions leading to a high degree of improvement.

The opposite of canonical systems are hybrid systems. In this case, it is complex systems in which several resistant schemes are combined. Thus, for example, in a hybrid bridge, a frame can be combined with a stayed system, or a tube with an arch. In these structures the structural behaviour is not obvious and depends, among other aspects, on the relative rigidity between the structural systems that coexist, the connections between the systems and the sequence of construction or loading the structure.

3.
CONCEPTUAL DESIGN OF HYBRID BRIDGES

In a hybrid bridge, when there are two superimposed subsystems, the structural response depends on the relative rigidity between the two subsystems (figure 1). Thus each structural subsystem takes a portion of the load proportionality to its rigidity relative to the rigidity of the whole system. That concept is applicable for live load as well as for dead loads. The designer can define a construction process, more or less freely, to decide which part of the dead loads is taken by each subsystem.

A clear example of this concept is extradosed bridges [1]. In this type of structure the selfweight is partially resisted by the stays system (typically the 60%) and the rest is taken by the deck. A deeper explanation of this structural type is included in the next sections.
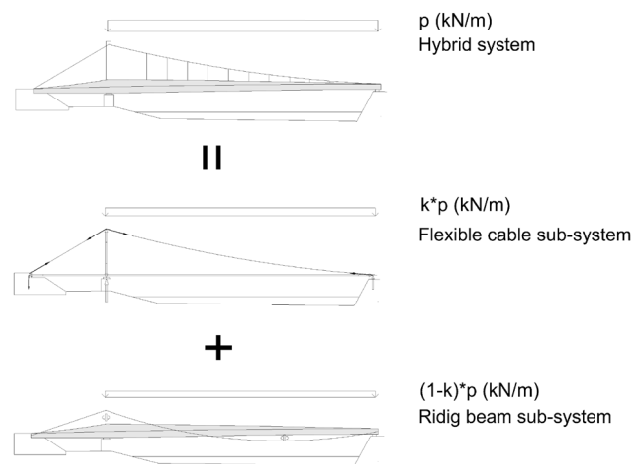
Figure 1. Structural behaviour of a hybrid structure (schematic).

4.
HYBRID BRIDGES IN CONSTRUCTION HISTORY

Hybrid structures are nothing new in the world of engineering. In some periods of the history of construction, a large number of hybrid structures were used. One of these periods coincides with the development of the railway, during that period a huge number of new bridges were built. Many of those structures do not follow what it could be called canonical types. That was a period of exploration where trial and error system were extremely used. In fact many of the bridges built during that period were what it could be named as hybrid structures. In many cases the engineers used more than one structural system at a time creating safer and redundant bridges. In the figure 2, an example of those early designs is shown.

Those structures were designed without any structural analysis that could support or explain the structural behaviour of the bridge. At that time, there were no tools to design such complex and redundant structures. After that initial period, the bridges built were closer to it could be called the canonical types. Probably the tools available at that time based on the equilibrium equations led to a kind of structurally more simple systems. In a way the structural solutions used were those which could be calculated

5.
CONTEMPORARY HYBRID BRIDGES

5.1 Introduction

Nowadays, the situation is rather opposite to the one explained above. Our contemporary conceptual and analytical tools allow the use of complex systems thanks to its sound comprehension. In a way today it is possible to use hybrid systems because of the evolution of the structural analysis

Figure 2. Early hybrid structures XIXth Century. Source: Structurae. Image-ID: 6316.

methods and tools. That is why, the very initial historical iron or steel structures from the XIXth Century are a good source of inspiration to the contemporary engineer. The modern techniques allow them to explore the fascinating and promising word of the hybrid structures, as it can be seen in the next chapters.

5.2 Extradosed bridges

The extradosed bridge is a good example of hybrid structure. In this type of bridges a deck with an "intermediate" rigidity is superimposed, with a flatter cable stayed system (figure 3).

During construction, it is usual to not completely compensate the permanent loads with the tightening. This percentage usually ranges between 50 to 60% [1].

The live load acts on the composite system deck and stays. By lowering the inclination of the stays, its effectiveness against live loads is low. As a consequence, only a very small fraction of the live load is resisted by the cables. Consequently, the oscillation of the tension in service conditions of the stays is very small and therefore the effect of the fatigue in them is negligible.

The extradosed bridge is the paradigm of hybrid structure. In it two systems are superimposed, the deck and the cables,
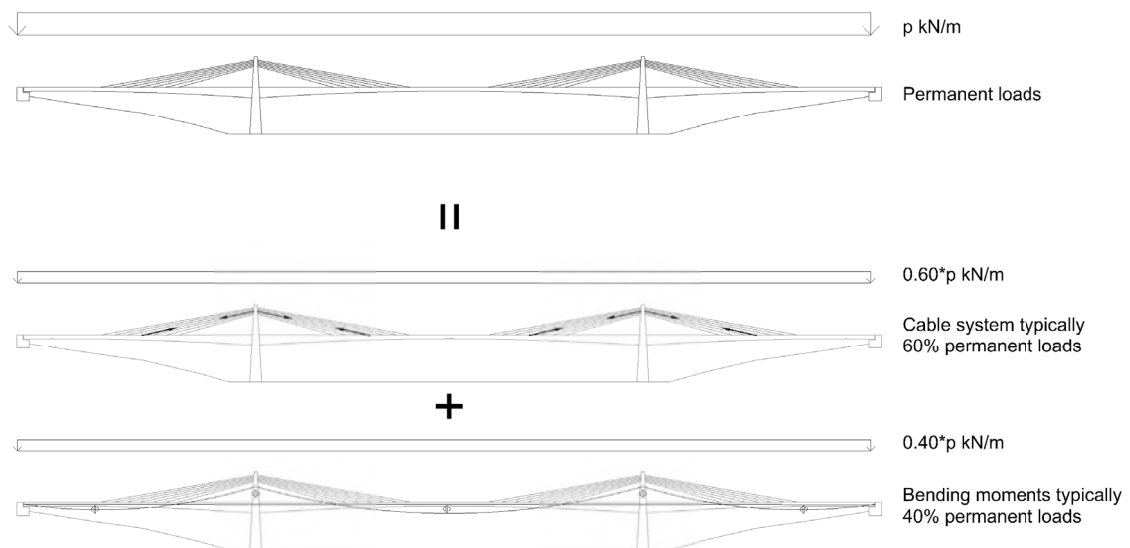
Figure 3. Structural behaviour of an extradosed bridge.

Figure 4. Brooklyn Bridge (John A. Roebling).
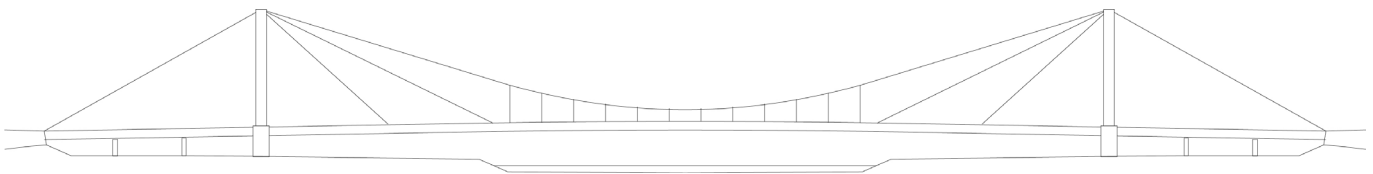
Figure 5. Köln-Mülheim Bridge across the Rhine, proposed by Dischinger in 1949.

combining their way of working at the designer's will. To do this, the angle of the stays can be varied with the horizontal, as well as the rigidity of the deck, to graduate the part of overload that each subsystem will take.

In this case, the fundamental objective is to reduce the variation of loads in the stays so that the fatigue oscillation is minimal. In this way the cables can be designed working at a higher stress than in the case of the canonical cable stayed systems, with the consequent savings.

5.3 Suspension and cable stayed combined systems

Besides de extradosed bridges there are other structural solutions used nowadays which could be considered as a hybrid structure. For instance, the combination of a cable stayed system with a suspension system in the same structure is a good example of that.

The superposition of both systems could be found as far ago as the John A. Roebling Bridge in Cincinnati, opened in 1867 with its 317 m world record span length at its time [2].

This bridge is the predecessor of Roebling's masterwork, the Brooklyn Bridge in New York.

In both bridges, Roebling used stays close to the pylons and superimposed with the global suspension system to increase the stiffness of the bridge. The hangers are located on the entire superstructure. That is why we could talk about a suspension bridge with a certain rigidity or stiffness.

Other example is the proposal for the reconstruction of the Köln-Mülheim Bridge across the Rhine, proposed by Dischinger in 1949 [3]. In this case, the bridge had the two systems, stayed and suspended, but in different zones of the bridge. Here in the area closer to the pylons the deck is just stayed meanwhile the central part of the deck is suspended from the main cables.

In this sense, the bridge is a perfectly hybrid bridge since the author has decided to differentiate two areas in which the subsistence system is different.

A recent example of the application of this kind of hybrid system is the "Third Bosphorus Bridge" designed by M. Virloguex and J.F. Klein with 1408 m of span [4]. Here the system

Figure 6. Third Bosphorus Bridge (M. Virlogueux and J.F. Klein).
Source: https://commons.wikimedia.org/wiki/File:Yavuz_Sultan_Selim_Bridge_IMG_3080.jpg

Figure 7. Orio Bridge. (FHECOR).
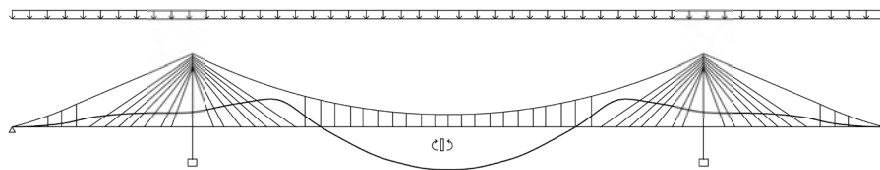
Figure 8. Orio Bridge: bending moments in the deck for a uniform live load applied to the whole deck. (FHECOR).

is conceptually similar to the Dischinger's proposal. However, while in the case of the Rhine Bridge, the cable stayed area and the suspended part do not overlap, in the case of the Bosphorus Bridge (figure 6), both areas overlap for an important magnitude, although not completely on the whole deck as on the Brooklyn Bridge . Again we can see in this example, how the designer can play with both the relative rigidities of the systems, and with their geometric configuration to achieve the desired structural behaviour.

A similar solution but with a central suspension system is the Orio Bridge [5] designed by the author. In this case the hy-

brid system was used for having low towers that blended into the horizontal landscape of the river Oria estuary. The bridge has only a central plane of cables, and the deck has a box steel cross section with a torsional rigidity enough to span from the torsional point the distance between the abutments.

One issue interesting to highlight is the greater rigidity of the hybrid bridge with respect to the traditional suspension bridge. Figure 8, shows for example the bending moments when a uniform vertical load acts on the whole deck. As it can be seen, there is an important reduction of the effective span length for the deck bending moments, compared with

Figure 9. Infante Dom Henrique Bridge. Adao da Fonseca & IDEAM.

Figure 10. Martin Vigil Viaduct.
Source: Luis Cortés, CC BY-SA 2.0, https://commons.wikimedia.org/w/index.php?curid=18329848

the case of the classic suspension bridge. Here the stay system are quite stiffer than the suspension system and therefore the general bending moment in the deck and the deflection in the center of the span are smaller than the one corresponding to a suspension bridge.

As seen through those examples, this hybrid solution has its own field of use. In many cases the combined stayed and suspended system improves the stiffness and therefore the performance of the bridge when is compared with a classic suspension bridge, which makes the solution applicable in the cases that the deformations can be critical, as it happens for example in the case of railway bridges.

5.4 Arches with rigid deck

This is again not a new idea, the combination of a rigid arch and a slender deck, or vice versa, a slender arch with a rigid deck, is present in the structural engineering from the XIXth Century.

The example of the figure 9 of Porto, is an example of the combination of a slender arch with a stiff deck.

As an opposite example, the Martin Vigil Viaduct by E. Torroja (1939) [6], is a paradigm of a stiff arch with a slender deck.

In both cases, the designer could define the way of live loads are shared between deck and arches as a consequence of their relative bending stiffness.

Figure 11. Obhur Bridge. (FHECOR).

It is obvious that the possible combinations are huge. One further idea could be the combination of a tubular truss deck with a more slender arch. This was the proposal for the Obhur bridge (Saudi Arabia) developed by the author. Here there was a limitation of the maximum height of the crown of the arch, because of the structure was closed to an airport. The conceptual design led to a shallow arch, with a relationship rise/length of the arch close to 1/10, to compensate that the deck was designed with a high stiffness. Therefore in this case the bulk of the moments caused by the uneven live loads are resisted by the deck.

5.5 Extradosed and frame systems

This section presents two examples of combined hybrid bridges designed by J. Manterola, the Andalusia Bridge [7] and

the Viana's Prince Bridge [8]. Both structures are extradosed bridges where there is a combination of a stiff deck with a system of cables with a low inclination. But beside that, J, Manterola introduces inclined struts to reduce the flexure of the deck adding a frame system to the structure. The bridges are therefore a combination of an extradosed and a frame structural system.

In both bridges the innovative and the smart engineering solution is also complemented with a typical flair for designing nice and elegant structures, which is a constant in the works of J. Manterola.

5.6 Arches and stressed ribbons

Another master in the use of combined systems is Jiri Strasky [9]. Some of his most important contributions to hybrid struc-

Figure 12. Andalusia Bridge (Córdoba) J. Manterola. Source: Carlos Fernández Casado S.L.

Figure 13. Viana's Prince Bridge (Lérida). J. Manterola. Source: Carlos Fernández Casado S.L.
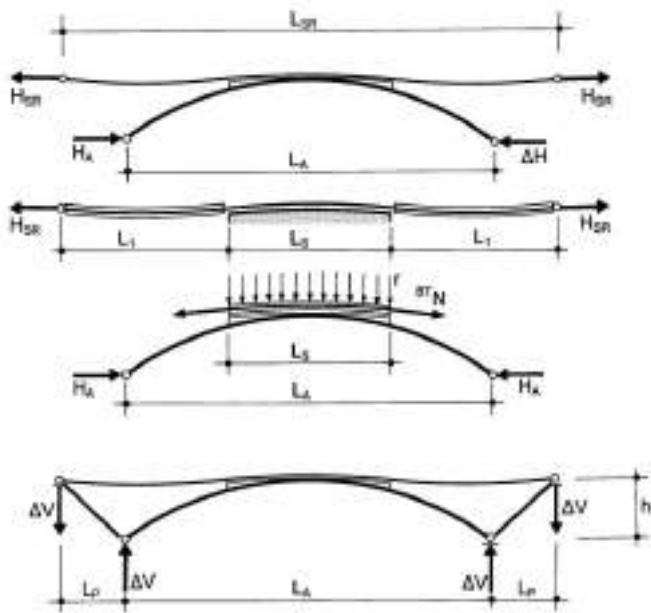
Figure 14. Stress ribbon supported by arch.
(Conceptual ideas by Jiri Strasky [10]).
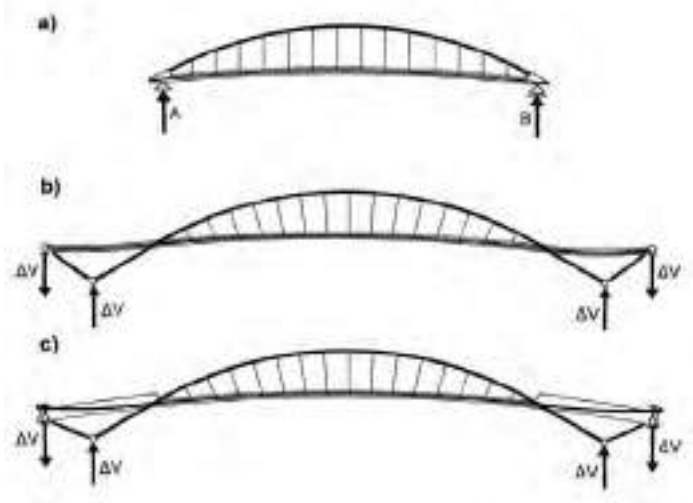
Figure 15. Stress ribbon suspended by arch.
(Conceptual ideas by Jiri Strasky [10]).

tures are those in which he combines an arch with a stress ribbon structure. Using that combination he achieves a self-anchoring system where the horizontal force from the stress-ribbon is transferred by inclined concrete struts to the foundation, where it is balanced against the horizontal component of the arch. With that disposition, there is no need to resist very large horizontal forces at the abutments, which determines the economy of that solution in many cases. In figures 14 and 15 the conceptual development stages of the solution are shown.

These two examples show that two canonical systems:

the arch bridge and the stressed ribbon can be combined to achieve a hybrid structure that effectively solves one of the problems that are critical for both types, its dependence on the ability to transmit horizontal actions to the ground.

5.7 Longitudinal adjacent combined systems

A completely different way to conceive hybrid bridges is by combining two structural systems longitudinally to solve the same span. It is quite normal to have different structural sys-

Figure 16. Franjo Tudjman Bridge. Source: Structurae, photographer Bernd Kramarczik [11].

tems longitudinal to solve different spans, for instance combining a main span with a cable stayed or an arch bridges with continuous approach viaducts designed as a continuous deck. What is quite unique is having two adjacent structural systems to solve the same span. Probably the most known example of that possibility is the Franjo Tudman Bridge in Dubrovnik, Croatia. Here in order to solve a main span of 304.05 m, a stayed system is combined with a cantilever concrete box-girder. The connexion of the two systems is hinged, and probably the asymmetry of the crossing led to that special structure.

This unique design is perhaps one of the few examples of the use of two different structural types combined longitudinally, in an exceptional hybrid bridge.

5.8 Summary

As seen through the above examples, there are nowadays, in real practice, some good examples of hybrid bridges that show the potentiality of this kind of concepts. A field of innovation in which more examples will be seen in the future, following for example, the ideas presented in the next section.

Many of the examples presented here were designed as a consequence of special requirements such as the need of stiffening in the case of cable supported bridges. In that opportunity the combination of a suspension and a stayed system gives the required rigidity to the system. In the case of the stress ribbon structures, the combination of the ribbon with an arch system makes the structure self-anchored and therefore the horizontal forces transmitted to the ground are successfully eliminated.

6. HYBRID BRIDGES POSSIBILITIES

6.1 Introduction

As described above, there are several types of hybrid bridges which have a clear field of application. It is obvious that it society will build more Extradosed Bridges or combination of Stayed and Suspended Bridges.

The extradosed bridges described in previous chapters are good examples of the possibility of a hybrid structure. Its range of application of 150 to 250 m lies between the classic continuous concrete box-girder deck built by cantilevering and the canonical cable stayed bridges. The extradosed bridges is an unbeatable solution in multi-span structures, which solves the problems of flexibility of continuous cable stayed bridges. Other hybrid solutions, such as the combination of suspended and stayed bridges are also of interest when the pure suspension system has not enough stiffness against live loads, which could be the case of railway bridges. This kind of structural hybrid system could also be necessary for stabilising long span bridges.

Beside those two types of hybrid bridges already presented, it is possible to foresee a wide range of other possible bridges.

Figure 17. Lascellas Bridge Spain. Source.: Biblioteca Nacional de España.
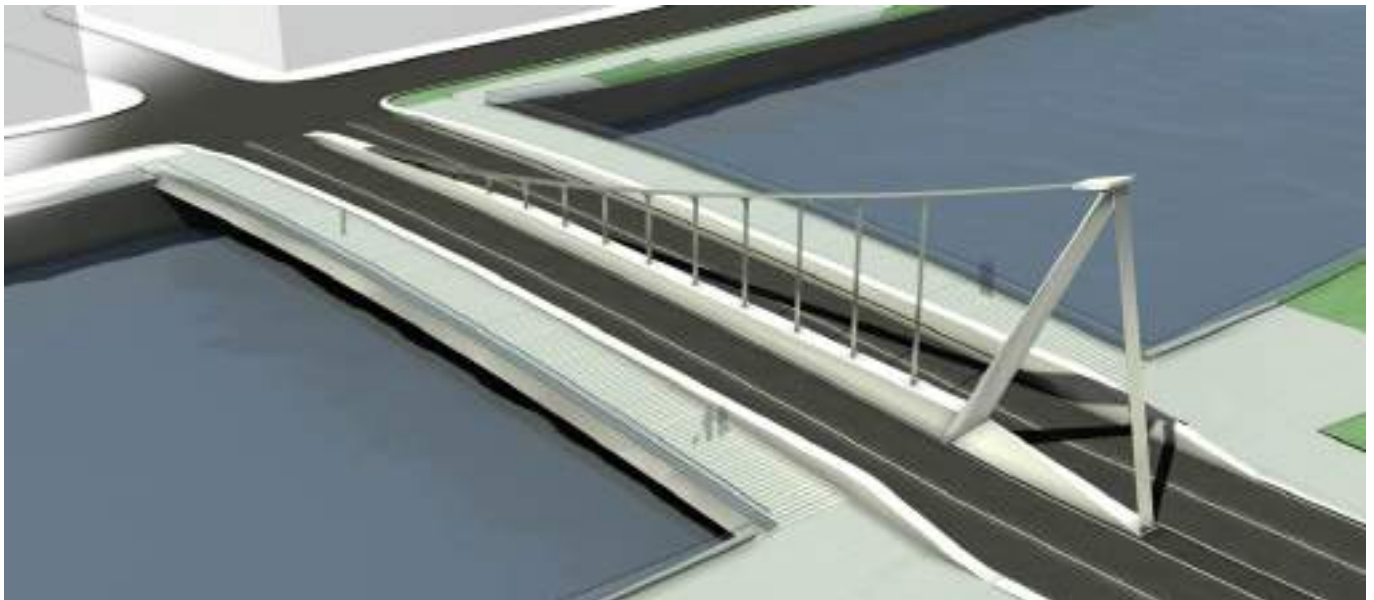
Figure 18. Zorrozaurre bridge. (FHECOR).

The following sections will present just a few examples, as a brief set of the enormous variety of combinations.

6.2 Suspension systems with a rigid deck

The combination of a rigid deck suspended by cables is not a new idea. Some of the early suspension bridges combined a rigid deck, usually a truss beam, with a suspension system.

The bridge of Lascellas built in 1867 in Spain is an example of the early design of a suspension bridge with a low sag/span ratio.

Here again, the designer could modify the main parameter to stablish which part of the dead and live load will be resisted for the deck or the cable.

Figure 19. Arga bridge. (FHECOR).

Figure 20. Dvorecky bridge. (FHECOR).

In general, the stiffness of the deck could be achieved by using a solid beam or by a truss structure.

An example of the first type is the proposal of the author for the first Zorrozaurre Bridge in Bilbao. The bridge has a stiff deck and a shallow suspension system. In this case, the stiffness of the deck was achieved by using two solid elevated steel box beams, which also divides the sidewalks for pedestrians, and the central zone for traffic. The distribution of the permanent load between the two systems can be selected as the designer can modify the forces taken by the hangers, while the distribution of the live loads between main cable and deck depends only of the relative stiffness of the two systems.

Other example of that is the proposal of the author for the Arga Bridge. The structure is a combination of a rigid truss deck with a shallow cable suspension system (figure 19). As in the Zorrozaurre Bridge, the distribution of the permanent forces between deck and cable can be selected by the designer meanwhile the distribution of the life load depends only on the relative vertical stiffness of both systems.

The following example is a proposal for the Dvorecky Bridge in Prague. Here a combination of a suspension system and a framed deck was used to reduce the height of the pylon more suitable with the landscape.

All those examples are just a short set of solutions, which show the field of application of that variety of hybrid bridges.

6.3 The hollow beam

The concept of the hollow beam tries to take full advantage of the resistant capabilities of a beam working at bending, reducing its own weight by lightening the beam wherever possible.

A beam, simply supported, working at bending has two different zones related to its structural behaviour. On one hand there is the mid-span where we have the maximum bending moments and the minimum shear forces, and on the other hand the support area in which the situation is reversed, with the minimum bending moments and the maximum shear forces.

At mid-span, it is sufficient to have an upper compressed chord and a lower tensioned chord to resist the existing forces. That is why in that area it is possible to lighten the section removing much of the web of the beam.

Figure 21. Cork Footbridge. (FHECOR).

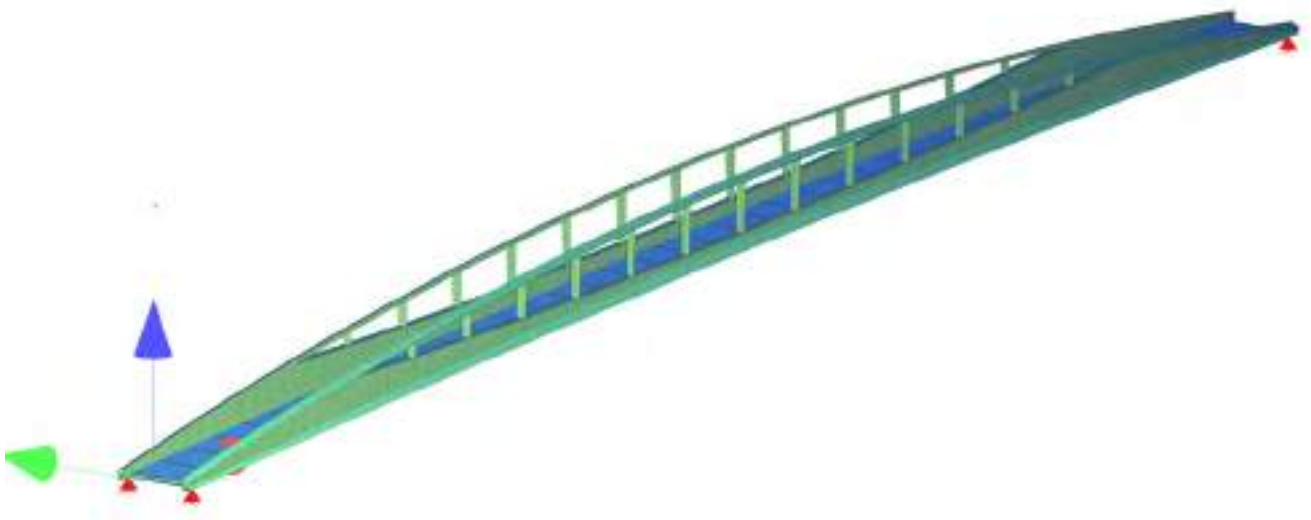Figure 22. New Danube. (FHECOR).

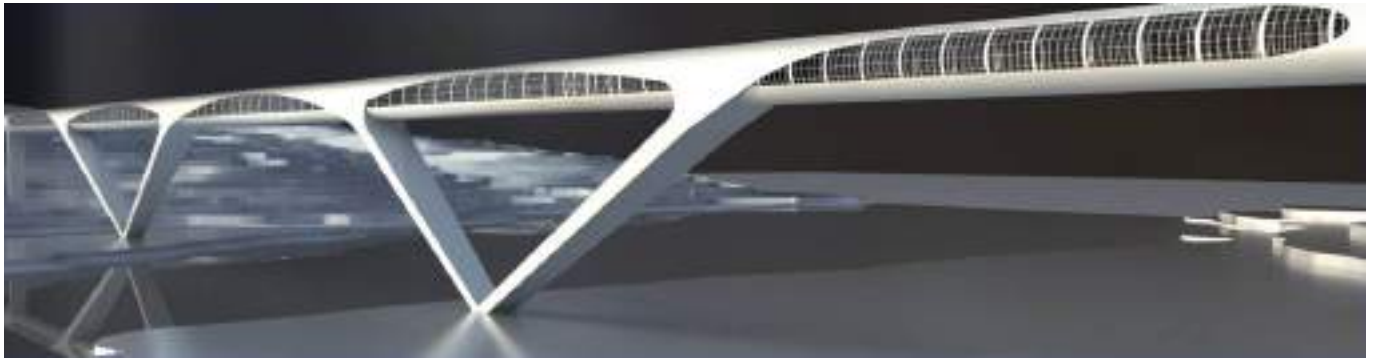Figure 23. Eibar footbridges. (FHECOR).

Figure 24. Ulla Bridge. (FHECOR).

On the contrary, in the support zone it will be necessary to have a solid web, since it is necessary to resist high shear forces, while the bending moments are not important, so it is possible to have a smaller depth than at mid-span.

An example of this hybrid concept, as an intermediate type between a pure beam and a shallow arch, is the proposal for a footbridge in Cork (Ireland) designed by the author. There a central beam built with an important voided central area, which emphasizess the slenderness of the structure.

The same concept was used for the New Danube Bridge competition in Budapest. In that case the structure had a span in the range of 500 m and the concept was developed together with Dissing and Weitling architects.

Other examples of that type of hybrid structure are the two footbridges in Eibar (Spain), currently under construction. There, the system is formed by two lateral beams with the same concept (figure 23).

6.4 Frames and tubes

As simple example of other hybrid structures is the proposal for the Ulla Bridge designed by the author [12]. Here a truss tubular deck cross section is combined with a frame supporting system. The frame with is inclined struts reduces the flexure of the deck, improving its deformational behaviour, which is critical due to the use of the bridge for a high speed railway line.

The struts of the frame have a precise inclination at each side to compensate the horizontal forces due to the permanent loads in the foundation.

It is also obvious from the former examples, that the combination of tubular decks with other structural systems such as arches, frames, stays or suspension systems opens another world of possibilities.

7
CONCLUSIONS

It is clear that the canonical structural types, such as: beams, frames, arches, cable stayed or suspension bridges, are very well developed, and in a sense structural engineering has been able to refine those solutions to their limits. In many cases, the ca-nonical types are the right and more suitable solutions. Nevertheless, in some cases, the functional requirements or just the context where the bridge has to be built, led to what it could be called hybrid bridges.

As it could be seen through the examples previously presented, the Hybrid solutions have a wide field of application. That is the case, for instance, of the extradosed bridges; that type of bridges is in between the concrete box bridges and the cable stayed bridges, but that is only one possibility out of the universe of possible combinations.

As part of the tradition developed by our masters, such as Javier Manterola, the hybrid structures are a field of developing news ideas or concepts, and therefore a vast space for innovation in structural engineering.

References

[1] KASUGA, A.; Birth, Development and Future of Extradosed Bidges. Hormigón y Acero 2019. Vol. 70. Nº 288

[2] Cable Supported Bridges: Concept and Design. Niels J. Gimsing John Wiley & Sons 1983 Chichester. Page 24

[3] DISCHINGER, Franz: Suspension bridges for the heavy traffic loads (in German): Der Bauingenieur 24 (1949) 3, S. 65–75, 4, S. 107–113.

[4] De Ville de Goyet, Vincent / Virlogeux, Michel / Klein, Jean-François / Duchêne, Yves (2015): The behavior of the Third Bosporus Bridge related to wind and railway loads. Presented at: Structural Engineering: Providing Solutions to Global Challenges, IABSE Conference Geneva, September 2015, pp. 2109-2116.

[5] ROMO J., Orio Bridge: an innovative cable stayed suspension hybrid structure. 36th IABSE Symposium, Kolkata 2013

[6] Torroja, E.; THE STRUCTURES OF EDUARDO TORROJA. F. W. Dodge Corporation. 1958. Pp 71- 81.

[7] 50 años Carlos Fernando Casado Oficina de Proyectos. CFC. Madrid 2017. Pp 60-62

[8] 50 años Carlos Fernando Casado Oficina de Proyectos. CFC. Madrid 2017. Pp 74-76

[9] Strasky, Jiri. (Search for the true structural solution). Hormigón y Acero. 2019. Vol. 70. Nº 288

[10] Jiri Strasky, 2008. "Stress Ribbon Pedestrian Bridges. Supported or Suspended on Arches", Chinese-Croatian. joint colloquium, Long Arch Bridges, Brijuni Islands, Croatia, 135-147

[11] Franjo Tudjman Bridge Šavor, Z. / Radic, J. / Prpic, V. (2003): Bridge Across Rijeka Dubrovacka, Croatia. In: Structural Engineering International, v. 13, n. 3 (August 2003), pp. 190-192.

[12] Romo, J.; Structural Types 3D Tensor (STT). IABSE-IASS Symposium Taller, Longer Lighter. Nº 234. Pp 39-40. London 2011.

REALIZACIONES
ESPAÑOLAS
OCHO AÑOS
DE INGENIERÍA
ESTRUCTURAL

2009
2016

SPANISH WORKS
EIGHT YEARS
OF STRUCTURAL
ENGINEERING

ACHE
Asociación Científico-Técnica
del Hormigón Estructural
Spanish branch of FIB

ACHE

Arch and tied-arch steel bridges – some applications

Arcos de acero: aplicaciones

Vicent de Ville de Goyet[a]

[a] Dr. Engineer. Director. GREISCH. (Belgica).

ABSTRACT

During 2000 years, the basic material to build a bridge was stone. The typical bridge was the semi-circular arch bridge. The first bridges made of metal were again arch bridges where the internal forces are essentially compression forces. The industrial revolution and the progress of the theoretical knowledge in the field of structural mechanics made it possible to design bridges with different shapes. Bridges with large spans were mostly suspended and yet arch bridges.

This paper presents some applications of steel arch bridges designed twenty years ago with, each time, the objective to obtain the most efficient structure, a slender structure, by using the last theoretical developments in the field of instability because an arch works essentially in compression. The examples of bridges were chosen with the aim to explain the reasoning for the design and, also, to show that, even for similar bridges, it is often possible to improve any detail.

© 2019 Asociación Española de Ingeniería Estructural (ACHE). Published by Cinter Divulgación Técnica S.L.L. All rights reserved.

KEYWORDS: Arch, tied-arch, steel, buckling, cables, construction.

RESUMEN

Durante 2000 años, el material básico para construir un puente fue la piedra. El típico puente era el de arco semicircular. Los primeros puentes de metal fueron de nuevo puentes de arco donde las fuerzas internas son esencialmente fuerzas de compresión. La revolución industrial y el avance de los conocimientos teóricos en el campo de la mecánica estructural hicieron posible el diseño de puentes de diferentes formas. Los puentes con grandes vanos eran colgantes y, todavía, puentes arco.

Este trabajo presenta algunas aplicaciones de puentes de arco de acero diseñados hace veinte años con el objetivo de obtener la estructura más eficiente, una estructura esbelta, utilizando los últimos desarrollos teóricos en el campo de la inestabilidad porque un arco funciona esencialmente en compresión.

Los ejemplos de puentes fueron elegidos con el objetivo de explicar el motivo del diseño y, también, para demostrar que, incluso para puentes similares, a menudo es posible mejorar cualquier detalle.

© 2019 Asociación Española de Ingeniería Estructural (ACHE). Publicado por Cinter Divulgación Técnica S.L.L. Todos los derechos reservados.

PALABRAS CLAVE: Arco de tablero superior, arco de tablero inferior, acero, pandeo, cables, construcción.

1.
EVOLUTION OF THE BUILDING MATERIAL

The Iron Bridge over the Severn River (UK, 1779) (Figure 1) is the first metal bridge in the world. It is still used today for pedestrians. The structural behaviour of cast iron multiple arches bridges is similar to that of arch bridges in stone masonry. It develops only compression stresses, which made it possible to use cast iron, which is mostly resistant to compression.

Iron, replacing cast iron, is a stronger material than stone. Its tensile strength is low, but significantly higher than any other material available before the mass production of steel appeared. One of the first modern suspension bridges was the

---

* Persona de contacto / *Corresponding author.*
  Correo electrónico: Vicent de Ville de Goyet: vdeville@greisch.com

Figure 1. Iron bridge – 60 m.

Menai suspension bridge (Figure 2) designed by Thomas Telford and completed in 1826. The 176 m span of this structure marked an important milestone in bridge construction.

Iron was also used to build arch bridges, by means of trusses to create the arches. A good example are the two major viaducts of Gustave Eiffel: the bridge Maria Pia in Porto (1877) and the viaduct of Garabit (1884) (Figure 3).

Steel, with its mechanical characteristics far superior to those of iron, gradually replaced iron in all types of structures and allowed reducing their weight. Taking both tension and compression, steel made it possible to produce lattices whose overall stability was ensured by only normal forces. In order to optimize these lattices, their overall geometry followed the longitudinal bending moment distribution, as in the case of the Firth of Forth bridge (1890), or was arranged creating arches, like in the Eads bridge in the United States (1874) (Figure 5). The advantage of this lattice-based design was to make possible the construction of large structures with individual elements of limited size, easy to transport and assemble on site.

2.
EVOLUTION OF THE BUILDING MATERIAL

2.1 Typologies

From this time, the arch bridges were defined in different forms by arranging the deck either above the arch (a), under the arch (b) or at mid-height (c). The configuration b is called a tied-arch bridge (Figure 6).

The choice of one or the other configuration depends essentially on the obstacle to be crossed:
- the arch below the deck (a): mountainous areas
- the arch above the deck (b): areas without relief
- the deck at mid-height (c): intermediate situations

and the mechanical characteristics of the soil:

- for configurations (a) and (c), the critical aspect is the arch foundations, which require a soil with good mechanical properties to be able to take over important inclined compression forces
- the tied-arch bridge is self-stable: the compression of the bow is balanced by tension in the deck and there are only vertical reactions.

The span-length/arch-rise ratio is often in the range of 5-6. The deck is positioned at the level of the abutments. Its thickness is relatively limited because it is supported by the hangers (config. b and c) or by the columns (config. a) that can be considered as multiple supports whose inter-distance is small, about ten meters. Therefore there are bending moments acting between these supports. In the case of tied arch bridges, the deck will also be in tension.

2.2 Deck above or at mid-height of the arch

In the configurations (a) and (c), large horizontal compression forces must be taken up by the abutments. The arches being in compression present a potential risk of buckling, but this risk is reduced because of their connection with the deck. The arches are either fixed or articulated at their base. With three hinges (hinges at the base and at the keystone), the arch is a statically determinate structure.

The deck above the arch is supported by columns in compression, or in the case of mid-height decks, the parts of the decks under the arch will be suspended.

2.3 Arch above the deck

In this case, tied-arch or bow-string bridges as an analogy of the form of a bow with its stretched string. The arches are not held by the deck. They are generally connected in their upper part by a bracing structure, often composed by transverse beams, perpendicular to the arches. They ensure their transversal equilibrium, for example under the action of the

Figure 2. Menai suspension bridge - 176 m.

Figure 3. Viaduct of Garabit – 165 m.

wind and to avoid the risk of instability due to compression in the arches. The deck is suspended from the arches; the hangers are stressed in tension, which explains their lightness.

2.4 Construction

Whatever the configuration, the main difficulty for this type of bridges is its construction. The overall scheme is such that each element, the arch, the deck and the hangers (counter) are slender (length-to-height ratio). For each configuration, deck above or under the arch, the bending is limited between hangers (columns) and the bending stiffness of the deck is small. During construction, each one of these elements, deck and arch must be supported at regular distances to limit bending. Thus the deck cannot be put in place by launching. The arch

is often assembled on temporary piers, for tied arch bridge, or is constructed, for example, using the cantilever method by stabilizing it with temporary bracing.

3.
TIED ARCH BRIDGES

3.1 Interest of tied arch bridges

Tied arch bridges are particularly well-suited for crossing a depression in a flat landscape. The deck is stretched over its entire length and bent between its hangers. It therefore has a small superstructure depth

Figure 4. Firth of Forth bridge (1890) – 2 x 521 m.

Figure 5. Eads Bridge (1874) – 3 x 158,5 m.
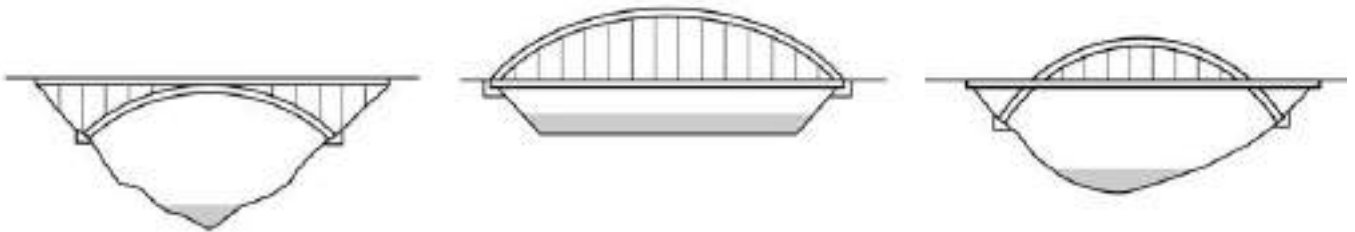
Figure 6. Different configurations of arch bridges .

- The vertical clearance under the deck is easy to guarantee
- The access ramps have a shorter length than for a beam bridge with a larger deck depth (Figure 8)

The deck is suspended at one or two arches arranged in vertical or inclined planes.

Bowstring bridges are internally, statically indeterminate systems and externally, determinate systems. They are supported by simple bearings (Figure 7).

3.2 Tied arch bridges over the Albert Canal

The Albert Canal, which connects the river Port of Liege with the seaport of Antwerp (Belgium), has been recently widened to allow traffic of pushed convoys with four barges and a total capacity of 9000 tons. This decision has required the replacement of the existing bridges by new structures with a much longer span length (roughly 165 m instead of 95 m). The topography where the bridges had to be erected is relatively flat. In that case, relatively few bridge typologies could be considered: girder bridges, cable-stayed bridges or bowstring arch bridges. The depth of the deck of a beam bridge is greater than for the other two types of bridges; it then requires longer access roads to get the required clearance under the bridge (Figure 8).

It explains the choice of cable-stayed bridges such as Lixhe, Lanaye and Wandre, whereas the case of tied arch bridges
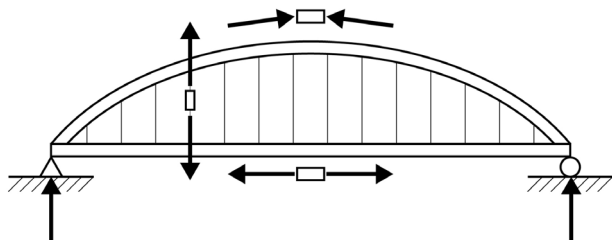
Figure 7. Internal forces.

could be supported by examples such as Haccourt, Hermalle, Marexhe and Misaucy (Figure 9).

In northern Belgium, a flat country, there are numerous examples of tied arch bridges. They are concrete bridges. The arches are braced over a great length and the hangers are vertical. The system of deck, arch and hangers works like a Vierendeel beam. For new bridges, the goals were to obtain slender structures, easier to build, with no (minimum) interruption of the river boats traffic. Designed in the same period, they gave an opportunity to try to optimize each structure, to adapt each one to the local configurations and to take advantage of the latest theoretical developments in the field of instability. Even though their main span-length is almost the same, each bridge is different (Tab. 1).

TABLA 1
Main Characteristics Of The Tied Arch Bridges Over The Albert Canal.

Location	Main span length (m)	Width length (m)	Arches	Bracing shape	Bracing location α=X/L
Haccourt (B)	139.5	20.90	2, parallel	/	/
Hermalle (B)	138.1	15.60	2, inclined	1 transversal top beam	0.5
Marexhe (B)	100.18	18.30	2, parallel	2 transversal beams	0.25/0.75
Milsaucy (B)	145.0	15.50	2, parallel	2 St. Andrew's crosses	0.20/0.80

The hangers are locked coil cables. Cross cables have been preferred to vertical and parallel ones for two reasons: to ensure a better distribution of the traffic loads to the arches (Figure 10) and to obtain a truss-like behaviour of the system of deck, arches and hanger. But, with this arrangement, it must be admitted that it also has some disadvantages: all cables are not in the same plane and, when the arches are inclined, as for the Hermalle bridge, the view of the suspension system is not clear (Figure 8).

3.3 Behaviour of the arches

The arches are in compression. It is necessary to verify their stability. Often, the instability in the plane of the arch is not preponderant, as the first buckling mode appears transversal to the arches plane. For this mode, the arch can be considered as a beam with compression stresses, restrained by the deck at each end. However, in contrast with a simple compressed column for which the ratio of the first two critical loads is about 4.0, in the case of tied-arch bridges, this ratio is around 1.0. The origin of this result is the stabilizing effect of the stretched hangers. The transversal instability of the arches is equivalent to a compressed beam on elastic foundation. The rigidity of this 'foundation' is equal to the tensile forces in the hanger divided by its length. (Figure 11). Based on several scientific papers and researches at the University of Liège, the stabilizing effect of the tension hangers has been considered to better explain this behaviour and also to optimize the rigidity and the location of the transversal bracing between arches [1-7].

For a preliminary design, it can be considered that the buckling length of the compression arch is equal to 0.35 L*, with L*, the developed arch length. The first instability mode shape is the same one as for the second buckling mode of a compression beam fully restrained at each support (Figure 12). Based on a parametric analysis of the arch bracing, a simple design method, [7], has been suggested which allows a satisfactory accurate assessment of the critical out-of-plane buckling load of arches. This method simply consists of evaluating
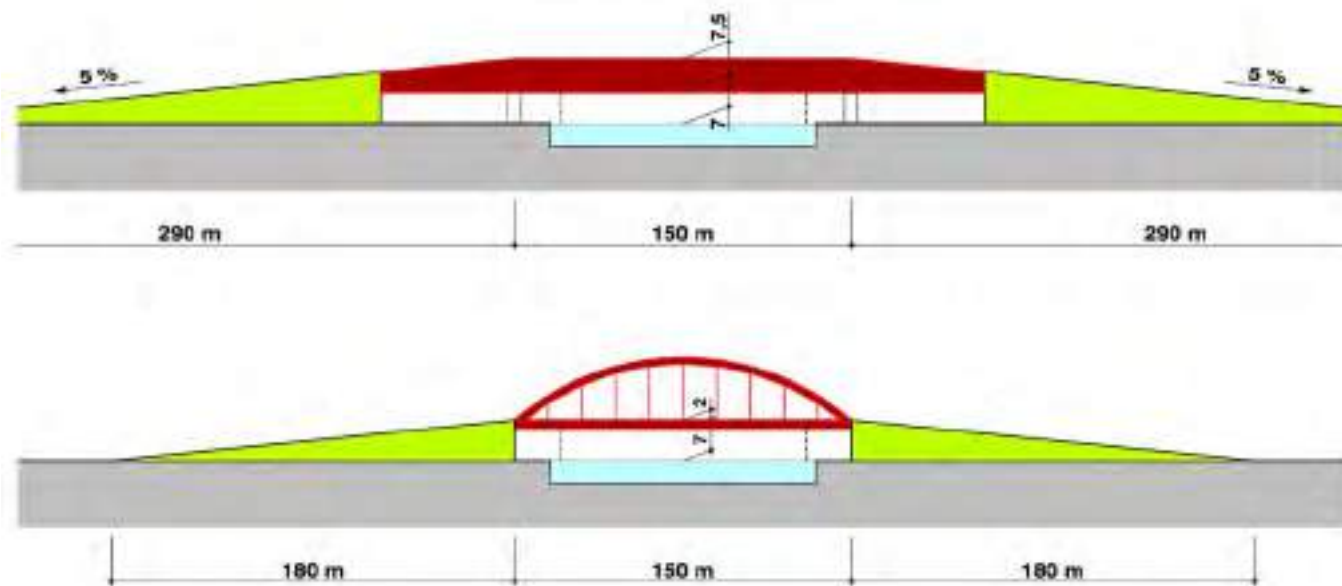
Figure 8. Approach spans combined with the two types of bridges.

Hermalle Bridge

Milsaucy bridge

Haccourt bridge

Marexhe bridge

Figure 9. Tied arch bridges on the Albert Canal.

analytically the instability of the set of bracing and arches submitted to compression in the arches transversally supported by an elastic foundation. This simple approach compared to the numerical values obtained by a finite element software shows that the understanding of the instability phenomenon appears to be correct.

Figure 13 shows the value the first critical transversal mode of the arches versus the location of the transversal bracing. The assumptions are: elastic constitutive law (Euler assumption) bracing beams with hollow cross section, only two bracing beams arranged symmetrically. It can be seen that the effect of the bracing beams is optimum with a location of 0.21 L* or 0.41 L*, with L*.

Taking into account the plasticity and the second-order effects, the gain is lower but the optimal location of the bracing is the same (Figure 14).

The efficiency of the bracing is clear but it is also possible to ensure the stability without it. For the four bridges on the Albert Canal (Figure 9), four solutions to ensure the transversal stability have been used, namely:
- Hermalle bridge: inclined arches 'connected' at the their crowns
- Marexhe bridge: two transversal beams
- Milsaucy bridge: two cross beams
- Haccourt bridge: without bracing.

Figure 10. Inclined - vertical hangers and traffic loads.

$$F_R = N_S . \sin(\alpha) = N_S . \alpha$$
$$d = h . \tan(\alpha) = h . \alpha$$
$$F_R = (N_S / h) . d$$

Figure 11. Elastic foundation induced by tension hangers.

Figure 12. Model to analyze the arches buckling.

Figure 13. Buckling load versus the location of bracing.

Figure 14. SLS, ULS safety factor respect the location of the bracing.

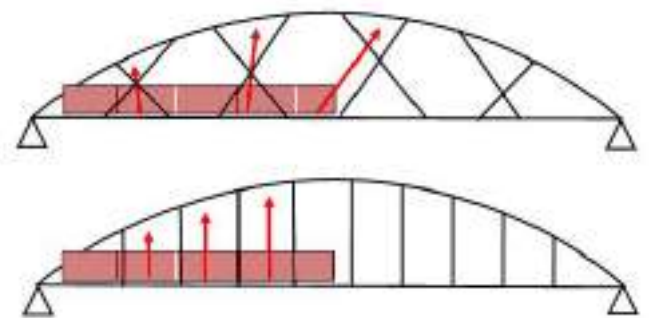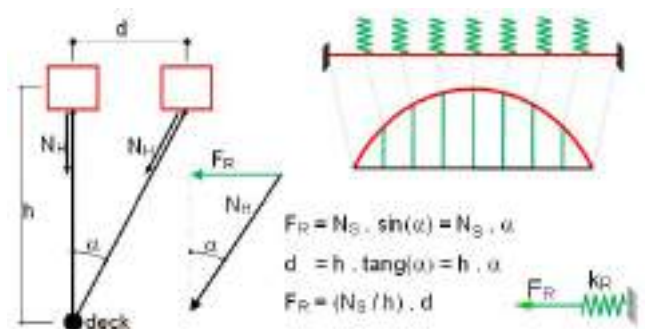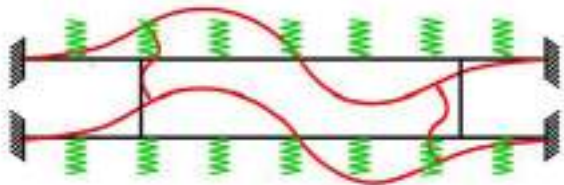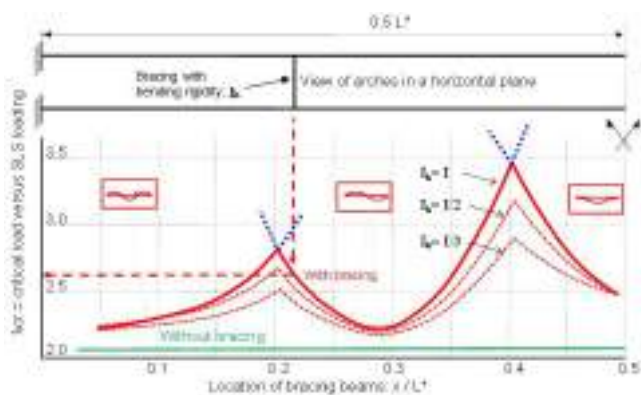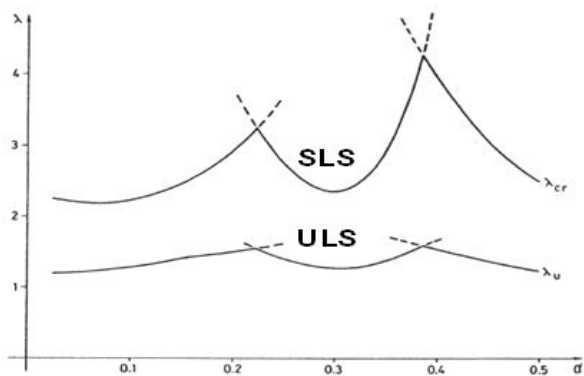The deck of the Haccourt bridge is larger. A bracing with transversal beams was also possible but the dimensions of the beam's cross-section would be too great, not only to ensure the stability of the arches, but also to support its own dead load. The solution was to suppress the bracing and to increase the bending rigidity of each arch. But, it is clear that, in that case, the hollow cross section of the arches must be larger to obtain the same safety. The comparison can be made between the dimensions of the arches' cross-section of the Marexhe and Haccourt bridges (Figure 15) but the global slenderness of the structure was maintained.

For the Hermalle bridge (Figure 16), with inclined arches, during their transversal displacements, each arch leans against the other; this behaviour adds a rigidity effect to the stabilizing effects of the strechted hangers. To incline the arches seemed to be an elegant solution; the stability is increased. However,

after several years of its opening, and despite a comfortable road clearance, the trucks were diverted the left of the traffic lanes when entering the bridge. Apparently, the trucks drivers are afraid to hit the arches. Perhaps, it would be interesting to increase the distance between the arch bases but, in this case, the deck width would also be increased.

The main stresses in the arches are in compressive and the plate buckling must be verified. Thirty years ago, it was typical to ensure the plate stability by adding numerous stiffeners. Moreover the loss of efficiency under compression stresses is also typical for the webs. For the upper and bottom flanges, a supplementary loss of efficiency appears due to the curvature of the plates (Figure 17). Under planar compression stresses, S1 and S2, transversal forces, TS, appear. In the projects designed by the Belgian administration, each plate was stiffened with a few T profiles along the whole length of the arches (Figure 17).

Based on researches carried out at the University of Liege, [8-9], it has been proposed, for the final design, to suppress each stiffener in order to limit the final cost. Of course the double loss of efficiency due to the plate buckling and to the transversal forces, TS, has been taken into account. It was more interesting to increase the plate thickness than to weld stiffeners obtaining a lower cost. Nonlinear simulations have been made with a finite element program to verify these assumptions.

3.4 Erection methods

After the brittle collapse of some steel bridges in Belgium between 1938 and 1940, the welding of steel elements on site was prohibited until the mid-1990's. Therefore the final connections of the arches for the new tied arche bridge on the Albert Canal were made with bolts (Figure 9.).

Two of these tied arch bridges were erected with temporary steel piers to assemble the deck and the arches: Milsaucy and Marexhe bridges. The two other structures, Hermalle and Haccourt bridges, were assembled on the ground and after that, transported on flat boats and installed on their final position.

3.5 Evolutions of the design

3.5.1 Chanxhe and Chaudfontaine tied-arch bridges
After the design of the tied-arch bridges over the Albert Canal, some other bridges with the same typology have been imagined and designed. The stability of the compression was well-known and understood; we could focus on other details of the structure. Two tied-arch bridges, with a span length around 50 m, have been designed in Chanxhe and Chaudfontaine (B) (Figures18-19).

The hangers are vertical and there is no bracing. With a ratio between the span length, L, and arch rise, f, equal to L/6, the road clearance would be difficult to be respected with a transversal bracing. Moreover, its suppression gives the impression of lightness.

A red colour has been adopted for the arches and the hangers for the Chanxhe bridge. For the Chaudfontaine bridge, the same red colour has been chosen for the arches and the deck and the white colour, for the hangers. This choice highlights the structural lines of the bridge.
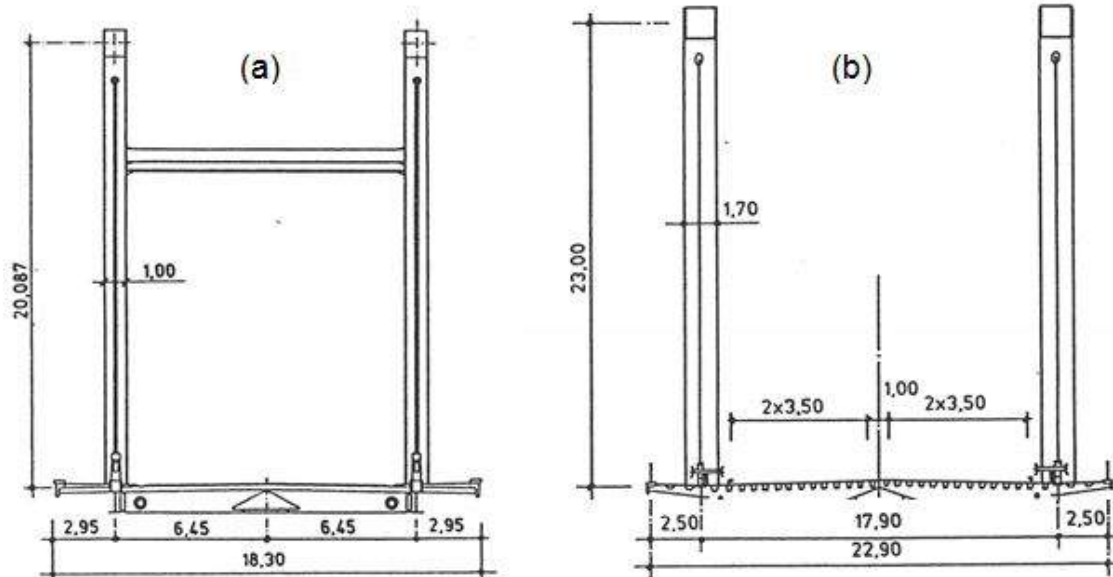
Figure 15. Marexhe (a) and Haccourt (b) bridges.
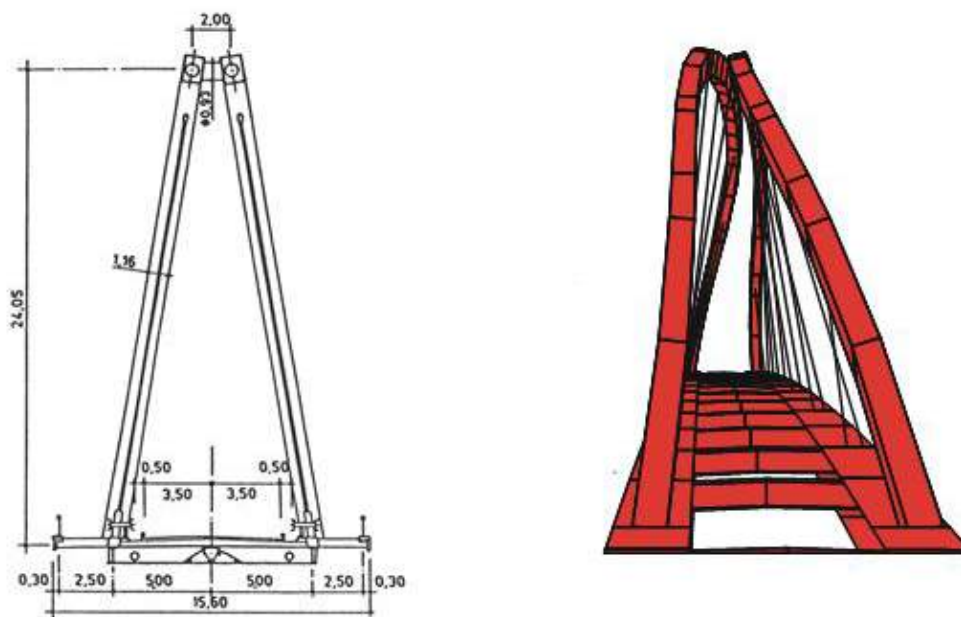
Figure 16. Hermalle Bridge – First buckling mode.

3.5.2 Hoge Brug in Maastricht

When it is possible to imagine tied-arch bridges with two arches without bracing, why not a tied-arch bridge with a single arch?

The Hoge Brug in Maastricht (Figure 20) is a footbridge and crosses over the river Maas in the centre of Maastricht (NL). It constitutes a link for pedestrians and cyclists between the new modern Ceramique district and the old city. With a 164 meters long main span without supports in the river, the bridge is perfectly integrated in its both modern and natural environment, but its elegance and its slenderness are also attractive. This impression of slenderness is due to the little dimensions of the structural elements (deck, arch, hangers) compared to their length, and is accentuated by the curve of the deck section, a box girder shaped as a

sector of a circle. It is constituted by 5 inner boxes with a maximum height of 1.2 m.

The main span is suspended by 14 crossed cables fixed to a single central arch which its cross section has a variable geometry. So, at the haunches, the cross section of the arch is 1.2 m wide by 1.2 m high, and at its crown 2.4 m wide by 0.8 m high. In this way, the steel is distributed in a efficient way: a vertical rigidity at the basis to transmit the longitudinal moments to the deck and a transverse stiffness at the crown of the arch to ensure its stability. This geometry reinforces yet the impression of slenderness. The single plane of hangers, anchored in the middle of the deck serves as a separation between the flow of pedestrians and cyclists. The main bridge was built on pontoons near its final position and was placed by barge driven by cables.
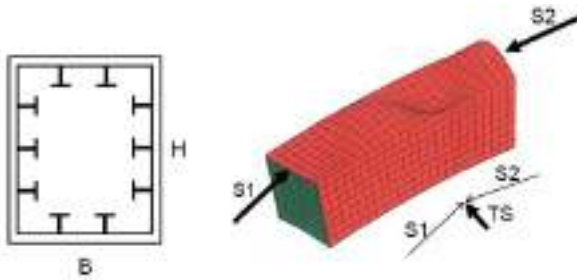
Figure 17. Arch flanges in compression.

Figure 18. Chaxhe bridge.

3.5.3 The Sado Viaduct

The railway Sado Viaduct (Figure 21) is a bridge in the south of Portugal. It carries two rail tracks. To limit the number of piers in the river, the choice of a multiple tied-arch bridge was quickly been adopted: three successive tied-arch bridges with 160 m long main spans. For the pre-design, two solutions were examined: tied arch bridges with two inclined arches or one single vertical arch. Of course, for this comparison, the deck shape was different for the two solutions. With two longitudinal arches, the longitudinal rigidity is ensured by two longitudinal beams located, each one, below each railway track. A transversely eccentric vertical load is equilibrated by an alternated loading in each arch. For the case of single arch, the deck cross section must be a composite box girder, with a sufficient torsional rigidity to transmit the torsional moment to the supports.

Both solutions were confronted with objective criteria on the basis of two preliminary designs carried out in parallel. Finally, the choice was made and the second design was selected for different reasons. Firstly, the single central arch is more effective. Its critical buckling load is greater and the overall deflection of the structure is lower. The variation of stresses in the hangers of the inclined arches is greater, thus making its design more prone to fatigue issues. The solution with two arches increases the number of elements to be assembled. The estimated cost for the two arches solution proved to be 10% higher. All these conclusions led to the final choice of three bowstring girders with a single arch [13].

The steel hollow cross section of the arch has a hexagonal shape of whose height and the width are variable from the basis to the top. The width is increasing to ensure the transversal stability of the arch and the height is decreasing to have the maximum vertical bending rigidity at the connection with the deck. The ratio between the length of the span and the height of the arch is 5.40. The deck is suspended from the arch, every 8 meters, by vertical and cylindrical solid steel bars. Their diameter is 200 mm and they are made of S355 steel.

One particularity of the main bridge, composed by three tied arch bridges, is its continuity. Under the dead load, in spite of the continuity between the bridges, the bending moment between two bridges is almost null. Under the variable load, it is not the case. This scheme doubtlessly distorts the behaviour of a real tied arch. But the interest in providing continuity was double: to suppress the problem of the rail track movement at the extremity of each tied arch bridge but also to have a single bearing device at the top of the concrete piers.

Figure 19. Chaudfontaine bridges.

Assembled on temporary steel frames upstream of the river, the total length of the three spans of the deck was erected by launching. For that, two steel temporary piers were installed in the river Sado between each final concrete pier. Temporary piers were also used to assemble the arches pre-fabricated in three elements. To suppress the bending moment in the deck, above the supports, due to the dead load, after the launching the internal bending moment in the deck due to the dead load after the launching, a vertical displacement of 1.3 m high has been imposed after the final launching. The instability of the arches was verified with finite element simulations. The first critical eigenvalues being not so high in comparison with the ULS load level (2.55 and 2.75 ULS), nonlinear elasto-plastic computations have been carried out with initial transversal deformed shape and several combinations of loading, dead load, wind and UIC loads, to ensure structural stability.

4.
CONVENTIONAL ARCH BRIDGES

4.1 Eau-Rouge Viaduct

The structure (Figure 22) is located between Francorchamps and Malmedy on the E42 motorway (Belgium) close to the border with Germany. The aggressiveness of the valley bottom soil, required a central span of 270 m to avoid the area of soil
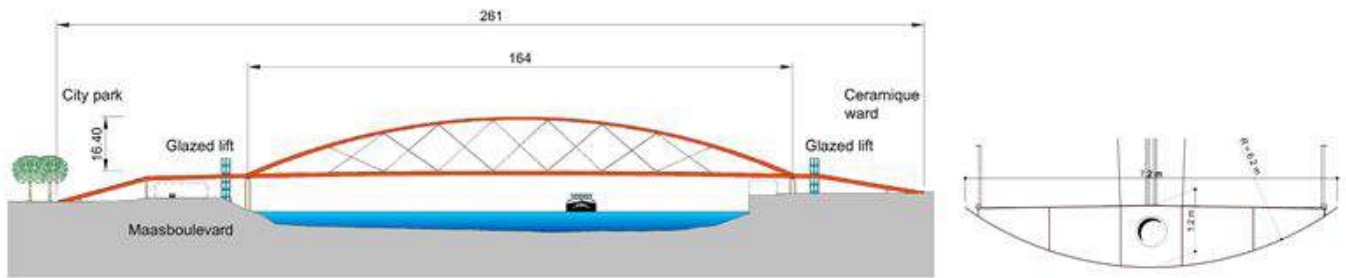
Figure 20. Hoge Brug in Maastricht (Netherlands).
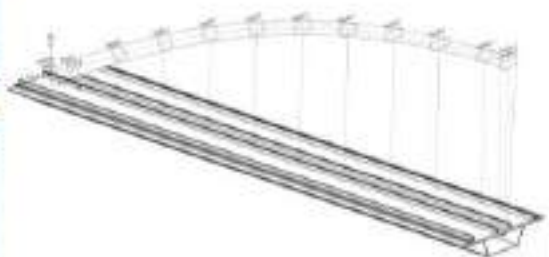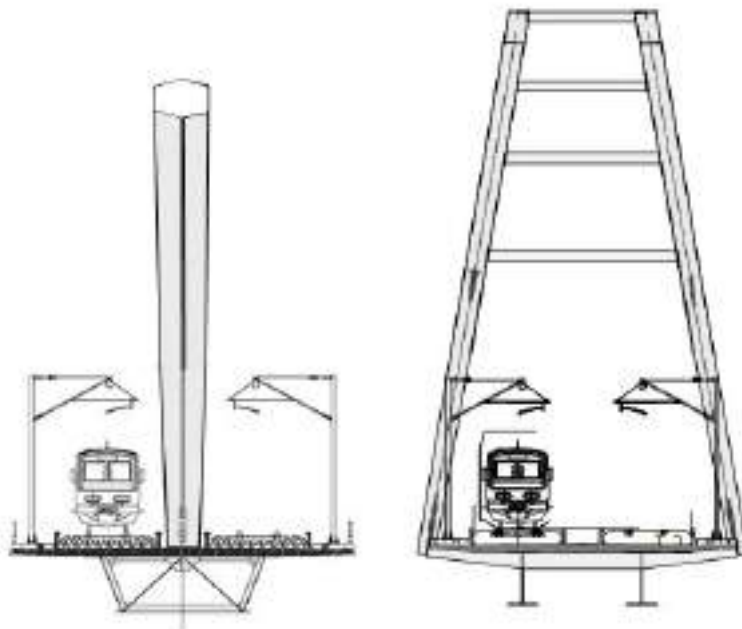
Figure 21. Sado Viaduct (Portugal).
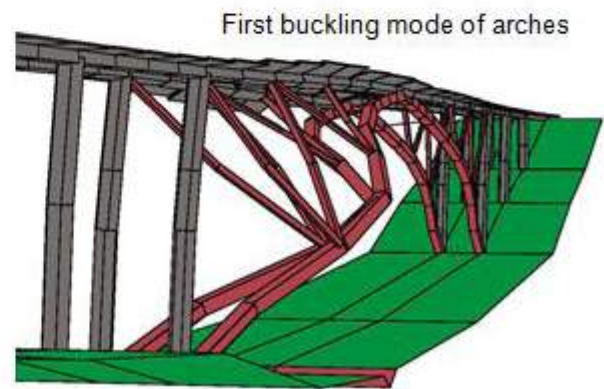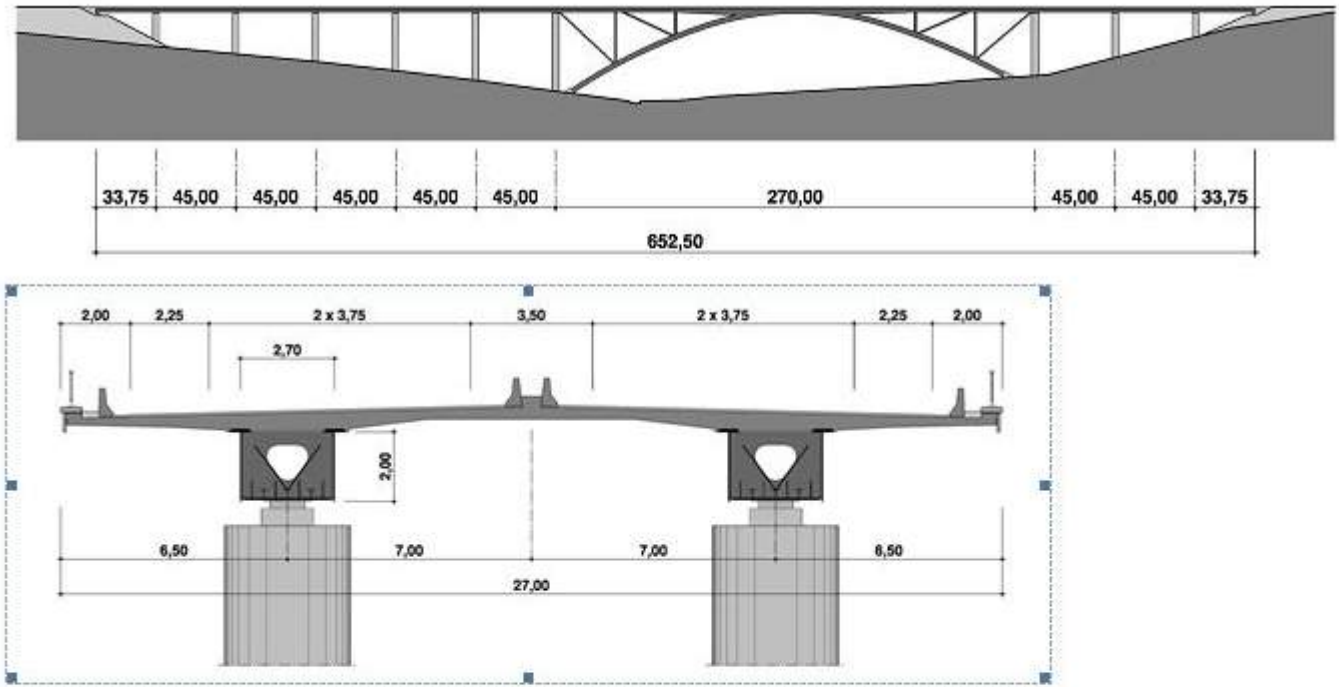
Figure 22. Eau-Rouge Viaduct.

with bad geotechnical properties. This central span is crossed with two arches made of steel hollow rectangular cross-sections spaced 14 m, supporting the composite deck with vertical members and diagonals. The approach spans are 258.75 m long on the north side and 123.75 m on the south side. The viaduct has a total length of 652.5 m. The composite steel-concrete deck is 27 m wide with two carriageways, each with two traffic lanes and one emergency stop lane.

The two steel arches have a parabolic shape of a minimum radius of 150 m and a rise of about 50.0 m. The two steel caissons are not interconnected by any bracing except during the assembly phases. At the top of the arch, the arch and the deck are combined to form a single box of variable depth (2.0 m up to 7.0 m).

The special character of the structure, its lightness, slenderness, and span length of the arch has led engineers to carry out a series of special simulations to verify:
- for the whole structure, its behaviour under the effect of an earthquake and its safety vis-a-vis the instability of the arches without transversal bracing. The first two instability load factor are equal to 4.84 and 5.09 versus the SLS loading (Figure 22.).
- for certain structural elements, the effects of the second order effect such as the vertical webs of the steel hollow caissons of the deck for which the phenomenon of web breathing for the common caisson deck-arch at the top of the arches would occured. [10].

The vertical webs of the steel caissons can be considered as restrained by the concrete slab. Then, when longitudinal stresses in the webs are close to the critical buckling stresses of the plate, transversal displacements appear and cause vertical stresses. So, there is a bi-dimensional stress state. Nonlinear computations with a finite element program have been made to evaluate the level of these stresses and an analytical model has been developed to give the opportunity to do a parametric study with the aim of better understanding the phenomenon, [12].

Figure 23. Arch bridge over the Ravine Fontaine.

This type of bridge, where the wish to simplify the structure is omnipresent, forces the engineer to use ever more advanced calculation methods. The software such as FINELG, [11], can better help understand the behaviour of the structure. But beyond a check, the interest also lies in the possibility of undertaking parametric studies that help guide the researcher in the development of a theory which should then result in design methods.

4.2 Bridge on the Ravine Fontaine

The arch bridge on the Ravine Fontaine (Figure 23) is a bridge on the road connection called "Route des Tamarins" in the West of the Reunion Island (F). It is one of four civil engineering works qualified as exceptional on this road because of their type, dimensions and/or location. The Tamarins road progresses on the sides of a volcano, approximately one km away from the coast and at an altitude close to 300 m. It must consequently cross innumerable ravines. The Ravine Fontaine has at the level of the road, an opening of 200 meters and a depth of 110 meters. The deck is 20.1 m width and carries 2 road lanes and an emergency lane in each direction [12].

As first approach, it was reasonable to consider that (Figure 24.):
- for a bridge whose reactions were vertical, the support zone must have been located 20 m back relative to the edge of the cliffs where a basalt layer sufficiently thick to allow the diffusion of the support reactions could be found.
- for a bridge with inclined reactions (arch type bridge), that it was necessary to consider the zone following the natural balancing slope as unstable, and that a support surface directly behind this zone was acceptable, as far as it was possible to find one or more basalt layers which were able to balance the horizontal component.

Reunion island is the seat of a very significant endemic flora of which many species are protected. In particular, certain birds
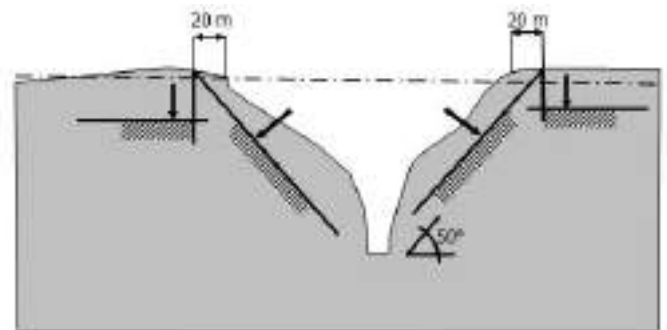
Figure 24. Ravine Fontaine profile and possible support zones.

such as the "puffins of the baillon" nest and reproduce in the cracks and fractures of the basalt layers. It was not possible to envisage a cable-stayed bridge that would have disrupted their flight. In consequence, the best choice was a bridge with a support structure below the deck: an arch bridge.

The length of the structure is strictly limited to what is needed for carrying out the crossing, this is 200 m. It is easily understood that if the geotechnical conditions allow the construction of an arch bridge, this solution will be the most interesting, both from an aesthetical technical and economic point of view. Within this scope, various solutions were subject of a comparative analysis, but the form of an arch was finally retained, for the purity and expressivity of its line.

The principle of an arch bridge is such that it is principally subjected to an almost constant compression force. It is therefore logical to design a constant section. The design takes account of this principle. However, to benefit from the possibilities of restraining the arch in the foundations and in the basalt layers, the height of the section was increased at the basis, which also made it possible to decrease it in the central part and to give the impression of a large slenderness. Transversely, the arch is mainly subjected to wind forces (mean wind speed, 50 m/sec, in cyclone regions). It behaves
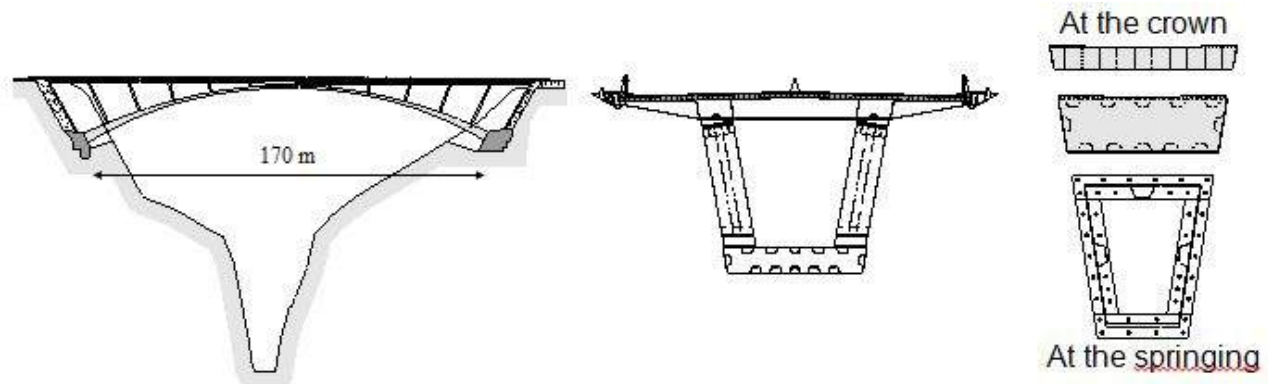
Figure 25. Bridge on Ravine Fontaine – Evolution of the arch transverse Cross section.

like a beam supported at its two ends, with a maximum bending moment in the central part. The width of its section develops proportionally to this bending moment. These principles have made it possible to fit the arch section between two inclined planes.

The geometry of the arch defined in such way was used as the basis for the geometrical construction of the columns and the deck. The deck is composed of two small caissons 2 meters high and 2 meters wide. These two small caissons are braced every 4 meters in order to support the reinforced concrete slabs. They are in addition supported by the radiating, inclined columns. The columns as well as the caissons of the deck fit in the planes of the arch.

The ratio f/L, arch height to span length, is usually guided by economic considerations and lies between 5 and 6 (see tied arch bridges on the Albert Canal). In addition to the general rule, other parameters had to be considered. The foundations must find a sufficiently rigid support on the basalt layers to take the compression of the arch. The abrupt face of the cliffs made the earthworks and the access to the bottom of the excavation particularly delicate. It was necessary to limit their depth to the minimum. But aesthetically, the economic ratio leads to a less dynamic aspect. This is why we made the choice to decrease the slenderness ratio to 1/7.5, which is a rise of 22.50 meters for a span of 170 meters.

The four sides of the box girder consist of stiffened steel panels (Figure 25). These panels were checked by means of Eurocode by taking into account the combined plate-column behavior.

Two by two and laid out every 16 meters, the columns transfer the loads coming from the deck onto the arch. They are provided with hinges at their two ends in order to be subjected only to normal forces. Indeed, under the effect of the asymmetrical forces (a longitudinally loaded half-bridge), the arch works exclusively in bending and significantly deforms, inducing significant relative rotations, particularly at the foot of the columns. An end restraint at this place would have imposed a bending moment in the columns incompatible with their resistance to fatigue. In order to ensure their functionality and to limit the maintenance works (inspection, replacement), the supports at the interface with the deck are carried out by means of steel grains on steel, and at the arch, by means of a welded plate (Figure 26.).

After execution of the earthworks, foundations and support abutments, the assembly of the metallic structure, with a total weight of 2000 tons, was erected by the cantilever method (Figure 27). Basic sections are manufactured in workshops in Italy before being conveyed by boat to Reunion Island. After assembly on site to create elements of a maximum weight of 100 tons, these assemblies were set up ones after the others by means of a derrick crane built explicitly for this work.

5.
CONCLUSIONS

Although numerous arch and tied-arch bridges have already been designed around the world, it is yet possible to imagine innovative structures. But, the most important thing is perhaps to design aesthetic and elegant structures with the due respect to their environment.

The beliefs of Greisch's founder about appropriateness of design in relation to efficiency, economy and functionality have been expressed in a series of works which have established the reputation and the references of Bureau Greisch. René Greisch was engineer and architect. His interest in architecture has instilled the Greisch team with a spirit of research and innovation and has led to many collaboration ventures with architects. Collaboration between engineers and architects is important in order to create an atmosphere where the design team is constantly questioning and searching for new solutions, both formal and technical. The team spirit and the attitude of quest, the determination to work through collaboration and synergy, constant innovation and dynamism, invention combined with imagination must become the working methods and principles that must underpin the design of structures and bridges.

The bridges must be designed to serve the city with the respect of three well-known principles: the statics, the aesthetics and the politics. Then, there will be many chances that citizens will be proud of ''their" bridges. The hope is that the bridges presented in this paper respect this challenge.
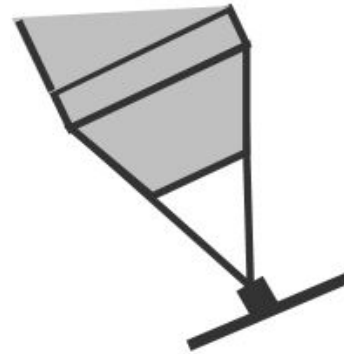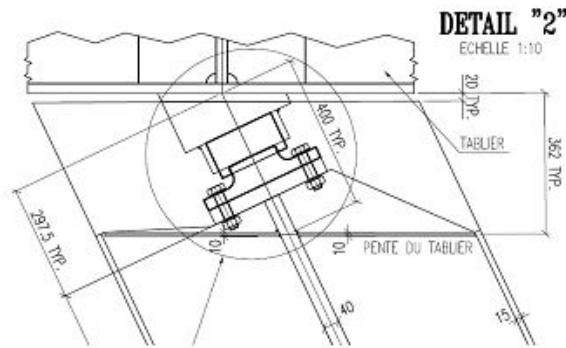
Figure 26. Interface between counters and the deck and the arch.

Figure 27. Erection stages of the steel structure.

References

[1] Sakimoto, T.: Elasto-plastic Finite Displacement Analysis of Three Dimensional Structures and its Application to Design of Steel Arch Bridges, Kurnato University, Japan, 1978.

[2] de Ville de Goyet, V., Fonder, Gh., Lothaire, A.: Stability of a Bowstring Bridge with Twin Inclined Arches, Proceedings of IABSE Workshop "lnformatics in Structural Engineering", Bergamo, 1982.

[3] Chaib, A., J.: Stabilité des ponts bowstring - Etude paramétrique, Master Degree, Department MSM, University of Liege, Belgium, 1987.

[4] de Ville de Goyet, V.: L'analyse statique non linéaire par la méthode des éléments finis des structures spatiales formées de poutres à section non symétrique, Ph.D., Department MSM, University of Liege, Belgium, 1988.

[5] de Ville de Goyet, V., Massonnet, C.E.: Comparative Study of the Stability of Various Dispositions of Tied Arch Bridges, Der Stallbau in Konstruktiven - Ingenieurbau Festive, Publication for Professor BAEHRE, Karlsruhe, 1988.

[6] Ney, L.: Etude paramétrique du contreventement de ponts en arcs, Master Degree, Department MSM, University of Liege, Belgium, 1989.

[7] Ney, L., de Ville de Goyet V., Maquoi R.: Optimum Bracing of the Arches of Tied-Arch Bridges, Journal of Constructional Steel Research, Vol.18, 1991.

[8] Dubas, P., Gehri, E.: Behaviour and Design of Steel Plated Structures, ECCS, nr 44, 1986.

[9] Jacques, Th., Maquoi, R., Fonder, G.: Buckling of unstiffened compression curved plates, Journal of Constructional Steel Research, no 1/1983.

[10] Creme, J.M., de Ville de Goyet, V., Lothaire, A., Radu, V.: Viaduc de l'eau rouge, études spéciales, Construction Métallique, no 1-1994.

[11] FINELG Nonlinear Finite Element Analysis Program, User's Manual. Engineering Office Greisch and ArGenCo Department, University of Liege, Belgium.

[12] Cremer, J.M., Del Forno J.Y., Klein, J.F.: the bridge over the ravine "la fontaine", Reunion Island, 7th International Conference on Steel Bridges, proceedings, Guimaraes, Portugal, 2008.

[13] de Ville de Goyet, V.: Illustration of Design Constraints for Composite Railway Viaducts with Some Recent Structures, Associacon Cientifico-tecnica del Hormigon Estructural, Madrid, 2009.

Bridge design – the Spanish approach by Javier Manterola and similarities in Germany

Diseño de puentes: el enfoque español por Javier Manterola y su similitud en Alemania

Mike Schlaich[a]

[a] *Dr. Engineer. Director. schlaich bergermann partner. (Alemania).*

ABSTRACT

For Javier Manterola engineering is both rationality and emotion, function and form, science and art. His bridges combine such classic virtues of structural engineering as efficiency and structural truth with a permanent search for innovation and progress. His work follows a tradition, which before him was defined by the now classic work of Carlos Fernandez Casado and Eduardo Torroja. He has further shaped and evolved this Spanish tradition for decades and sees it now taken over by the next generation. Similarly, in Germany the classic Fritz Leonhardt was followed by Jörg Schlaich, who is of the same age as Javier Manterola, and now the present generation of engineers. The two engineers know and respect each other and there is also a similarity in their approach to bridge design. To illustrate this and to pay tribute to Manterola, some projects by schlaich bergermann partner will be presented here.

© 2019 Asociación Española de Ingeniería Estructural (ACHE). Published by Cinter Divulgación Técnica S.L.L. All rights reserved.

KEYWORDS: Cable-stayed bridges, composites deck, shell bridges, carbon fiber, stress-ribbon bridge, innovation, structural art.

RESUMEN

Para Javier Manterola la ingeniería es racionalidad y emoción, función y forma, ciencia y arte. Sus puentes combinan las virtudes clásicas de eficiencia y verdad estructural, en una búsqueda permanente de la innovación y el progreso. Su trabajo sigue una tradición, que antes de él fue definida por la obra ahora clásica de Carlos Fernández Casado y Eduardo Torroja. Él ha forjado y desarrollado esta tradición española durante décadas y que ha sido ahora asumida por la próxima generación. Del mismo modo, en Alemania, el clásico Fritz Leonhardt fue seguido por Jörg Schlaich, que tiene la misma edad que Javier Manterola, y que es ahora seguido por la generación actual de ingenieros. Los dos ingenieros se conocen y respetan entre sí y también existe una similitud en su enfoque del diseño de los puentes. Para ilustrar esto y rendir homenaje a Manterola, algunos proyectos de schlaich bergermann und partners se presentan aquí.

© 2019 Asociación Española de Ingeniería Estructural (ACHE). Publicado por Cinter Divulgación Técnica S.L.L. Todos los derechos reservados.

PALABRAS CLAVE: Puentes atirantados, tableros mixtos, puentes lámina, fibra de carbono, puentes en banda tesa, innovación, arte estructural.

1.
INTRODUCTION

A very recommendable little book which contains a series of papers and lectures by Manterola and that gives good insight into his thinking, is *"la obra de ingeniería como obra de arte"* [1]. It is the writing of an intellectual who knows all aspects of his profession and can connect them with ease to other fields like the arts, painting and sculptures, as well as music, politics and philosophy.

It shows that Manterola feels obliged to the classic tradition with its leitmotiv *"lo resistente en la forma construida"* and *"la verdad estructural"*. But this should not become "toda una religion". His work always shows the search for new solutions to leave behind the engineering classicism of the 1960s, because *"la ingeniería no podía quedarse en una repetición al infinito de las buenas soluciones encontradas"*. However, he opposes so-called landmark bridges and bridges designed by architects, especially if the engineer is not called at an early stage but only late in the design to make things stand up. It is the engineer who designs bridges and now *"es el momento de crear formas resistentes nuevas que amplíen las muy optimizadas formas*

* Persona de contacto / *Corresponding author.*
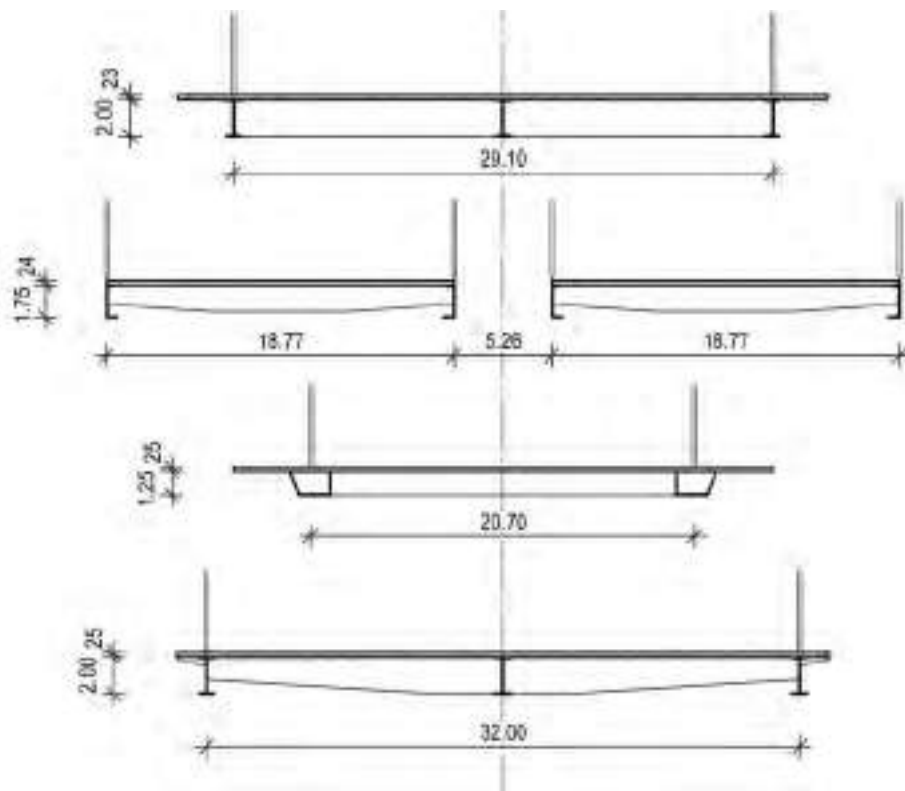Correo electrónico: Mike Schlaich: m.schlaich@sbp.de

Figure 1. Schematic cross sections of composite decks in the same scale from top to bottom: Second Hooghly Bridge, Ting Kau Bridge, K03 over Albert Canal, Signature Bridge in New Delhi. ©schlaich bergermann partner

heredadas". He sees the future of bridge design in the use of new materials such as glass and carbon fibers and in the introduction of 'intelligent' structures which can change their stiffness and flexibility according to exterior requirements. He goes as far as foreseeing a revolution in construction like the one at the beginning of the XIX century when science entered engineering.

The final chapter of the booklet contains a fictional dialogue between an old and a young engineer. The younger person attacks the elder one for the views just given in the paragraph above which shows Manterola´s inner discussion and how carefully he has studied all points and reasons of other views. But he, the elder stays firm *"yo estoy muy lejos de pensar que la fuente de las formas que se obtienen con un enfrentamiento serio con los materiales, su disposición structural y los nuevos métodos de construcción se haya agotado"*.

In our office, schlaich bergermann partner we are following an approach that subscribes to such points of view. There is proven technology which we use and develop further over the years and there is the search for new approaches. Manterola is often working on bridges with concrete decks and has refined them further and further, coming up also with beautiful bridges made of well-shaped precast concrete segments. We have often worked with composite decks. Four cable-stayed bridges, all with such decks (Figure 1), will be presented. Regarding new technologies, two small bridges will show that we are also testing the new ways Manterola is looking at. An 'intelligent' carbon fiber bridge and a shell bridge, which combines state-of-the-art techniques with

traditional methods in form-finding and fabrication will be introduced.

2.
PROVEN TECHNOLOGY - FOUR CABLE-STAYED BRIDGES WITH COMPOSITES DECKS

Composite decks for long-span cable-stayed bridges have numerous advantages: they are comparatively light and robust, because both concrete and structural can be exploited ideally, concrete mainly in compression and steel mainly in tension. They are cost effective because of ease of construction and maintenance. The light steel grid can be transported and installed in large segments and it acts as falsework for an *in-situ* concrete slab or, even better, as support for precast concrete panels.

The actual configuration of main girders and the arrangement of the cable planes needs to be decided individually depending on the boundary conditions of each project. A composite deck should be supported along the edges, as this leads to compression of the concrete also in the transverse direction. For deck widths above 25 to 30 m an additional central main girder, that distributes local loads over several cross girders, usually pays off. For deck widths beyond 30 m and very windy conditions four cable planes can be envisaged in order to reduce the span of the cross girders and hence the overall depth of the bridge deck.

Figure 2. Second Hooghly Bridge (Vidyasagar Setu), Kolkata, India. ©Roland Halbe

Figure 3. Ting Kau Bridge, Hong Kong. ©schlaich bergermann partner

The choice of open or closed steel sections and welded or bolted connections depends on the context, mainly on the possibility of transporting large segments, on-site welding, lifting capacities and experience of the contractor. Precast concrete panels for the deck slab are always advantageous, because formwork is saved and, due to their age, creep and shrinkage effects are reduced. The hoop joints in between the precast panels, that were developed and thoroughly tested for the Ting Kau Bridge, allow for fast erection and result in a continuous, durable and robust bridge deck.

Vidyasagar Setu – Second Hooghly Bridge, Kolkata, India
The Second Hooghly Bridge in India, now known as Vidyasagar Setu, was designed in the early 1970s by Jörg Schlaich and Rudolf Bergermann when they were still working in Fritz Leonhardt´s office and later became the first large project of their own office. It bridges the Hooghly River and connects the suburb Howrah with central Kolkata (Figure 2). The total length of the bridge is 823 m with a main span of 457 m and a width of 35 m. The construction finally started 1978 but could not finish before 1992 due to local political issues [2].

Since weldable steel and High Strength Friction Grip (HSFG) bolts were not available at that time in Kolkata, only a riveted structure was possible. Vidyasagar Setu was not only record span for cable-stayed bridges at the time, it also became the first cable-stayed bridge designed with a composite deck. In-situ concrete was used for the deck slab, which is in good conditions today still.

Ting Kau Bridge, Hong Kong
The Ting Kau Bridge in Hong Kong is one of the few multispan cable-stayed bridges built so far. It crosses the rambler channel and an under-water hill in its middle offered the opportunity to build a central mast, which led to economical deck span dimensions and a total cable-supported deck with a length of 1177 m (Figure 3). The design was also governed by the typhoon wind loads in Hong Kong. Aerodynamic stability of the deck for wind speeds up to 95 m/s had to be achieved. A slender deck of only 1,75 m height supported by four cable planes reflects this. The high wind loads also led to slender masts, shaped for minimum wind resistance, which are stabilised in the transverse direction by cables just like the masts of a sail boat. The bridge was completed in 1998, after only 44 months for design and construction [3].
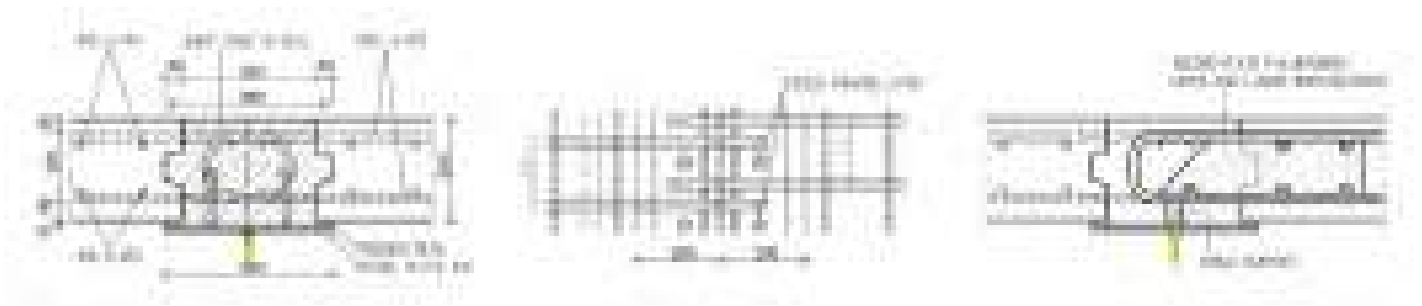
Figure 4. In-situ concrete joint to connect the precast concrete panels and the steel work. ©schlaich bergermann partner

Figure 5. Bridge K03 over Albert Canal, Belgium. ©Jan de NUI, Patrick Henderyckx

The cables are spaced at 13,5 m with cross girders at 4,5 m distances. They support precast reinforced concrete panels with a thickness of 24 cm and 30 cm closer towards the masts. The panels have a size of approx. 4,5 m by 4,5 m and are made of a concrete grade 60 (equivalent to C50/60 in Eurocode terms). All the panels have been cast three to six months prior to their installation in order to reduce creep and shrinkage effects.

The in-situ concrete joints between the panels mentioned above guarantee the continuity of the deck slab and connect it to the steel grid (Figure 4). Tests on site not only confirmed the load bearing capacity of the connection but also showed a pattern of closely spaced small cracks not exceeding 0,25 mm at SLS.

Bridge K03 over Albert Canal, Kempen, Belgium

This semi-integral bridge forms part of a large infrastructure project in Belgium, Kempen North South Connection, which comprises several bridges, tunnels and underpasses (Figure 5). The design is characterized by the harp configuration of the

cables and a relatively short back span. Its axis crosses the canal at a skew angle of 70°. The harp configuration was chosen to have a harmonic appearance of the cables even with the skewed alignment of the masts. The main span of 122 m has a lightweight composite deck with precast slab elements placed on hollow box steel main girders. The relatively short back span with no intermediate tension ties required a heavy and stiff deck for the back span. This led to a thicker concrete slab and to a stiff frame configuration between the masts and the back-span girders in the cable planes. The back-span deck was cast monolithically with the southern abutment to make the bridge semi-integral. The bridge is the results of a successful BOT competition where the winning contractor not only constructs the bridge but also operates it for several years after its completion in 2013 [4].

A large portion of the steel grid, about 70 m by 30 m in size and consisting of main and cross girders, could be prefabricated in the workshop and transported to site on large barges. After completion of the concrete side span, the masts and abutments, the steel grid was lifted to temporary towers

Figure 6. Image of the Signature Bridge in New Delhi, with ornamental painting on the pylon. ©schlaich bergermann partner

that rested directly at the quay walls and was welded together during a remarkably short closure period of the channel. Once connected with the remaining steelwork at the mast and the opposite abutment, the cables with a spacing of 12 m and the skewed precast panels with a typical size of 9 m by 4 m and thickness of 25 cm have been installed step by step beginning from the mast. The deck cantilevers are also made of precast panels which were supported by temporary steel girders.

Signature Bridge, New Delhi

This "Signature Bridge" in New Delhi connects the city Ghaziabad and its surrounding across the river Yamuna to the inner city (Figure 6). The bridge shall be the landmark to a new park and recreation area which shall be created from a now heavily spoiled and contaminated site. In this sense the bridge can be looked at as the signature under the promise to improve a neglected neighborhood. The dynamically shaped pylon consists of two inclined legs, which are rigidly connected to the deck girders and bend mid-way. The upper portion of the pylon anchors the back-stay cables as well as the main-span cables, arranged in a semi-harp like manner. The tip of the pylon is created by a 30 m high steel-glass structure, which can be illuminated to create a landmark visible from afar at night. The bridge was completed at the end of 2018 [5].

The asymmetric cable-stayed bridge has a main span of 251 m (corresponding to a symmetric bridge with two pylons of 500 m span) and total length of 675 m. Its composite deck carries 8 lanes (4 in each direction) and is approximately 35 m wide. The main span is supported by lateral cables spaced at 13,5 m intervals. Towards the approaches the same deck section continues with piers supporting it at 36 m intervals. The

height of the steel tower is approximately 150 m.

The bridge deck consists of three main girders with a height of 2 m and cross girders at a spacing of 4,5 m, very similar to the Second Hooghly Bridge. To provide sufficient space for 8 lanes, the two outer main girders, supported by cables, are spaced 32 m apart from each other. The emergency footpath has been placed on 1,5 m long cantilevers outside of the cable planes. Similar to the Ting Kau Bridge, all steel joints have been designed as HSFG connections.

A major difference between the bridges presented above and the Signature Bridge in New Delhi is that the latter is relatively low above water which is shallow outside of the monsoon period. Therefore, it was possible to erect the entire deck on temporary trestles and not by free cantilever method. This way, full composite action, also for dead load, could be achieved, so that the concrete slab is transmitting even more compression force than in the other cases. This is reflected in the distribution of the concrete slab thickness. Outside of the cable-stayed part the precast reinforced concrete panels have a thickness of 25c m which gradually increases to 35 cm thick panels towards the pylon and ends in a 70 cm thick in-situ portion around the pylon legs. The deck panels are made of grade 50 concrete (equivalent to C40/50 in terms of Eurocode) with a size of 4,5 m by 8 m to minimize the amount of transverse joints. Due to the positive experience gained from the joint detail developed for the Ting Kau Bridge the same detailing has been used again (Figure 7).

The four examples described above show the wide variety of solutions only in the field of composite decks for cable-stayed bridges. We are far from having exploited all the

Figure 7. Deck erection with precast elements (left) and in-situ joints between precast elements and steel girder (right).
©schlaich bergermann partner

possibilities this method of building offers but we should also look for new approaches in bridge design. Small structures, footbridges, offer the possibility for experiments.

3.
NEW APPROACHES IN BRIDGE DESIGN

Carbon fiber stress-ribbon bridge, Technische Universität, Berlin.

Up to now, Carbon Fiber Reinforced Plastics (CFRP) are used in structural engineering mainly to reinforce existing structures. However, its economic and structural potential for new structures is still largely unused. To show this potential, in 2007 a stress-ribbon bridge with carbon fiber ribbons was built in the laboratory of the Department of Civil and Structural Engineering at the Technische Universität Berlin (Figure 8). Stress-ribbon bridges are among the most elegant and lightest bridges. The ribbons are anchored in the abutments on both sides. Pedestrians walk directly on the ribbons that are covered and stabilised by open-jointed concrete plates. Usually the ribbons are steel plates or steel cables. The use of carbon fiber ribbons instead of normal steel ribbons gives an opportunity for progress in the design of stress-ribbon bridges. Compared with normal structural steel, the tensile strength of this material is ten times higher and the specific weight is five times lower. This allows building longer spans and smaller cross sections but also makes such lightweight structure lively.

The high vibration sensitivity of the bridge led to studies on new new damping or control strategies. Active control stat-

egies allowed to make the bridge 'intelligent'. Sensors in the deck detect any movements of the bridge an their signals are sent to a processor unit, which in real time triggers the inflation of artificial pneumatic muscles installed in the handrail. These muscles contract and counteract the movements of the bridge (Figure 9). This way damping can be increased by a factor of ten and the rocking bridge is calmed [6]. The system has been working now for more than ten years and has become a very useful tool for research and for the students as a 'life' introduction into the field of dynamics.

Another very interesting application of carbon fibers in concrete bridge design and construction is pre- and posttensioning. At the TU Berlin a research project for integral road bridges of some 45 m span made of precast concrete girders which are post-tensioned with carbon fiber elements is showing considerable benefits of such an approach.

Shell bridges

The stainless-steel footbridge in Ditzingen, Germany, is a shell that forms both structure and deck (Figure 10). The double-curved shell spans 20 m with a plate thickness of only 20 mm. Laser cut holes in the shell not only make the structure lighter and translucent, but also the remaining steel work reveals the path of the principal membrane forces, thus making the bridge more understandable [7].

In spite of all the modern form-finding techniques available, in this case initial form-finding was done in a most traditional way. Oranges in a German supermarket come in quadrilateral plastic nets, which, when tensioned, deform in a way that loads are carried only by principal membrane tensile forces because the net cannot take shear in its plane. A simple

Figure 8. Load test with Department of Civil and Structural Engineering at TU Berlin. ©Technische Universität Berlin
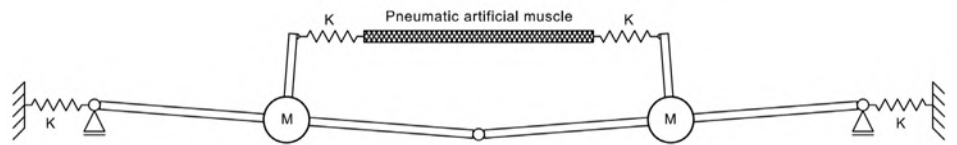

Figure 9. Simplified system for damping the first mode vibration and the first installed pneumatic muscles. ©Technische Universität Berlin

Figure 10. Shell bridge (TRUMPF-Steg) in Ditzingen, Germany. ©sbp / Andreas Schnubel
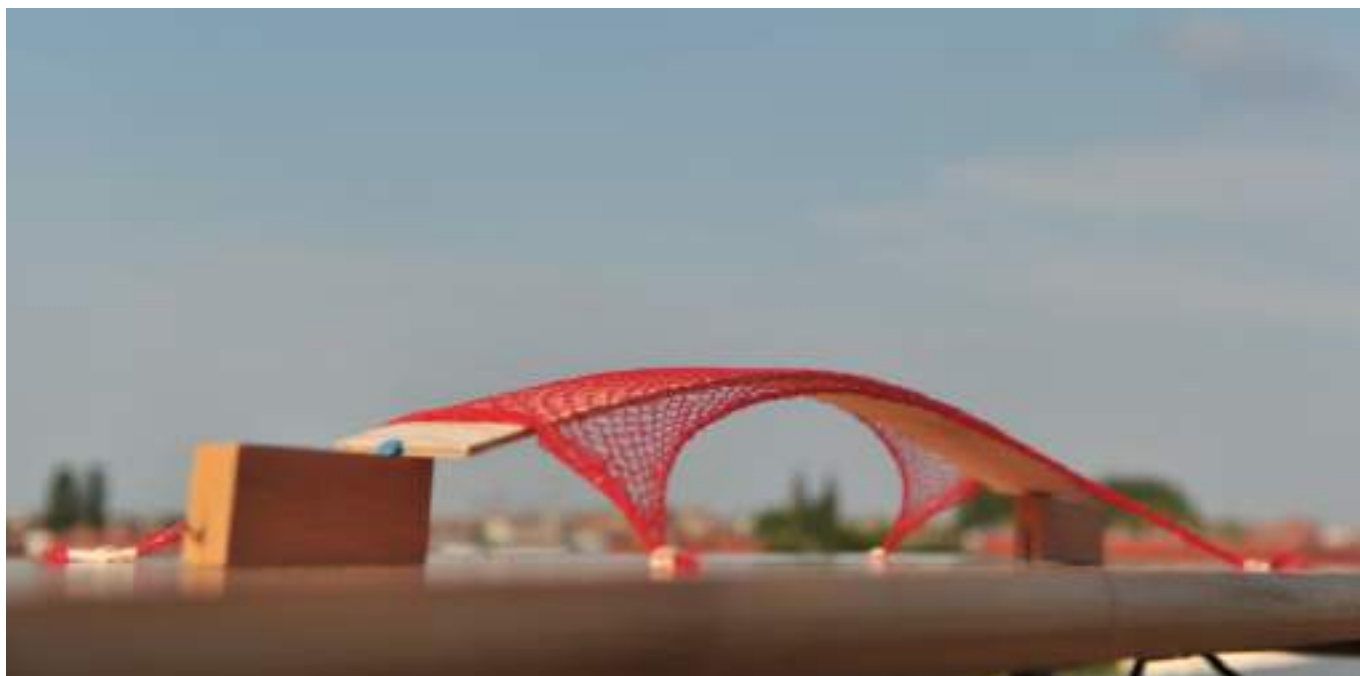
Figure 11. Orange net model. ©schlaich bergermann partner

model made of such a net with a curved timber plate to push the net upward - like an inverted distributed walkway load - was made to achieve a tension-only geometry. The photograph of the model in Figure 11 shows the deformed net and the distribution of the principal membrane forces. Naturally, later modern parametric design tools and nonlinear Finite Element Analysis was used to fine tune the design.

For building the shell, state-of-the-art laser cutting was combined with traditional ship building methods. Steel plates of up to 3x6 m were laser-cut in the Netherlands (Figure 12) and were brought into shape by plastic deformation in a ship building yard in Stralsund, Germany. There, six individual segments, large enough to fit on trucks were welded together and shipped to site. Final assembly of these segments was done under a tent which allowed safe welding and a surface finish with glass powder blasting. Then the entire bridge was lifted into its final position where it is supported on four ball bearings.

This project shows that combining almost traditional techniques with state-of-art technologies is no contradiction. On the contrary, this can lead to surprisingly different results.

4.
SUMMARY

The enormous and beautiful body of Javier Manterola´s work relies on the successful use and further development of proven technologies together with daring new approaches in bridge design. The examples presented here show that this is also the way we are working in Germany. Looking at other recent bridges in France and Great Britain also reveals such approaches. Is the European idea also appearing here with the present generation of bridge engineers, forming a European tradition of bridge design? That would be nice!

Figure 12. Laser cut plate in front of the laser cutter. ©Outokompu

References

[1] Manterola J.: la obra de ingeniería como obra de arte. *Editorial Laetoli*, Pamplona, 2010.

[2] Schlaich J., Bergermann R.: Cable-Stayed Bridges with Composite Stiffening Girders - The Second Hooghly Bridge in Calcutta. *Proceedings of the Sino-American Symposium on Bridge and Structural Engineering*, Peking, 1982.

[3] Bergermann R., Schlaich M.: The Ting Kau Bridge in Hong Kong. *Proceedings IABSE Symposium Kobe*, Japan, 1998.

[4] K03 bridge over Albert Canal - project description online. www.sbp.de/en/project/k03-albert-canal-cable-stayed-bridge/ [02.09.2018].

[5] Schlaich M., Subbarao H., Kurian J.: A Signature Cable-Stayed Bridge in India - The Yamuna Bridge at Wazirabad in New Delhi. *SEI Journal*, 1/2013.

[6] Bleicher A., Schlaich M.: Active vibration control with artificial pneumatic muscles for carbon fiber stress-ribbon bridge, *Proceedings 17th Congress of IABSE, Chicago*, 2008.

[7] Schlaich M.: Shell bridges – and a new specimen made of stainless Steel. *IASS Journal*, September 2018.

Evolution of suspension bridges
Evolución de los puentes colgantes

Klaus H. Ostenfeld[a]

ª Expert Bridge consultant and past CEO of COWI.

ABSTRACT

The suspension of bridges by cables is one of the oldest methods used for spanning relatively long distances with no intermediate supports. Though utterly simple in its basic concept, this system offers excellent opportunities for even very long spans.

The paper describes the evolution from medium span suspension bridges with relatively simple technology towards increasingly more sophisticated technologies, which lead to modern suspension bridges comprising many new innovations, such as continuous aerodynamic bridge decks, internal corrosion protection by dehumidification, using wind flow improving devices, wind screening, deflection control via hydraulic damping and buffer devices, wear reduction systems at bearings and expansion joints and the analysis of anchorage structures with detailed consideration of the soil/structure interaction.

The paper covers the most significant worldwide examples while focusing particularly on several Danish bridges of this typology and how the examination of previous experiences resulted in multiple design optimizations.

Future developments, which would allow extreme spans in the 3- 5 000 m range that are suitable for the Messina and Gibraltar straits, are also presented. This includes a review of the potential of innovative technologies such as new materials and aerodynamically driven active control systems.

© 2019 Asociación Española de Ingeniería Estructural (ACHE). Published by Cinter Divulgación Técnica S.L.L. All rights reserved.

KEYWORDS: Suspension Bridge, box girder, contrapeso, flutter, dehumidification unit.

RESUMEN

La suspensión de puentes por cables es uno de los métodos más antiguos para salvar vanos de longitud considerable sin soportes intermedios. Aunque es muy simple en su concepto básico, este sistema ofrece excelentes oportunidades incluso para vanos muy largos.

El artículo describe la evolución de los puentes colgantes de longitud media con tecnología simple, pasando por tecnologías más y más sofisticadas hasta llegar al puente colgante moderno que incluye muchas innovaciones como el tablero aerodinámico continuo y protección contra la corrosión interna mediante deshumidificación con dispositivos de mejora del flujo del viento, cribado del viento sin efectos adversos sobre la estabilidad aerodinámica, dispositivos hidráulicos de amortiguación para el control de la deformación y la reducción del desgaste de las juntas de dilatación y los rodamientos, así como estructuras de anclaje avanzadas, teniendo debidamente en cuenta la interacción suelo/estructura.

El presente artículo abarca los más significativos ejemplos en el mundo enfocándose en particular en varios puentes daneses de esta tipología y en cómo el análisis de experiencias previas llevó a optimizaciones en el diseño.

Desarrollo futuro con revisión del potencial de nuevos materiales como las fibras de carbono y otras nuevas tecnologías con sistemas de control activo aerodinámicos, permitirían tramos extremos de 3- 5 000 m adecuados para el estrecho de Messina y el estrecho de Gibraltar.

© 2019 Asociación Española de Ingeniería Estructural (ACHE). Publicado por Cinter Divulgación Técnica S.L.L. Todos los derechos reservados.

PALABRAS CLAVE: Puente colgante, sección cajón, anchor block, flameo, sistema de deshumificación.

1.
INTRODUCTION

Suspension bridges are one of the oldest solutions for spans exceeding by far those attainable with simple beam structures.

They are based on one of the simplest structural systems ever devised, namely a rope suspended between elevated supports and anchored to some form of structure founded on the ground. The first suspended structures based on this principle

---

*   Persona de contacto / *Corresponding author.*
    Correo electrónico: Klaus H. Ostenfeld: kho@khoconsult.dk

Figure 1. Bamboo Suspension Bridge - Min River - China.

Figure 2. Tacoma Narrows Bridge - Washington State, USA.

are know from China, where ropes were crafted with twisted lianas. Bamboo fibers were later used in China, Tibet, Japan India and South America.

The Chinese, pioneers in the construction of suspension bridges, used iron chains for this purpose already before 600 AD. At the time, the deck was generally placed directly over the main cables and followed the chain suspension lines of those.

Later came the suspension of the deck from the main cables via clamped hangers.

The first major suspension bridges of rational design appeared some 200 years ago. The suspension bridge concept has since then undergone a steady and continuous development eventually reaching the longest spans in the world, with even much greater spans envisaged for the future.

While other structural systems like cable stayed bridges have also evolved with spans increasing over the years, the original suspension concept remains unsurpassed as the most suitable and economically feasible support concept for very long spans of up to 3 000 m, for the Messina Bridge, and even up to 5 000 m, as envisaged for a bridge on fixed foundations across the Strait of Gibraltar.

New materials, like carbon fibers with their much higher strength/weight ratio, will open the doors for even lighter and longer spans, which may consequently then call for active stabilization systems for adequate aerodynamic stability.

The article will present some of the major evolutionary steps in the suspension bridge technology which have contributed to longer and longer spans, with some indications of further possibilities for development into super long spans with new advanced materials and technologies.

2.
PAST DEVELOPMENTS

As it is generally the case, bridge engineers have always strived for reaching longer and longer spans, in a constant endeavor to beat records. Sometimes in this process, size effects inevitably become critical.

This was the case on the first Tacoma Bridge near Seattle, with a span of 854 m. On a November day, only four months after its inauguration in 1940 and under moderate wind speed conditions, the bridge exhibited large torsional oscillations. These resulted eventually in deformations and accelerations which caused the total collapse of the span.

Earlier suspension bridges, like the iconic Golden Gate Bridge in San Francisco completed only 3 years earlier, had all comprised a stiffening girder in the form of a truss system with large inherent stiffness and a quite acceptable aerodynamic behavior, albeit not optimum in terms of wind resistance.

For the Tacoma bridge, the truss concept was replaced by a slender plate girder with very high slenderness compared to the bridge span, which resulted in a section with practically no torsional stiffness and very poor aerodynamical properties. Thus, the collapse was caused by aerodynamical instability called "flutter" at moderate wind speeds.

One can only speculate if this accident could have been prevented had the designers consulted the Boeing aircraft designers, located in the same neighborhood, as they certainly were very familiar with the problem of flutter which has catastrophic consequences for aircrafts.

The accident obviously set back the development of suspension bridge for some years, until it was determined that it could be avoided by providing adequate torsional stiffness compared to the deck vertical stiffness, and with the improved shaping of the girder for better aerodynamic performance.

Even the earlier Golden Gate Bridge suffered from oscillations in the first part of its life, until torsional stiffness of the trussed girder was increased with the addition of adequate bracing at the lower chord level.

The Golden Gate Suspension span, directed by J.B. Strauss, set new standards for long span bridges with its 1280 m span, a clear record at the time.

The bridge employed tall riveted steel towers acting as a huge cantilevered Vierendeel trusses with no cross bracing from ground up and the girder was one of the slenderest at the time.

The sag ratio for the main cables is relatively high at approx. 1/8 with corresponding tall pylons, which contributes to the iconic gracious shape of the bridge with its iconic overall proportions.

Figure 3. Golden Gate Bridge, San Francisco, USA.

Undoubtedly, the Golden Gate Bridge stood as the finest example of the art of long span bridge engineering for a very long time and is still one of the most successful suspension bridges of all times also because of its scenic location.

The much later Verazzano Narrows Bridge in New York is with its 1 298 m span only marginally longer than the Golden Gate and employs basically the same technology.

A technological leap in suspension bridge technology came with the 988 m span Severn Bridge project in UK. The British designers developed a single slender and rather aerodynamically shaped box girder design for this bridge, and they even utilized its closed shape for sailing the individual segments of the prefabricated girder as ships on the estuary of Severn during high tides.

Further, the designers introduced inclined hanger systems with the aim of providing a triangulated truss-like behavior of the girder, suspension cables and hanger system and thus increased stiffness for wind and traffic loads.

The inclined hangers have however later been replaced by conventional vertical hangers in connection with a major overhaul and strengthening of the bridge because of fatigue concerns.

The nineteen sixties gave rise to increased developments in suspension bridge technology.

While the Severn bridge was under development in the UK, the project for the Little Belt Bridge in Denmark was taking shape.

3.
MODERN SUSPENSION BRIDGE

A. The Little Belt Bridge, Denmark

The basis for this first modern suspension bridge in Scandinavia were extensive studies of the worldwide suspension bridge technology.

The historic Brooklyn Bridge in New York by J.A. Roebling, with 488 m main span, completed in 1,883 comprising the first application of parallel galvanized steel wires for its 4 main cables and the Golden Gate and Verrazano Narrow Bridges were of course among the bridges looked at.

In particular, the Tancarville Bridge across the Seine in France and many others were intensively studied – all with the aim of extracting the very best experiences from past designs in order to create a unique design combining best structural performance with optimum advantages for the Owner regard-

Figure 4. Verrazano Narrows Bridge, N.Y. USA.

Figure 5. The Little Belt Bridge, Denmark.

Figure 6. The aerodynamic box girder with wind deflectors.

ing design and construction, as well as operation, maintenance and aesthetics.

The most important advances of technology and innovations which resulted from this global research were:

I. Use of symmetrical, as opposed to asymmetrical air foils, aerodynamic steel box girders with wind deflectors (guide vanes) as a result of consultations with aeronautical engineers and aircraft designers.

The girder section was developed with special consideration for fabrication of box girder segments at a naval shipyard with similar technology. Furthermore, it was refined by extensive wind-tunnel testing for stability against divergence and flutter related oscillations for all relevant wind speeds. As the shape could not be optimized just for aerodynamics, because wind can blow from both sides and because the primary purpose of the girder is to carry traffic, the edges of the girder would comprise rather sharp and less aerodynamical bends between the flat deck and bottom surfaces and the aerodynamic noses/trailing edges.

However, the resulting release of vortices was found to be greatly attenuated by adding wind-deflector plates to the top edges of the girder.

Such plates have later been used also for the rather bluff section of the cable stayed Saint Nazaire Bridge and Great Belt Bridge with excellent results.

The box girder was presented to the bidding consortia as an alternative to a more traditional truss-based girder in order to generate a basis for competitive bidding amongst the consortia and methods. The result was that the box girder design provided an approximately 20% lower cost than the truss, and thus was ultimately selected for construction as it also presented considerable operation and maintenance advantages for the Owner.

II. Introduction of dehumidification for internal corrosion protection of the box girder and the main cable anchorages.

The internal steel surface area of the girder, including stiffeners and cross bracings or diaphragms, amounts easily
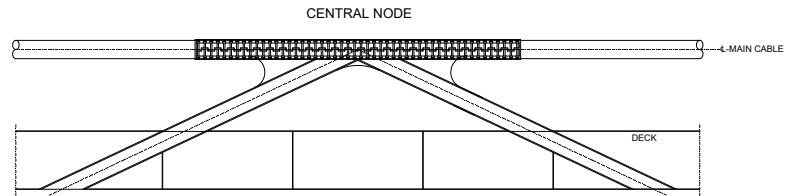
Figure 7. Central Node and dehumidification unit in box girder.

to more than 80% of the total steel surface area of the girder as the exterior is desired to be as slick and smooth as possible for aerodynamic reasons, and the riding surface is covered by mastic corrosion protection and pavement.

The principle of dehumidification for corrosion protection stems originally from the "moth-balling" of heavy military equipment and is based on the simple fact that steel does not corrode in atmospheres with relative humidity below 60%.

The advantages are multifold: The installation using standard off-the-shelf dehumidifier units and simple air circulation systems known from buildings can be accomplished at much lower costs than painting systems, and further the environmental and occupational safety concerns with internal painting is completely eliminated. As a bonus, dehumidification is even a much safer and more efficient method as the risk of quality deficiencies related to occasional nonpainted areas because of difficult access, and resulting localized corrosion, is also effectively eliminated.

Presently, dehumidification is considered the *de-facto* standard for corrosion protection of closed volumes in steel structures because of its proven efficiency and low cost of operation of the dehumidification units.

The concept has been further developed in Japan to comprise permanent corrosion protection of the main cables on existing bridges by means of circulating dehumidified air longitudinally in the cables taking advantage of the voids between the individual wires in the cable and using an airtight PE sheet wrapping on the cable.

III. Use of prefabricated twisted ropes as part-cables for the main cables instead of traditional spinning.
The standard for major suspension bridges was at the time the spinning of parallel galvanized approximately Ø5 mm wires between anchorage shoes arranged at both anchorage structures and subsequently wrapping of the wire bundles with a wire wrapping applied by a specialized purpose-designed machine.

In order to facilitate competitive pricing, the requests for pricing included both traditionally spun cables and prefabricated cables constituted by a number of parallel long lay twisted part cables –called "ropes"– which –after suspension by pulling over the catwalks as always used for suspension bridge construction– would be wrapped by a

galvanized steel wire for assembly of the cable with a circular shape suitable for the cable clamps which in turn suspended the deck via the hangers. The bidding resulted in the prefab cable solution being selected for the Little Belt Bridge.

IV. Use of a central node connection between the main cables and the girder at mid-span for deflection reduction under asymmetrical loading.

The conventional suspension principle leads to relative longitudinal displacement between the main cables and the bridge deck. This means that shorter hangers will alternatively incline in either direction during passage of high concentrated loads like a heavy vehicle. This can cause fatigue on the short hangers, particularly at the anchorage sockets.

By fixation of the main cable to the deck at mid-span through the so-called central node, these relative movements are efficiently arrested and the vertical deflections as a result significantly reduced.

Therefore, this principle was adopted for the Little Belt Bridge and other later bridges.

V. Development of a unique underground anchorage slab structure for the main cables suitable for the fractured Little Belt Clay with adverse soil characteristics and with aesthetic advantages.

The Little Belt bridge is within in a zone with a geology of fractured fat clay. This over-consolidated fat clay is characterized by its susceptibility to slippery fractures and consequently the concerns over the shear strength at these fractures, which is highly un-predictable, make the design of anchorage structures under horizontal forces, which are typical for suspension bridges, critical.

The unique solution developed involved balancing the essential part of the horizontal component by an inclined 1.0 m thick underground anchorage slab ballasted with soil so as to generate by friction enough capacity to resist the live-load related anchorage forces, whereas the dead loads component of cable forces in combination with the self-weight of the anchorage plate and ballast soil is perpendicular to the underside of the large surface anchorage slab.

In addition, the deck over the dehumidified anchorage chambers, where the main cables separate into vulnerable
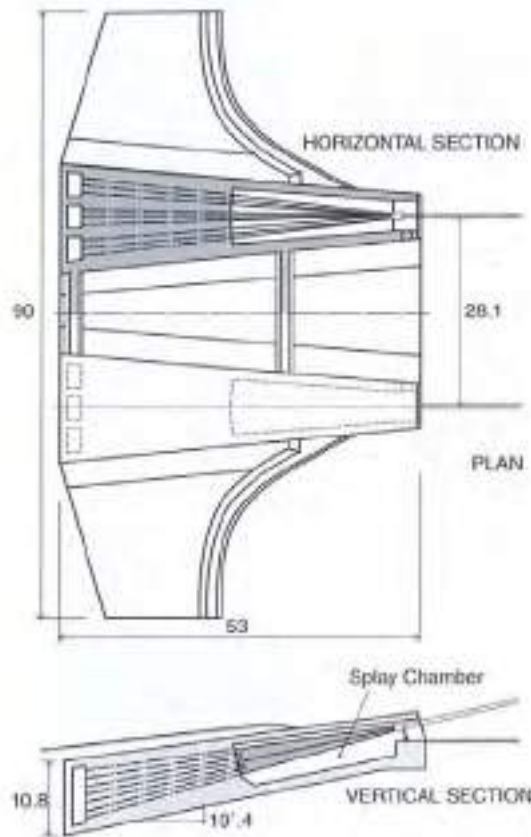
Figure 8. Little Belt Buried Anchorage slab structure.

individual ropes, was particularly investigated for potential aircraft crashes and thus also –almost prophetical– for terrorist attacks.

An aesthetical side benefit of this unusual concept is that the anchor structures are completely buried in the side slopes of the Little Belt and thus nearly not visible and not disturbing the light elegant appearance of the bridge.

vi. Development of a special concrete mix design for the pylons with low cement content, low heat of hydration and excellent durability.

As the pylons along with the main cables essentially are non-replaceable for a major suspension bridge without the total disassembly of the whole structure, a meticulous research was carried out to develop very durable concrete for the piers and pylons. In this endeavor, attention was paid so as to minimize cracking in the massive structures by using of minimum cement content and thus generating minimum heat of hydration. This was achieved by the adequate selection of aggregate sources with optimum gradation.

vii. Pioneering design of main pylon piers with regard to risk for ship collisions based on systematic probabilistic approach.

As the main piers for the pylons are in the Little Belt water, investigation was made to safeguard the bridge against catastrophic ship collisions. This has resulted in the world's first systematic research of causes for ship collisions based on statistical data and the ship/pier interaction forces in the event of a collision.

As ship collisions later have unfortunately become more frequent – some with very tragic outcomes with many casualties – the probabilistic methodology developed has proven very beneficial for the adequate analysis and decision making for later bridges.

The methods having been published in various technical papers are now universally used for major bridges crossing navigable waterways.

viii. Involvement of an architect for assisting with the overall shaping of the bridge components to in the best possible way to fit into the hilly landscape with its gentle light curved and yet springy light nature of the bridge.

The Little Belt Bridge – although with a modest span of 600 m measured with today's eyes – set at the time of its inauguration in 1970 a new standard for modern suspension bridges which has subsequently been the basis for further development of much larger bridges.

B. The Great Belt Bridges in Denmark, 1977-78 proposals

The final decision to construct the Great Belt Bridge in 1976 provided an excellent opportunity to continue the development of the suspension bridge technology from the basis created for the Little Belt Bridge, but this time for much longer spans and heavier loads.

The design was to be for a 6-lane motorway and a dual track heavy duty railway to be carried on a bridge crossing over the international waterway of the Great Belt with some of the world's biggest ships and tankers..

After extensive studies of alternative solutions with due consideration of risks and consequences of ship collisions in the Great Belt, it was concluded that a minimum main span of 780 m was required. This was considered the maximum conceivable at the time for cable stayed, a world record for cable stayed span with a double track railway. However, a longer span was desirable so as to minimize the risk of collisions, which led to consider a long suspension span as the only feasible solution. The inherent flexible nature of suspension spans was a potential concern for railways because of their heavy loads and strict requirements for deflections and restricted allowance for angular alignment and profile changes at expansion joints.

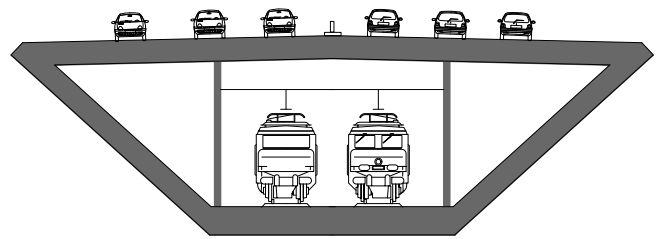Figure 9. Great Belt rail cum motorway bridge design 1,416 m span.

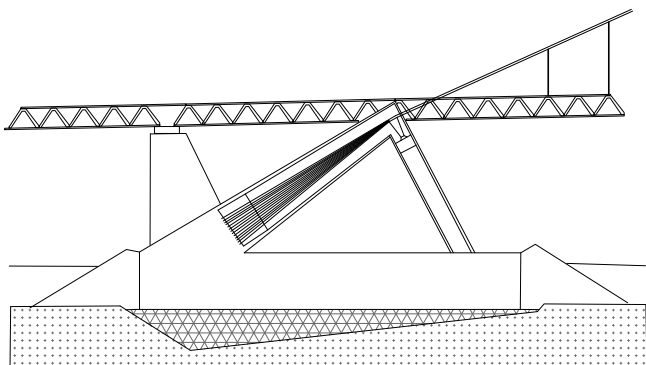Figure 10. Double deck Bridge girder.

Figure 11. Anchor block structure for 1416 m main span.
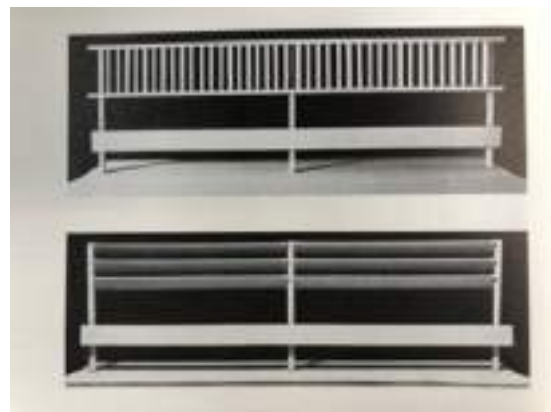

Figure 12. Wind screen concepts with excellent aerodynamic properties.

The continued studies concluded that a relatively long and heavy suspension span would actually generate a corresponding very desirable high main cable force which would be advantageous for sustaining relatively high concentrated train loads with reasonable deflections, and thus it was determined that a 1416 m double deck suspension span with dual railway tracks on the lower deck and 6 a lane motorway on upper deck would be feasible and meet railway stiffness criteria. This was found feasible because rotations at expansion joints could be controlled by using a partially fixed girder at the anchorages.

Building on the experience from the design and construction of the Little Belt Bridge the continued development of the suspension bridge suitable for heavy train loads comprised the following:

I. A 1416 m main span suspension bridge with relatively short side spans for increased stiffness.

The studies of spans from 1200 m up to 1800 m indicated that short spans would be too flexible for heavy loads and the stiffening girder would be easily overstressed because of inadequate main cable force. Conversely, very long spans –although leading to much higher main cable forces and dead load– were not found economical.

Thus, the selected 1416 m span was a reasonable technical and economical optimum which provided adequate lateral ship navigation clearances and overall cable/girder system stiffness for concentrated train loads.

II. A continuous double-deck girder from anchorage to anchorage with semi-fixity at the anchorages and with inclined triangulated trusses with closed box members connecting the 2 decks. All box members dehumidified for corrosion protection.

Contrary to previous suspension bridges at the time, which comprised expansion joints at the pylons – it was found advantageous to let the girder float continuously through the pylon structures suspended only by the hangers and thus avoiding hard points and the complications of expansion devices for the rail with associated angular rotations and maintenance issues.

Furthermore, the anchorage structure, conveniently shaped with a massive counterweight pier at the rear end, Figure 11 provided a convenient support possibility for the girder in addition to the support at the front of the anchorage structure. The relatively short distance between these supports provided an elastic fixity of the girder and thereby assured very small relative angular rotations at the expansion joints which would be acceptable even for high speed trains.

III. In order to further increase stiffness for short term loads like train passages, the bridge would include a central node as the Little Belt Bridge and huge hydraulic lock-up devices at the anchorages which would allow slow temperature variation generated movements, whereas the girder would be virtually fixed for short term passing train loads and

Figure 13. Great belt Suspension Bridge - 1,624 m main span.

thus reduce short term deflections.

IV. For the long span, aerodynamic stability was a concern, as was wind exposure to vehicular traffic on the high-level bridge, which needed a vertical clearance of min. 65 m for international shipping in the Great Belt.

It was known that ordinary wind barriers would create undesirable turbulence and lead to instability and/or buffeting of the bridge for relative low wind speeds.

However, extensive wind tunnel tests revealed that a barrier shaped so as to allow free flow of wind below the barrier and equipped with a semi-open barrier up higher acting like a huge wind resistor (reducing wind speed) would not only ensure stability as without barrier, but in reality, increase the aerodynamic stability of the bridge deck. In addition, such a barrier would be much more effective in reducing the overturning wind loads on high light vehicles because the wind forces would be reduced at a higher level. The effect is well known from aerodynamics of airplane wings using small turbulence generators.

V. In an attempt to minimize the visual impact of the colossal anchorages, the structure was designed as optimum fit for purpose by a triangulated tension and compression leg supported on a sand filled caisson to be placed by the floating off shore method similar to the Ekofisk platform in the North Sea. For balancing the loads for central loading at the underside of the anchorage, a sand filled counterweight pier was provided at the rear end of the anchorage.

The Great Belt Project was developed ready for construction in 1978, when the 2nd energy/economic crisis struck, and the project was shelved for another 8 years.

C. *The Great Belt Bridge 1992 -1998*

The Great Belt Bridge project was relaunched in June 1986 and this time with a requirement for a separate railway tunnel and 4 lane motorway bridge instead of the previous rail cum road bridge for 1978.
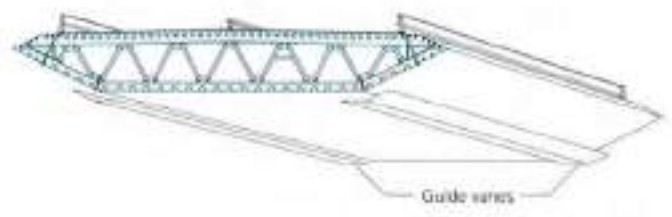

Figure 14. Great Belt Bridge girder with wind guide vanes.

Again, several studies for selection of the most appropriate solution were performed. The selection criteria was based on extensive studies of spans vs price comparisons with due regard to the need for compensating excavations in the sea bottom for the water flow blocking effect of the piers in the belt as well as through ship impact risk assessment by probabilistic analysis, statistics, theoretical and psychological navigation behavior of captains, as well as real time simulations in a new navigation simulation facility.

The end result of the extensive studies was the selection of a 1 624 m main span solution for the East Bridge of the Great Belt as the solution which best satisfied all criteria.

The selected solution brought the suspension bridge technology another step forward:

I. Longest span continuous box girder length in the world with its approx. 2 700 m continuity without expansion joints.

The box girder is continuously suspended between anchorages, where huge expansion devices with capacity of +/- 1 m expansion capability are located. The configuration of the box girder is developed for industrial fabrication in a shipyard with even more production-oriented details than the Little Belt Bridge and of course corrosion protection of the internal volume by dehumidification.

In order to assure adequate stability of the rather sharp-edged girder it was necessary to install wind deflector
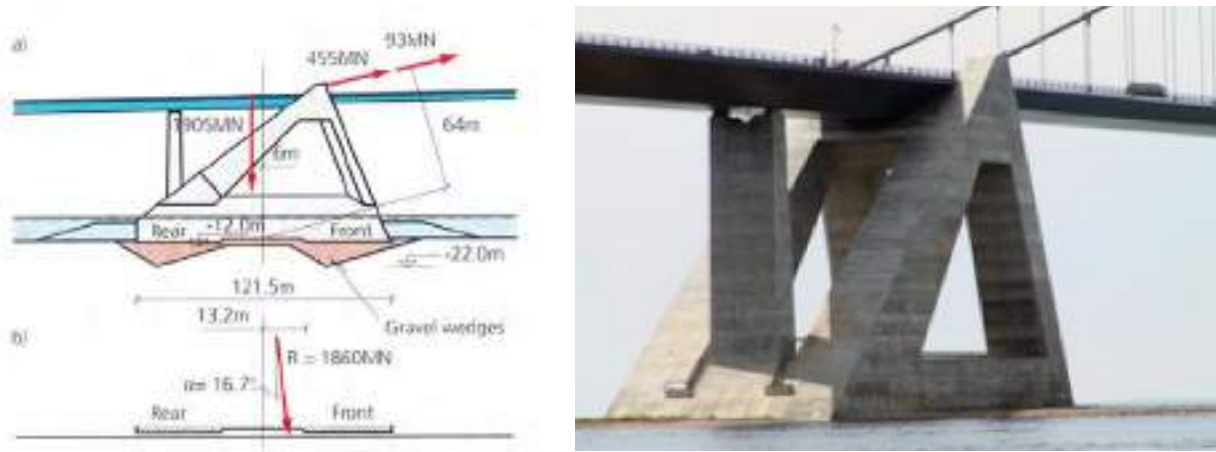
Figure 15. Anchor Block Structure - 1 624 m main suspension span.

plates at the soffit to guide the wind flow around the corners between the horizontal soffit and the inclined sides of the box girder.

II. In order to limit deflections and improve aerodynamic stability, the bridge comprises, as Little Belt, a node connection of the main cables with the deck at mid-span through longitudinal fixation. Furthermore, huge hydraulic buffers were installed at the anchorages as developed already in 1977 in order to prevent longitudinal movements of the girders for short term loads passing the bridge, whilst at the same time permit long term slow expansion and contraction of the bridge deck caused by temperature variation. This system has reduced the accumulated movements of bearings and expansion joints to a very small fraction of the movements which would have taken place without such devices and thus wear and tear is reduced by several orders of magnitude.

III. The main cables, comprising 18 648 Ø 5.38 mm galvanized wires, were spun by an advanced accelerated spinning method using 4 spinning wheels. This allowed spinning the complete cables with 8 wires per spinning passage in only 4 months. This was again the result of putting prefabricated parallel wire strands PPWS in competition with conventional spinning at the time of tender.

IV. The 255 m tall concrete pylons were designed for ship impacts, on deterministic basis, of even the biggest oil tankers, 250 000 dwt ships at 16 knots, because of their proximity to the main navigation channel.

The usual cross beam below the bridge deck, which would inhibit the clear view of the free-floating suspended girder through the pylon, was in collaboration with the architects moved to an optimum mid-height position on the pylons and thus provides for the light appearance of the deck through the pylons with no visual disruption of the elegant lines of the sleek girder.

V. The configuration of the anchorages was inspired on the 1978 solution in order to create a simple and open structure with minimal visual obstruction as a triangulated structure supported on a sand ballasted caisson built in dry dock and floated to the site and ballasted to sit on the previously prepared sea floor with inclined gravel pads – also inspired by the Little Belt anchorage structure configuration.

VI. All piers, including the main piers for the pylons, the anchorages and the approach span piers were built on shore for lowest cost and floated to the site for installation using the now common off-shore technique.

4.
FUTURE DEVELOPMENTS

It is expected that bridges in the future at certain locations will require longer spans, in the range of 3 000 m and even up to 5 000 m.

Studies have been made for the Messina Bridge for more than half a century. The span currently envisaged is 3 300 m for a bridge comprising a double track railway and a six lane motorway. It will be one of the most challenging bridge projects ever with almost 400 m tall pylons and a huge span located in a known earthquake prone zone. However, the suspension bridge concept is well suited for earthquakes because its natural frequencies are very low and far from typical earthquakes frequencies, and thus the structures are not susceptible for large accelerations apart from those parts close to the foundations.

A detailed design has been developed ready for construction as and when decided.

The UN as well as the Spanish and Moroccan governments have shown interest in investigating the technical feasibility of a fixed link across the Strait of Gibraltar at several occasions.

This has led to the development of technically feasible, albeit not financially, bridge schemes on two different alignments across the very deep and geologically complex Gibraltar Strait.

The shallowest is a 28 km long alignment taking advantage of a saddle-like bathymetry with the possibility of
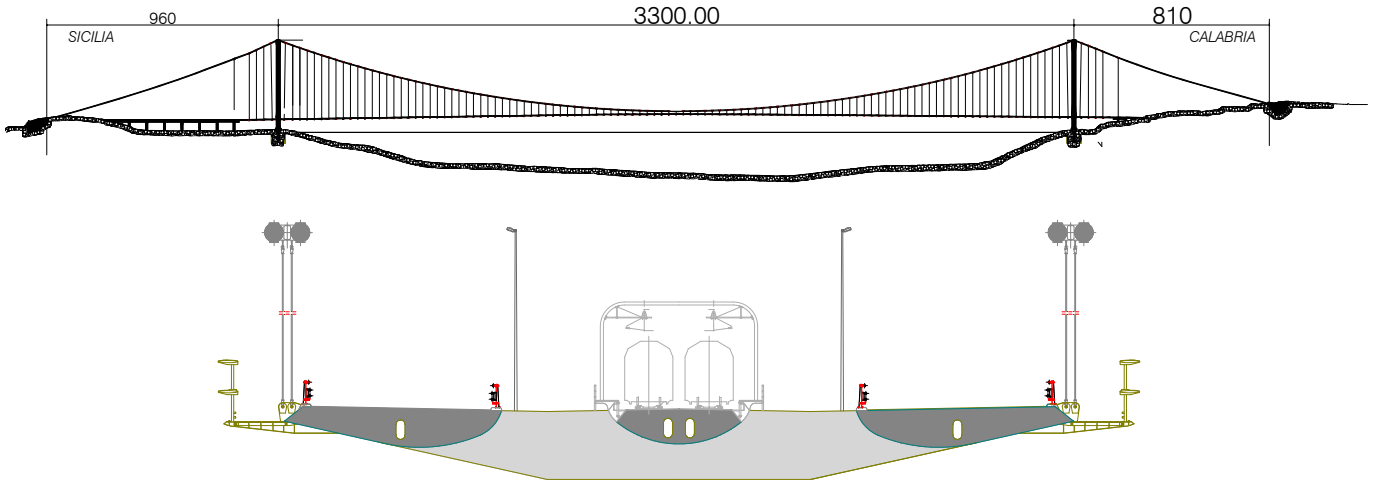
Figure 16. Messina bridge 3 300 m span road cum rail bridge.

Figure 17. Gibraltar Strait - 3 x 3 500 m suspension bridge solution.

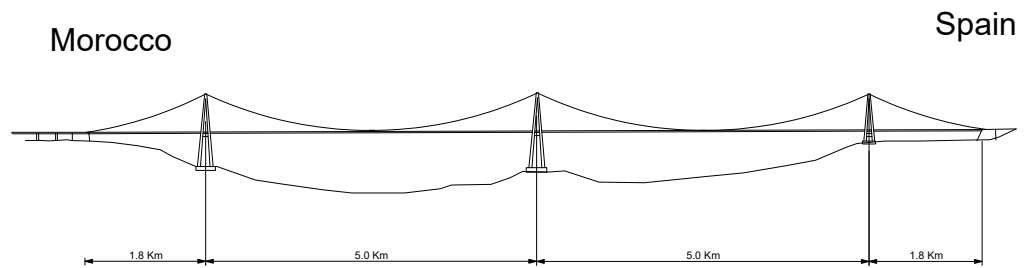Figure 18. Off shore type bridge pier concept for 300 m water depth.

Figure 19. Gibraltar Strait 2 x 5 000 m span solution.

placing off-shore type piers on water depths of 300 m approximately, which is similar to the deepest existing off shore oil and gas platform (Troll in the North Atlantic Sea). This concept would require 3 consecutive 3 500 m spans using A-shaped pylons for rigidity.

A solution of much shorter length of 14 km has also been investigated, but water depth would dictate 2 consecutive 5 000 m spans, and one center pier placed on approximately 450 m deep water.

A further serious complication is the risk of ship collisions and very difficult foundation conditions with chaotic geological strata and risks of earthquakes.
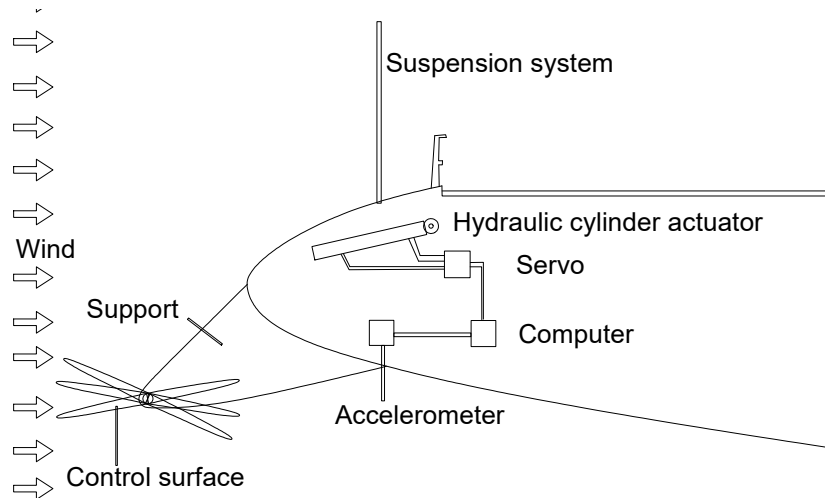
Figure 20. Active control system for aerodynamic stabilization of bridge decks.

The further development of such extreme bridges will require new considerations and the development of new technologies with materials of much improved strength/weight ratios like carbon fibers or similar.

These bridges will be lighter and use less material in the interest of saving on resources and cost as well as being environmentally friendly.

As a result of this development, it is inevitable that these bridges become more susceptible to aerodynamic instabilities, which can only be controlled by active systems.

Such a system, inspired by commonplace autopilots in airplanes, has been developed and patented as a suitable means for efficiently stabilizing bridge decks utilizing the destabilizing forces generated by the wind to also stabilize the bridge deck movements using actively controlled control surfaces as illustrated in the figures below.

References

[1] Chr. Ostenfeld & W. Jønson, Motorway Bridge across Lillebælt, Technical Publications I – XIV, 1970

[2] Chr. Ostenfeld, Ship Collisions against Bridge Piers, IABSE Twenty Fifth Volume of "Publications" 1965

[3] Erik Kalhauge, Georg Haas, Klaus Ostenfeld, Great Belt Bridge – Tender Projects, IABSE Congress Report, 1980

[4] Klaus Ostenfeld, Georg Haas, Torsional Fixation of Girders in Cable Suspended Bridges, IABSE Congress report, 1984

[5] Javier Manterola, Miguel Astiz, Klaus Ostenfeld, Long Span structures for the Gibraltar Crossing, IABSE Congress Report, 1988

[6] Klaus H Ostenfeld, Designing Bridges, To Bridge the Danish Way, Danish State Railways and The Road Directorate, 1986

[7] Georg Haas, Klaus H Ostenfeld, Recent Danish Contributions to Bridge Engineering, To Bridge the Danish Way, Danish State Railways and The Road Directorate, 1986

[8] Klaus H. Ostenfeld, Aerodynamics of large Bridges, Structural Engineering International, Vol 2, 1992

[9] Klaus H. Ostenfeld, From Little Belt to Great Belt, AFGC Symposium Deauville, France 1994

[10] Klaus H. Ostenfeld, Design of the Great Belt East Bridge, Structural Engineering International, Vol 5 1995

[11] The Storebælt Publications, East Bridge, A/S Storebæltforbindelsen, 1998

[12] Klaus H. Ostenfeld, Evolution of bridge foundations for constructability, economy, sustainability and safety, IABSE Colloquium, New Delhi, 1999

[13] Klaus H. Ostenfeld, Dietrich L. Hommel, Dan Olsen, Lars Hauge, Planning of Major Fixed Links, Bridge Engineering Handbook, CRC Press, 2000

[14] K. H. Ostenfeld, The Storebælt East Bridge, Structural Control and Health Monitoring, John Wiley & Sons, Ltd. 2004

[15] Klaus H. Ostenfeld, Jørgen S. Steenfelt, Flemming M. Petersen, Carsten S. Sørensen, Transcendent foundation solutions – 75th anniverary of K. Terzaghi's "Erdbaumechanik"

[16] Klaus H. Ostenfeld, Henrik Andersen, Modern suspension bridges from a global viewpoint, Steelbridge symposium, Millau, France, 2004

[17] Klaus H. Ostenfeld, An integrated Multidisciplinary Approach to Design of Major Fixed Links, IABSE Symposium, Venice 2010

[18] Klaus H. Ostenfeld, Major Fixed Links – approach to the future climatic, environmental and societal requirements in planning, design and construction, IABSE-JSCE Joint Conference in Bridge Engineering – II, Dhaka, 2010

[19] Klaus H. Ostenfeld, Erik Y. Andersen, Major Bridge projects, - a multidisciplinary approach, Frontiers of Architecture and Civil Engineering in China, Vol 5 2011

[20] Klaus H. Ostenfeld, Cross Border Technologies in Major Bridge Structures, IABSE conference, Egypt 2012

[21] Niels J. Gimsing, Klaus H. Ostenfeld, Eminent Structural Engineer: Dr. Techn. Christen Ostenfeld (1900-1976), Structural Engineering International Vol 22, IABSE, 2012

[22] Klaus H. Ostenfeld, European Patent, A system and a method of counteracting wind induced oscillations in a bridge girder, 1996

[23] Michel Morgenthaler, Klaus Ostenfeld, Un Grand Ingénieur Passionné, Travaux, Janv/Fevr. 2019.

ACHE
MONOGRAFÍAS

ACHE

MONOGRAFÍA **33**

M
EVALUACIÓN DE ESTRUCTURAS DE HORMIGÓN ARMADO

Grupo de Trabajo G.T. IV/1 Evaluación
de estructuras de hormigón armado
Comisión 4 "Uso y mantenimiento"

SOFiSTiK | 2020

- **SOFISTIK | 2020** es el siguiente paso en la estrategia BIM de SOFiSTiK.
- Nuevos interfaces para manejar las diferentes fases del proyecto.
- Colaboración con modelos IFC y flujos con Dynamo y Grasshopper.
- Modelos de puentes con parametrización axial mediante CABD.
- Nuevas barras de menú para el SOFiSTiK Structural Desktop SSD.
- Árbol de tareas en el TEDDY para una mejor organización de los elementos.

VIII CONGRESO DE ACHE

ASOCIACIÓN ESPAÑOLA
DE INGENIERÍA ESTRUCTURAL

CONGRESO INTERNACIONAL DE ESTRUCTURAS

SANTANDER
| 24, 25 y 26 de junio de 2020

Resúmenes

La **fecha límite de recepción de resúmenes será el 31 de mayo de 2019**. En la página web www.CongresoACHE.com podrán encontrarse las instrucciones para los autores.

El **30 de junio de 2019 el Comité Científico comunicará a los autores la aceptación de su resumen** o, en su caso, la propuesta de cambios a realizar.

Comunicaciones completas

La **fecha límite para la recepción de las comunicaciones completas será el 31 de octubre de 2019**. Las normas específicas para su redacción podrán encontrarse en la página web del Congreso.

Antes del 31 de enero 2020 se notificará a los autores la aceptación provisional o el rechazo de su trabajo y, en su caso, las modificaciones requeridas por el Comité Científico. La aceptación definitiva se comunicará a los autores antes del 28 de febrero de 2020.

Tanto los resúmenes como las comunicaciones completas pueden ser escritas en idioma **español** o **inglés**.

Publicación

La revista indexada **Hormigón y Acero** publicará un número especial con los resúmenes aceptados. Para que el resumen sea incluido en esta publicación será necesario que al menos uno de sus autores se haya inscrito en el Congreso antes del 30 de abril de 2020. **Las comunicaciones completas se publicarán en acceso abierto en la página web de dicha revista, www.hormigonyacero.com**.

Adicionalmente, el Comité Científico realizará una selección de las mejores comunicaciones completas presentadas al Congreso para su publicación como artículos de realizaciones o de investigación en números ordinarios de la revista Hormigón y Acero. Dichos artículos también estarán disponibles en acceso abierto en **www.hormigonyacero.com**.